Democratic and Popular Republic of Algeria

Ministry of Higher Education and Scientific Research

University Mohamed Khider of Biskra

Faculty of Exact Sciences and Science of Nature and Life

Department of Material Sciences

Thesis

Presented to obtain the degree of

Doctorate of Sciences

Speciality: Physics of Materials

Synthesis and characterization of Zinc Oxide (ZnO) Thin films deposited by spray pyrolysis for applying: electronics and photonics

Presented by:

OTHMANE MOHAMED

Publicly defended on: .. / .. / 2018

To the Jury composed by:

M^{r}. H. Bentamam	Professor	University of Biskra	President
M^{r}. A. Attaf	Professor	University of Biskra	Supervisor
M^{me}. H. Saidi	MCA	University of Biskra	Co-Supervisor
M^{r}. N. Attaf	Professor	University of Cons1	Examiner
M^{r}. A.B. Bouzida	Professor	University of Batna1	Examiner
M^{r}. D. Belbacha	Professor	University of Batna1	Examiner

Academic year 2017-2018

DEDICATION

To

my family

To my friends

Table of Contents

Chapter II : Realization and characterization Of thin films

Chapter III : Effect of solution flow rate and deposition air pressure on ZnO properties deposited using Pneumatic Spray Pyrolysis

Chapter IV : Effect of substrate temperature and dopants on ZnO properties deposited using Utrasonic spray pyrolysis

Acknowledgments

« PRAISE BE TO ALLAH»

I am grateful to my Supervisor Professor **Mr.Abdallah Attaf**, Professor at Mohamed Khider University of Biskra for his continuous guidance advice effort and invertible suggestion throughout the research.

A big thank you to **Mrs. Saidi Hanane**, Co-Supervisor of my thesis, assistant Professor at Mohamed Khider University of Biskra for her support and advice, encouraged me, and helped me to carry out this work.

I am honored that **Mr. Elhachmi Bentamam**, Professor at Mohamed Khider University of Biskra, has agreed to chair the jury of my thesis. I thank him warmly.

I also thank **Mr. Nadhir Attaf**, Professor at the University of Constantine 1, **Mr. El- Djemai Belbacha**, Professor at the University of Batna 1, and **Mr. Aissa Belgacem Bouzida**, Professor at the University of Batna 1, for having agreed to do part of the jury of this thesis as examiners. That their remarks and their criticisms are welcome. i thank everyone in the discussion committee for accepting the request and i am grateful to them for reading my thesis and thanks and gratitude to Professor **Mr. Aida Mohamed Salah,** a Professor at King Abdulaziz University, Jeddah for his advice and opinions, which he did not hesitate to give with confidence in this work.

I would tkank **Mr. Fouad Bouaichi** without his continuous support this study would not have been possible.

I am also grateful to **Mr. Saad Rahmane** Professor in the Department of Physics of the Faculty of Exact Sciences of the University of Biskra for providing me the logistic support and his valuable suggestion to carry out my research successfully. I thank **Mr.Toufik Tebermacine**, Professor in the Department of Physics of the Faculty of Exact Sciences of the University of Biskra, for all the electrical measurements made on my thin films, My utmost gratitude to **Mr. Gasmi Brahim**, engineer at the Mohamed Khider University of Biskra for his kindness and help for his contribution to X-ray diffraction measurements (XRD). I would also like to thank everyone who collaborated to characterize our samples.

I thank **Mr. Nabil « Mourad » kara** for helping to carry out my research. I would also like to thank **Mr. Salah Yahiaoui** for encouraging me to carryout this project.

My thanks also go to all of my colleagues from our laboratory (Laboratoire de Physique des Couches Minces et Applications « LPCMA »)

Finaly I would like to express my sincere appreciation to my familly for encouraging and supporting me throughout the study.

List of Tables

List of figures

General Introduction

In the recent years, Growing request for clean source of energy has increased the industry of solar cells for converting sun energy directly into electricity. Transparent and conductive oxides (TCO) are remarkable materials in many areas. The existence of their double property, electrical conductivity and transparency in the visible, makes them ideal candidates for Optoelectronics, photovoltaic or electrochromic windows.

Research has been carried out around the world to make a cheaper and more efficient solar cell technology by employing new architectural designs and developing new materials to serve as light absorbers and charge carriers.

In this context, advances have been made in the field of solar cells. Zinc oxide (ZnO) is a material belonging to the family of transparent oxides Conductors (TCO). The non-toxicity and abundance on Earth of its components make it an ideal candidate as transparent electrical contact for solar cells in layers thin films of amorphous and / or microcrystalline silicon.

The technique of spray pyrolysis deposition makes it possible to obtain layers of ZnO Rough and thus efficiently diffusing the light that passes through them. This high power Diffusing layers of ZnO makes it possible to lengthen the path that the light travels in the Solar cell, and thus to increase the optical absorption and the photogenerated current in the cell.

The present education incorporates the recognition of critical spray parameters and redress issues concerning to these parameters to optimize the interpretation of the spray pyrolysis unit. thereby this study being for demonstrating the optumal parameters for obtaining of thin films of transparent conducting oxide for various applications, via two kinds of spray pyrolysis method which are pneumatic spray pyrolysis and ultrasonic spray pyrolysi

Worth knowing to indicate that transparent conductive Oxides (TCO) thin films are used as a window material in the solar cell these days. Its increased stability in the reduced ambient, less expensive and more abundance make it popular among the other TCO’s. It is the aim of this work to obtain a significantly low resistive ZnO doped thin film with good transparency. Detailed electrical and materials studies is carried out on the film in order to

expand knowledge and understanding, where The work reported in this thesis sets out to answer three questions :

- What are the apropriate conditions for synthesis thin films via Spray Pyrolysis and pneumatic spray pyrolysis?
- Does the relationship between the deposition pressure and the solution flow rate be strong, and what is optimum point for the best properties?
- What is the best doping rate of fluorine and aluminium concerning zinc oxide thin films and what are their affected on the electrical properties?

This thesis consist of four chapters ; where the first chapter presents a review about the general properties of transparent conductive oxides (TCO's)and zinc oxide and their doping trends.

The second chapter titled by Realization and characterization Of thin films, where we bring a detail informations about Spray pyrolysis system also the Empirical conditions occured in our laboratory, then we listed the characterization methods which have used for Microstructural, optical, and electrical measerments.

In the third chapter which is titled by results and discussions, our study were about the pneumatic spray pyrolysis where we devided it into two sections; the first on the impact of solution flow rate on the whole properties of zno thin films, the second section was about the effect of the deposition pressure on the structural, optical and electrical properties, and at the end we indicate the nature of relation between the both parameters.

Chapter four presents a description of the experimental ultrasonic spray pyrolysis and its method of use, where the investigations of ZnO thin films were into two parts, the first was about the substrate temperature, where We studied the influence of substrate temperature on the properties of the zinc oxide thin films, we carried out a serie from 250 to 500 ^{o}C when the whole parameters are fixed all samples have characterized on the optical, structural, and electrical, the second part to carried out the effect of aluminum and flourine doping on the properties of zinc oxide thin films.

Finally we will conclude our work by a general conclusion including details results of characterization of zinc oxide thin films which we have found through our experimental work and their behavior with a five factors which are the solution flow rate, deposition air pressure, substrate temperature, aluminum and fluorine doping concentration.

Chapter I

Conductive Transparent Oxides

I.1.Transparent conducting oxides

Transparent conducting oxides (TCOs) are a specific category of materials that can be electrically conducting and optically transparent and, as such, are a critical component in almost all thin-film photovoltaic devices. TCOs are very useful materials to transparent optoelectronics because they have unique features of optical properties in the visible light region such as the transparency over ~ 85% and optical band gap greater than 3 eV and controllable electrical conductivity such as carrier concentrations of at least 10^{20} cm^{-3} and resistivity of about 10^{-4} Ω.cm [1]. Notwithstanding their extraordinarily wide controllable conductivity range including that of semiconductor behavior, their applications are limited to transparent electrodes ,TCO's consists of a group of materials that can be thought of as 'conjugate property materials' in which one property, [in this case conductivity], is strongly coupled to a second property, namely, the extinction coefficient, Their resistivity could be as low as 10^{-4} Ω.cm, and their extinction coefficient *k* in the optical visible range (VIS) could be lower than 0.0001, owing to their wide optical band gap (E_g) that could be greater than 3 eV [2].The challenge for achieving materials that are both electrically conducting and optically transparent is to understand the fundamental material structure/property relationships that control these properties so that they may be decoupled such that the material retains transparency while becoming electrically conductive; furthere, (TCO) are binary or ternary compounds, containing one or two metallic elements.

The most widely studied TCO semiconductors are impurity-doped ZnO, In_2O_3, SnO_2 and CdO, as well as the ternary compounds Zn_2SnO_4, $ZnSnO_3$, $Zn_2In_2O_5$, $Zn_3In_2O_6$, In_2SnO_4, $CdSnO_3$, andmulti-component oxides consisting of combinations of ZnO,In2O3 andSnO2 [3]. Later, it was recognized that thin films of ZnO, SnO_2, In_2O_3 and their alloys were also TCOs. Doping these oxides resulted in improved electrical conductivity without degrading their optical transmission. Tin doped In_2O_3 (ITO), Al doped ZnO (AZO) and antimony or fluorine doped SnO_2 (ATO and FTO), are among the most utilized TCO thin films in modern technology. In particular, ZnO is used extensively.

The actual and potential applications of TCO thin films include: transparent electrodes for flat panel displays, transparent electrodes for photovoltaic cells, low emissivity windows, window defrosters, transparent thin films transistors, light emitting diodes, and semiconductor lasers.

I.2.Trends in the development of TCO materials

low resistivity and low optical absorption are always significant,when the development of new TCO materials is mostly dictated by the requirements of specific applications, basically, The most widely used for manufacturing TCO films have been made using indium or tin based oxides[4]. Indium is in limited supply and relatively expensive, and the price of tin has risen rapidly in the past few years [5]. Whereas, Tin doped Indium oxide (ITO) is the most commonly produced TCO followed by fluorine doped tin oxide (FTO) [6]. Thus, there is a need to find alternative materials that can be employed in optoelectronic devices. However, Zinc oxide films have been recognised as suitable alternatives based on the low cost, greater earth abundance and comparable optoelectronic properties. As shown in Table 1.1. The master strategy dopes known binary Transparent Conductive Oxides with other elements, which can increase the density of conducting electrons, more than 20 different doped binary TCOs were produced and characterized, of which ITO was preferred, while AZO , GZO and AZO come close to it in their electrical and optical performance. Doping with low metallic ion concentration generates shallow donor levels, forming a carrier population at room temperature. for example in FZO, fluorine is known to improve electrical conductivity. Fluorine is incorporated into the lattice by substituting an O^{2-} site with F^{-}, where O^{2-} : 1.24 Å; F^{-} : 1.17 Å , resulting in one more free electron making fluorine a suitable dopant for n-type, The concentration of F^{-} dopant ions should not exceed an upper limit, which is studied in part two chapter III, as an increase in carrier scattering by F ions led to a decrease in the conductivity [7]. Similarly, aluminum is often used for intentional n-type doping of ZnO, but other group III impurities, such as Ga and In, and group IV, such as Sn and Ge, also work. Doping by Al produced the relatively high conductivity AZO [8]. Doping with non-metallic elements is also common, e.g., ZnO:Ge (GZO), SnO_2:F (FTO) and SnO_2:Sb (ATO). lately, AZO films with resistivity ρ~$8.5.10^{-5}$ Ω.cm was reported by Agura et al [9]. FZO, with lower resistivity ρ ~10^{-5} Ω.cm, was also reported. This value is approaching to the lowest resistivity of ITO of $7.7.10^{-5}$ Ω.cm.

Table 1.1 **:** TCO Compounds and Dopants [10]

TCO	Dopants
ZnO	Al, Ga, B, In, Y, Sc, F, V, Si, Ge,Ti, Zr, Hf, Mg, As, H
SnO_2	Sb, F, As, Nb, Ta
In_2O_3	Sn, Mo,Ta, W, Zr, F, Ge, Nb Hf, Mg
CdO	In, Sn
$GaInO_3$	Sn, Ge
$CdSb_2O_3$	Y

I.3.Zinc oxide (ZnO) Properties

I.3.1.Basic informations

Zinc oxide is an inorganic compound with ZnO formula. Where, commonly appears as a white powder, almost insoluble in water, basic properties of Zinc Oxide are tabulated in Table 1.2. The powder is widely used as an additive into many materials such as ceramics, glass, cement, rubber (car tyres), lubricants, paints ointments, adhesives, sealants, pigments, foods (source of Zn nutrient), batteries, ferrites, fire retardants, etc. ZnO is present in the Earth crust as a mineral zincite; however, most ZnO used commercially is produced synthetically.

In materials science, Zinc oxide is an attractive material for applications in electronics, acoustics, photonics, and sensing. In optical emitters, its high exciton binding energy (60 meV) gives ZnO an edge over other semiconductors such as GaN if reproducible and reliable p-type doping in ZnO were to be achieved. ZnO is a semiconductor named a II-VI due to the zinc and oxygen belong to the second and sixth groups of the periodic table, respectively. ZnO has various favorable properties: high electron mobility, wide bandgap, good transparency, strong roomtemperature luminescence, etc. Those properties are already used in emerging applications for transparent electrodes in liquid crystal displays and in energy-saving or heat-protecting windows, and On the electronic side, zinc oxide holds many potential in transparent thin film transistors due to its high optical transmissivity and high conductivity. Among the other promising areas of application for ZnO are acoustic wave devices, due to large electromechanical coupling in ZnO, and devices utilizing nanowires/nanorods such as biosensors and gas sensors and solar cells.

Table 1.2 : Properties of Zinc Oxide

Properties	
Molecular formula	ZnO
Molar mass	81.408 g/mol
Appearance	White solid
Odor	odorless
Density	5.606 g/cm^3
Melting point	1975 °C (decomposes)
Boiling point	2360 °C
Solubility in water	0.16 mg/100 mL (30 °C)
Band gap	3.3 eV (direct)
Refractive index (nD)	2.0041

I.3.2.Structural Properties

Zinc oxide is a wide-bandgap II-VI compound semiconductor. It may have crystal structures of three forms: the rarely observed cubic rocksalt, cubic zincblende and hexagonal wurtzite. Which are illustrated in figure1.1, a, b and c, respectively. It has been theoretically found that the wurtzite structure is energetically a more favorable structure of ZnO compared to rock salt and zinc blende structures. The zinc blende ZnO structure can be stabilized only by the growth on cubic substrates, the rocksalt NaCl-type structure is only observed at relatively high pressures (~10 GPa).

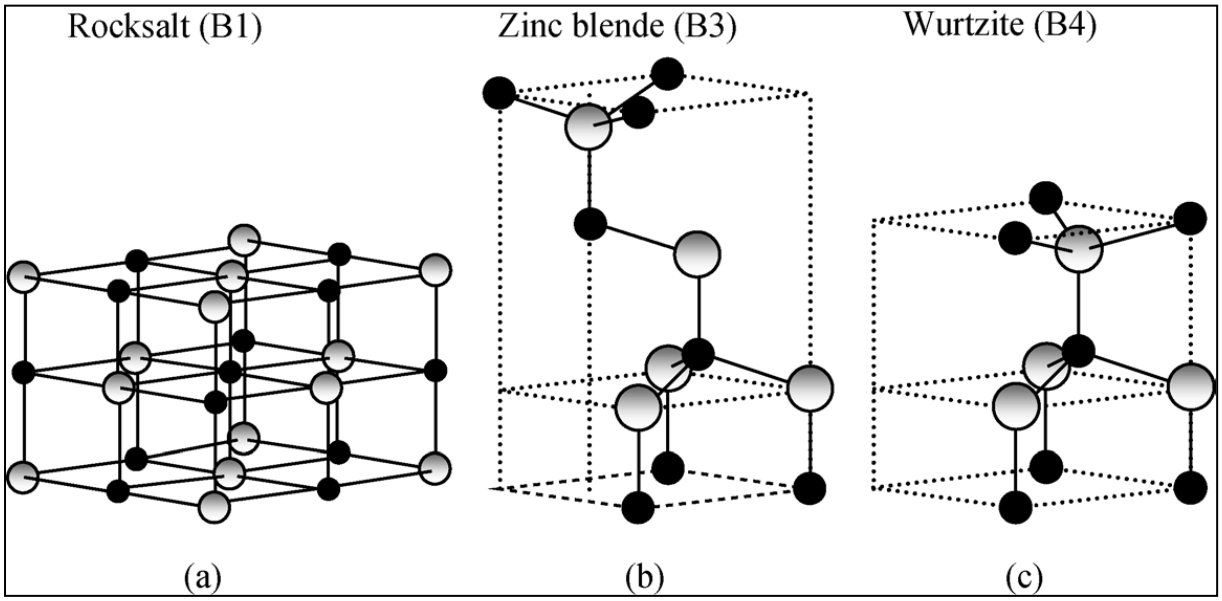

Figure 1.1 : Crystal structures of ZnO (a) cubic rocksalt , (b) cubic zinc blende and (c) Hexagonal wurtzite, O atoms are shown as white large spheres, Zn atoms are small black spheres [11].

The hexagonal lattice is characterized by two interconnecting sublattices of Zn^{2+} and O^{2-}, in such a way that each Zn^{2+} ion is surrounded by a tetrahedron of O^{2-} ions, and vice-versa. The tetrahedral coordination in ZnO results in non-central symmetric structure which subsequently results in strong piezoelectric, pyroelectric effects and spontaneous polarization which is also a key factor in crystal growth, etching and defect generation [12,13].

In the hexagonal wurtzite structure. It has a polar hexagonal axis, the c-axis, chosen to be parallel to Z (0001) .The zinc atoms locate almost in the position of hexagonal close packing, as shown in following figure1.2:

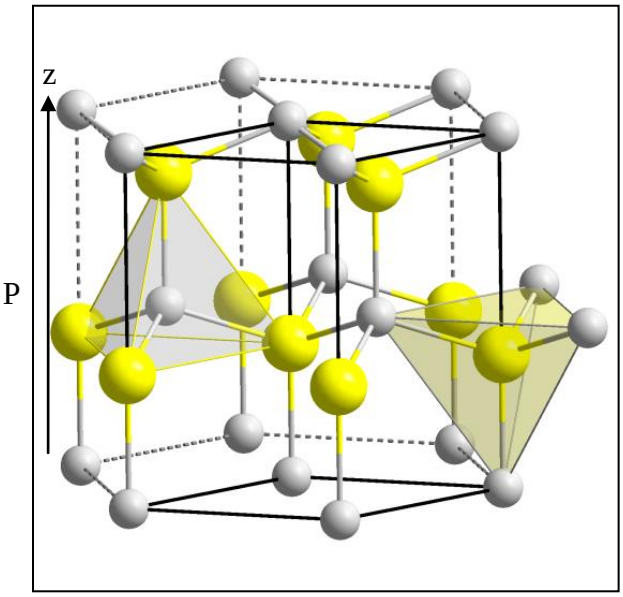

Figure 1.2 The wurtzite lattice of ZnO: small circles represent zinc atoms, whereas large circles depict oxygen atoms. The tetrahedral coordination of Zn–O is shown; it has a polar hexagonal axis, the c-axis, chosen to be parallel to Z.

In the wurtzite structure each sublattice includes four atoms per unit cell and every atom of one kind (group II) is surrounded by four atoms of the other kind (group VI), or vice versa, which are coordinated at the edges of a tetrahedron. In a real ZnO crystal, where the wurtzite structure may deviates from the ideal arrangement, and by varying the value u parameter which is defined as the length of the bond parallel to the c axis, in units of c; or the c⁄a ratio [14]. The following formula describes a strong correlation exists beween the c/a ratio and u parameter:

$$u = (1/3)\,(a/c)^2 + 14 \qquad (1.1)$$

It is obviously that, when the (c/a) ratio decreases, the u parameter increases. In other context, and through the deformation of tetrahedral angles due to long-range polar interactions, those four tetrahedral distances remain almost constant.

I.3.3.Optical Properties

The important optical properties of ZnO thin film are:

- Transmission, T
- Reflection, R
- Absorption, A
- Refraction Index, n
- Extinction Coefficient, k
- Band Gap, E_g
- Geometry

Geometry is an extrinsic property which encompasses the physical attributes of the film, including thickness, uniformity and surface roughness.

Transmission, reflection and absorption are intrinsic properties of the film dependant on the chemical composition; they are determined by the resultant two properties refractive index, extinction, band gap and geometry. The properties of ZnO that differentiate it from other semiconductors or oxides or render it useful in many applications:

- Large exciton binding energy: ZnO has some significant advantages in its large free exciton binding energy (60 meV compared to 21-25 meV for GaN) [15, 16], that allows for efficient excitonic emission in ZnO can persist at room temperature and higher [15].

  Since the oscillator strength of excitons is typically much larger than that of direct electron–hole transitions in direct gap semiconductors [17], the large exciton binding energy makes ZnO a promising material for optical devices that are based on excitonic effects.

- Direct and wide band gap : ZnO has a band gap of 3.44 eV at low temperatures and 3.37 eV at room temperature [18], which corresponds to emission in the UV region. This band gap is very close to that of GaN (3.39eV), and GaN has been the subject of much research over the past years, even being incorporated into the recent Blu-Ray drives. For comparison, the respective values for wurtzite GaN are 3.50 eV and 3.44 eV [19]. this enables applications in optoelectronics in the blue UV region, including laser diodes, light-emitting diodes and photodetectors [20,21]. Optically pumped

lasing has been reported in ZnO platelets [15], thin films [16], ZnO nanowires [22] and clusters consisting of ZnO nanocrystals [23]. Recently a many of reports on p–n homojunctions have appeared [24,25,26], but stability and reproducibility have not been established.

I.3.4.Electrical properties

Many reports have made alot of studies on the electrical properties of Zinc oxides films for understanding the conduction behavior, due to two reasons. First, n and μ cannot be independently increased for practical TCOs with relatively high carrier concentrations. At high electron density, carrier transport is limited primarily by ionized impurity scattering i.e., the Coulomb interactions between electrons and the dopants. Higher doping concentration reduces carrier mobility to a degree so that the conductivity cannot be increased.

Most Zinc oxide has *n*-type character, even in the absence of intended doping. Native defects such as oxygen vacancies or zinc interstitials are often assumed to be the origin of this, an alternative explanation has been proposed, based on theoretical calculations, that unintentional substitutional hydrogen impurities are responsible.

Controllable n-type doping is easily achieved by substituting Zn with group-III elements Al, Ga, In ; then major of reports in ZnO films, deposited using various methods, resistivity and mobility were nearly independent of the deposition method and limited to about 2×10^{-4} Ωcm and 50 cm^2/Vs, respectively [27,28]. Furthermore, it is difficult to be sure about ZnO in p-type, this problem originates from low solubility of p-type dopants and their compensation by abundant n-type impurities, and it is pertinent not only to ZnO, but also to similar compounds GaN and ZnSe. Measurement of p-type in "intrinsically" n-type material is also not easy because inhomogeneity results in spurious signals. However such high levels of *p*-conductivity are questionable and have not been experimentally verified [29].

Moreover it decreases the optical transmission at the near-infrared edge. With the increase in dopant concentration, the resistivity reaches a lower limit, beyond which it cannot decrease.

I.4.Review of doped zinc oxide thin films

Many types of dopants have been used (Al [30], In [31], As [32], S [33], Sn [34], Mn [35], etc.) for many important applications in ZnO thin films; these dopant elements offer a manner to regulate the electrical, optical, and magnetic properties, which are make Doped ZnO films are promising candidates as conductors with high transparency in the visible light range and high conductivity. Even though the standard transparent conductors in industry are ITO and FTO, there is huge interest in finding more stable and cheaper alternatives.

In Table 1.3 some doped films are summarized, and their transmittance in the visible range, and lowest resistivity values too, There are a Typical dopants that have been used to increase the conductivity of ZnO are group III (B, Al, In, Ga) and group IV (Pb, Sn) elements of the periodic table.

Table 1.3 : Summary of different doped ZnO thin films as transparent conductors.

Dopant	Methods	Transmittance in visible range	Lowest resistivity
Al	Pulsed laser deposition (PLD) [36,37]	~90%	$\sim 10^{-4}\Omega$cm
	Radio-frequency (RF) magnetron sputtering [38]		
	Solution processed [39]		
Ga	PLD [40]	~85%	$\sim 10^{-3}\Omega$cm
	Solution processed [41]		
In	Solution processed [42]	~80%	~20 Ωcm
N	Plasma-assisted molecular beam epitaxy [43]	~80%	$\sim 10^{-2}$ Ωcm
	RF magnetron sputtering [44]		
	Solution processed [45]		

I.5.Major applications of zinc oxide thin films

It might come as a shock but over 50% of that Zinc Oxide used is in the rubber industry. ZnO along with stearic acid is used in the vulcanization of rubber to produce such things as tires, shoe soles, and even hockey pucks.

A very important use is that Zinc Oxide is widely used as the buffer layer in CIGS (Copper Indium Gallium Selenide) solar cells. Some current experiments are focusing on the effect of the thickness of ZnO on maximum power output for the cells.

Another main use in concrete manufacture, the addition of Zinc Oxide aids the processing of concrete and also improves water resistance.

Zinc Oxide also has antibacterial and deodorizing peroperties. For this reason it is employed in medical applications such as in baby powder and creams to treat conditions such as diaper rash, other skin irritations and even dandruff. Due to its reflective properties it is also used in sunblocks and can often be seen on the nose and lips of lifeguards at the beach.

I.6.Thin Film Deposition Techniques

The thin film deposition can be broadly classified into two major processes: chemical deposition and physical deposition processes [46]. The chemical methods comprise gas phase deposition methods and solution techniques. The gas phase methods which are employ precursor solutions as: chemical vapour deposition (CVD) [47,48] and atomic layer epitaxy (ALE) [49], while spray pyrolysis [50], sol-gel [51], spin-coating [51] and dip-coating [51]. The physical methods include physical vapour deposition (PVD), laser ablation, molecular beam epitaxy, and sputtering.

For selecting of the deposition method there are many factors should be taking into account:

- Nature of the substrate on which the film is to be deposited
- Material to be deposited.
- Thickness of the film required.
- Structure of the film expected.
- Application of the thin film.

Careful selection of the appropriate deposition technique is essential for control over the properties of the resultant films, the following figure 1.3 shows the classification of methods :

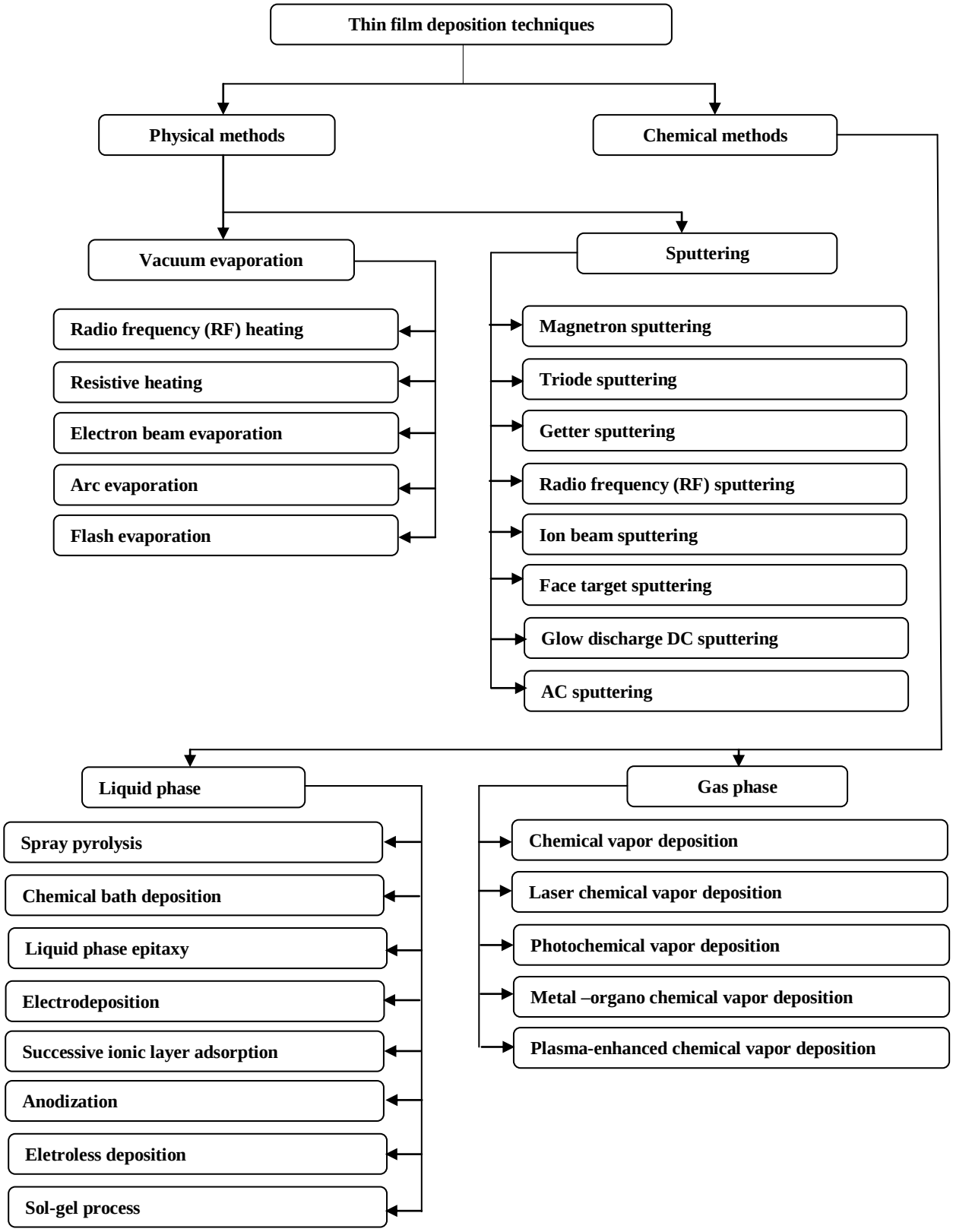

Figure 1.3: The classification of deposition methods.

I.6.1.Physical vapor deposition

Physical Vapour deposition techniques are the range of techniques used to deposit thin films onto a substrate using purely physical processes, PVD processes are environmentally friendly vacuum deposition techniques consisting of three fundamental steps Figure 1.4:

- Vaporization of the material from a solid source assisted by high temperature vacuum or gaseous plasma.
- Transportation of the vapor in vacuum or partial vacuum to the substrate surface.
- Condensation onto the substrate to generate thin films.

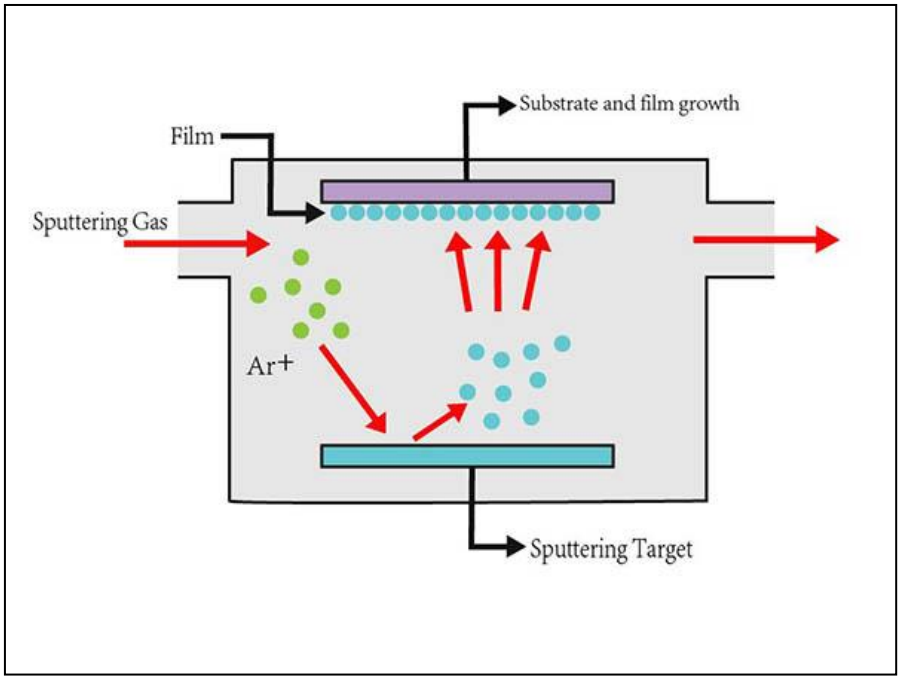

Figure 1.4: Physical vapour deposition method.

The choice of deposition PVD techniques used in production are basically two in nature:

- Thermal evaporation by resistively heating or by using an electron-beam heating
- Sputtering, a non-thermal process

And may depend more on what technology is available for the specific material at the time:

The two most common PVD processes are thermal evaporation and sputtering. Sputtering is a plasma-assisted technique that creates a vapor from the source target through bombardment with accelerated gaseous ions (typically Argon). Thermal evaporation is a deposition technique that relies on vaporization of source material by heating the material using appropriate methods in vacuum.

- Evaporation condensation of metal vapor in high vacuum to deposit a thin film on wafer.The vacuum is required to allow the molecules to evaporate freely in the chamber, and they subsequently condense on all surfaces. This principle is the same for all evaporation technologies, only the method used to the heat (evaporate) the source material differs. There are two popular evaporation technologies: e-beam evaporation and resistive evaporation [52].
- Sputtering is a process that uses plasma and acceliration of ion towards a surface of solid target material. Material sputtered from the target and deposited on wafer the atoms are deposited to form an extremely thin coating on the surface of the substrates. It is a technique often used to deposit thin films of semiconductors, CDs, disk drives, and optical devices. Extensively used Si technology moderate step coverage. Sputtered films exhibit excellent uniformity, density, purity and adhesion. It is possible to produce alloys of precise composition with conventional sputtering, or oxides, nitrites and other compounds by reactive sputtering.

Process of sputtering:

- Ions of inert gas are accelerating into target.
- Target is eroded by the ions via energy transfer and is ejected in the form of neutral particles.
- Neutral particles from the target traverse and are deposited as a thin film onto the surface of the substrates.

I.6.2.Pulsed laser deposition (PLD)

With the pulsed laser deposition (PLD) method, thin films are prepared by the ablation of one or more targets illuminated by a focused pulsed-laser beam (see figure 1.5).
It is a physical vapor deposition process, carried out in a vacuum system, which shares some process characteristics common with molecular beam epitaxy and some with sputter deposition.

In laser ablation, each ablation pulse will typically provide material sufficient for the deposition of only a submonolayer of the desired phase. The amount of film growth per laser pulse will depend on many experimental parameters, which have a strong influence on film properties. Laser related parameters such as laser fluence, including target–substrate separation; background gas pressure and laser spot size, and laser energy density. Under typical conditions, the deposition rate per laser pulse can range from 0.001 to 1A° per pulse [53].

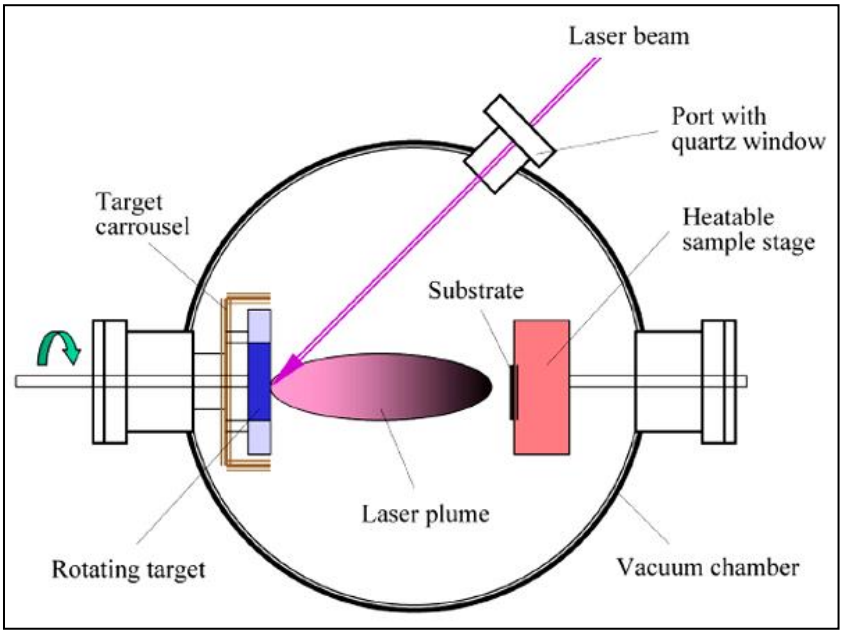

Figure 1.5: The pulsed laser deposition (PLD) method.

Another potential issue with PLD is the ejection of micron-size particles in the ablation process. This is often observed when the penetration depth of the laser pulse into the target material is large. If these particles are deposited onto the substrate, they present obvious problems in the formation of multilayer device structures.

The use of highly dense ablation targets and ablation wavelengths that are strongly absorbed by the target tends to reduce or eliminate particle formation. Mechanical techniques have been developed to reduce particle density in the event that target density and laser wavelength optimization fails to eliminate particulates [54].

The advantages of PLD are the simplicity and versatility of the experiments. By using high-power pulsed UV-lasers and a vacuum chamber, a variety of stoichiometric oxide films can be grown in a reactive oxygen background gas without the need for further processing.

I.6.3.Chemical vapor deposition (CVD)

CVD is one of the important techniques for producing thin film of semiconductor material, the chemical vapor deposition technique involves reaction of one or more gaseous species reacting on a solid surface (substrate), typically, a material in its solid form is vaporized and diluted with an organic reactant, which will assist the material's surface mobility. The chemical combination is transported to the heated surface where it decomposes,

leaving the material on the heated surface to migrate to the growing film as shown in figure 1.6. Nature of the decomposition process varies according to the composition of the volatile transporting species. The decomposition condition should be such that the reaction occurs only at or near the substrate surface and not in the gaseous state to avoid formation of the powdery deposits which may result in haziness in the films, this process requires volatile and stable precursors. The precursors usable for CVD can be categorized as halides, hydrides, metal organic compounds, alkyls, alkoxides, carbonyls, dialylimides, and diketonates, to name a few.

The chemical vapor deposition used to deposit thin film of solid material in various applications like fabrications of novel powder, fiber, preforms of ceramic composites, coatings for corrosion and wear resistance, and synthetic diamond. It is the most widely used technique in IC microfabrication for the oxide and nitride layers of the wafers.

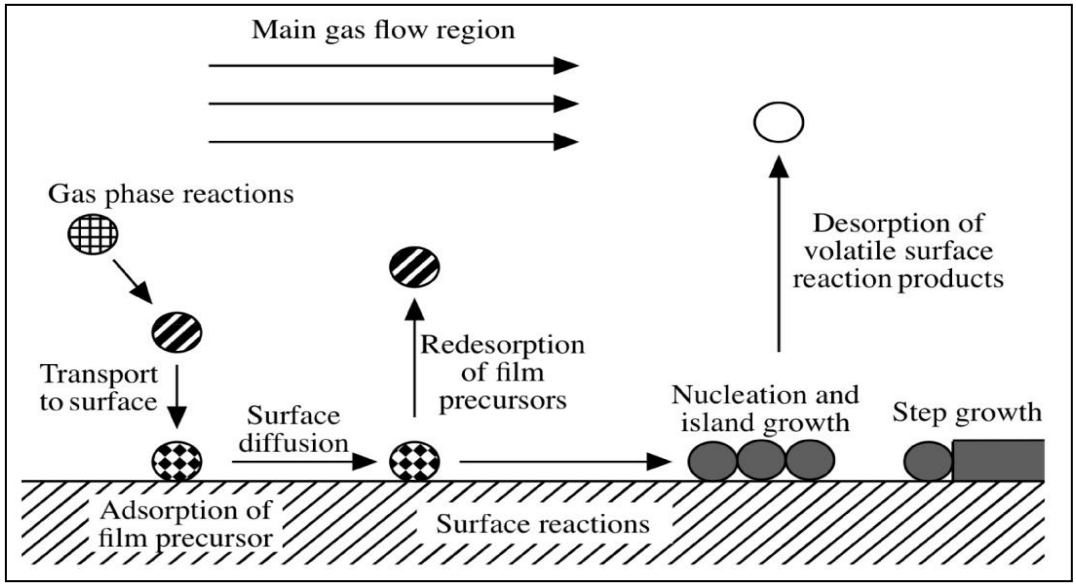

Figure 1.6: Steps of chemical vapor deposition technique [55].

I.6.4.Wet chemical Sol-gel

Including, amongst others, chemical bath techniques and Sol–Gel techniques, which are a wet chemical process that involve the use of a chemical precursor solution, The sol-gel process, as the name implies, involves the evolution of inorganic networks through the formation of a colloidal suspension (sol) and gelation of the sol to form a network in a continuous liquid phase (gel) [56].

The precursors for synthesizing these colloids consist of a metal or metalloid element surrounded by various reactive ligands. Metal alkoxides are most popular because they react readily with water. When monolithic inorganic gels were formed at low temperatures and converted to glasses without a high temperature melting process [57]. Through this process, homogeneous inorganic oxide materials with desirable properties of hardness, optical transparency, chemical durability, tailored porosity, and thermal resistance, can be produced at room temperatures, as opposed to the much higher melting temperatures required in the production of conventional inorganic glasses [57,58].

The specific uses of these sol-gel produced glasses and ceramics are derived from the various material shapes generated in the gel state, i.e., monoliths, films, fibers, and monosized powders. Many specific applications include optics, protective and porous films, optical coatings, window insulators, dielectric and electronic coatings, high temperature superconductors, reinforcement fibers, fillers, and catalysts [58].

- Dip Coating [59] : In a dip-coating process, a substrate is dipped into a liquid coating solution and then is dragging from the solution with controlling withdrawal speed as discribed in figure 1.7. Generally the thickness increases at faster dragging speed. The measurement of thickness by the equilibrium of forces at the stagnation point on the liquid surface. The thickness is primarily affected by fluid viscosity, fluid density, and surface tension.

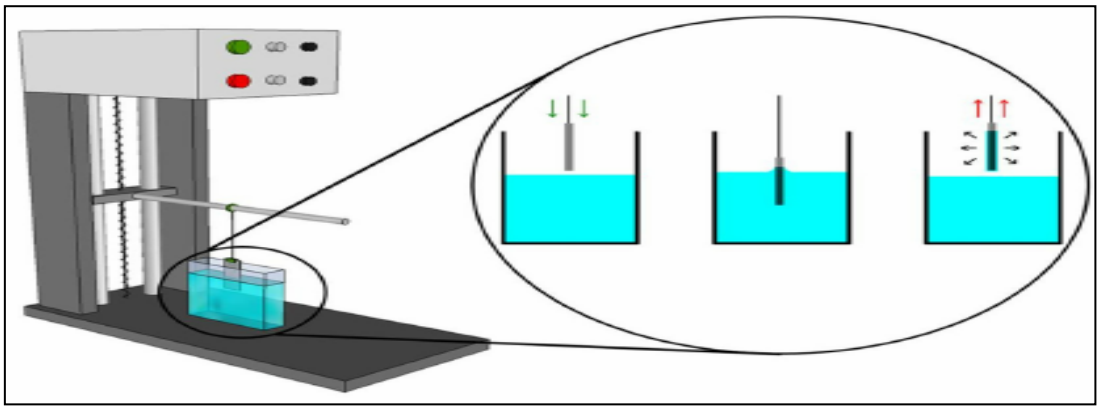

Figure 1.7: Schematic model describing the film formation during the dip-coeting process.

Therefore, a faster dragging speed pulls more fluid up onto the substrate before it has time to flow back down into the solution, should be occur. While excellent for producing high-

quality, uniform coatings, requires precise control and a clean environment. The applied coating may remain wet for several minutes until the solvent evaporates. This process can be accelerated by heated drying

- Spin Coating [60]- The precursor is dropped onto the centre of a spinning substrate which then spreads out quickly and evaporates the solvent,see figure 1.8. The Spin coating an exemplary process includes depositing a small puddle of a solution onto the center of a substrate and then spinning the substrate at high speed (typically around 3000 rpm). Centripetal acceleration will cause most of the resin to spread to, and eventually off, the edge of the substrate, leaving a thin film of material on the surface.

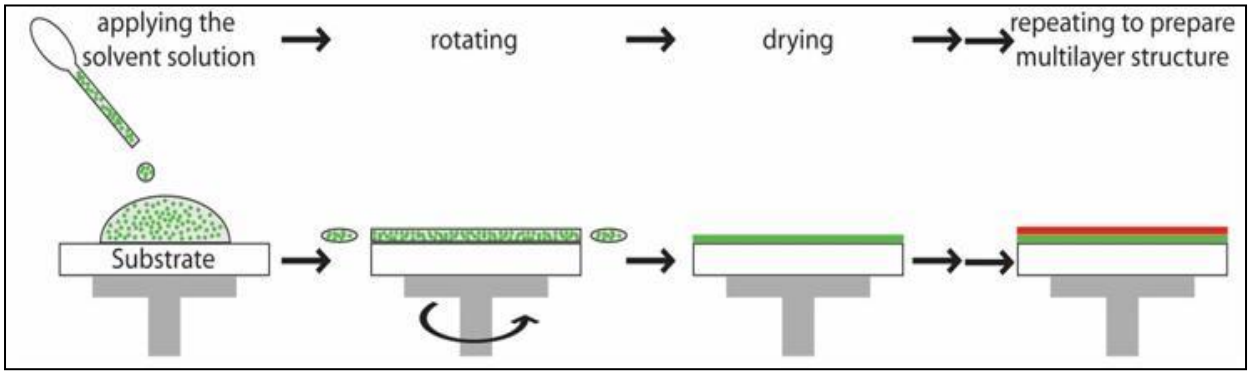

Figure 1.8: Schematic model describing the film formation during the sping-coating process.

Final film thickness and other properties will depend on the nature of the fluid material (viscosity, drying rate, percent solids, surface tension, etc.) and the parameters chosen for the spin process. Factors such as final rotation speed, acceleration, and fume exhaust affect the properties of the coated films. One of the most important factors in spin coating is repeatability, as subtle variations in the parameters that define a spin-coating process can result in drastic variations in the coated film.

I.6.5.Spray Pyrolysis

I.6.5.1.Working principle

Spray Pyrolysis (SP) This coating technique was the predecessor of the chemical vapor deposition (CVD) techniques [61]. The coating is applied at elevated temperatures by spraying droplets of liquid precursors onto hot substrates. The method is considered a modification of vapour deposition, again using a fine spray of precursor solution (generated by a spray nozzle using compressed gas) which delivers the precursor metal organic molecules to the substrate surface for thermal reaction and film formation figure 1.9 shows the schematic of spray pyrolysis process.

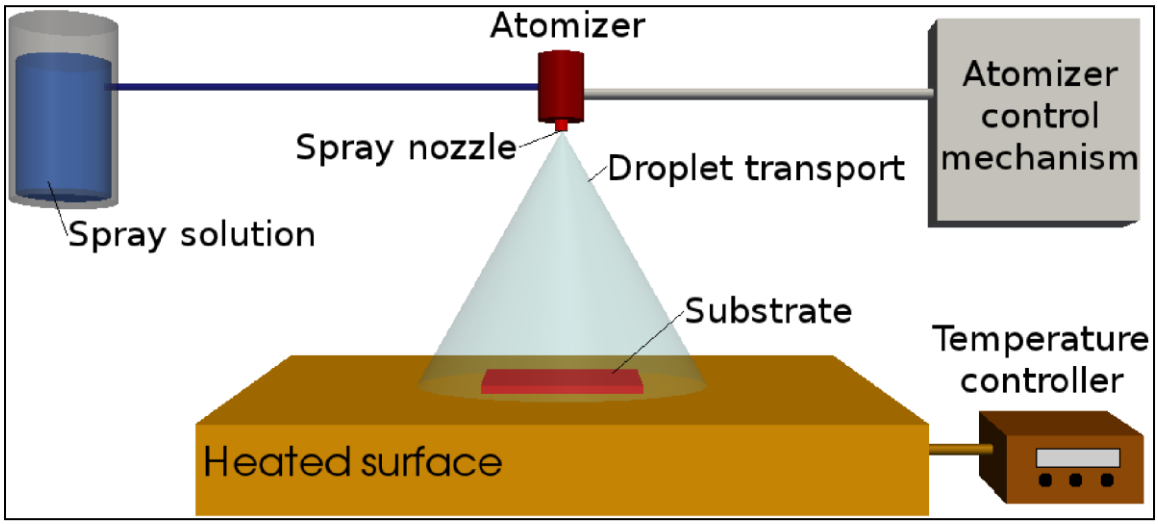

Figure 1.9: General schematic of a spray pyrolysis deposition process [62].

The droplet size depends on the process of atomization; aerosol and ultrasonic spraying produce larger and smaller initial droplets, respectively.

Spray pyrolysis is based on the pyrolytic decomposition of a metallic compound dissolved in a liquid mixture when it is sprayed onto a preheated substrate. In CSP, doping process is rather simple; just by varying the concentration of the dopant in the solution; one can vary the percentage of doping in the sample. A major drawback of this technique is that it cannot be used for the deposition of very thin films. Another shortcoming lies in the selection of substrate since it is a high temperature process. Effects of substrate temperature on the structural, electrical and optical properties of ZnO films, prepared using CSP technique had been studied [63].

The major advantages of spray pyrolysis are that the coatings are more durable than vacuum deposited coatings, the variety of precursors could be used, and the process can be employed at lower cost than CVD or vacuum deposition.

The disadvantage is that the coatings are not uniform in thickness. CVD consists of vaporizing the precursors and directing the resultant gases onto a hot substrate.

I.6.5.2.Advantages of Spray Pyrolysis Technique

The main advantages of spray pyrolysis over other similar techniques are:

- Spray pyrolysis is cost effective and can be easily performed.
- Substrates with complex geometries can be coated.
- Spray pyrolysis deposition leads to relatively uniform and high quality coatings.
- No high temperatures are required during processing (up to ~ 500 °C).
- Films deposited by spray pyrolysis are reproducible, giving it potential for mass production.

The major interest in spray pyrolysis is due to its low cost, while it is increasingly being used for some commercial processes, such as the deposition of a transparent layer on glass [64], the deposition of a SnO_2 layer for gas sensor applications [65], the deposition of a YSZ layer for solar cell applications [66], anodes for lithium-ion batteries [67], and optoelectronic devices [68].

The composition of the film can be adjusted by changing the precursor solutions. The method used for the deposition of dense films, porous films, and for powder production. Even multi-layered films can be easily prepared using this versatile technique, Spray pyrolysis has been used for several decades in the glass industry [69] and in solar cell production to deposit electrically conducting electrodes [70].

One of the major advantages of spray pyrolysis over the vapor-phase routes is the possibility of producing multicomponent particles with exact desirable stoichiometry in the final product.

I.7.Refrences

[1] J.H.Kim, A.Cho, H. Yin, D.A. Schafer, G. Mouneimne, K.J. Simpson, K.V. Nguyen, J.S. Brugge, D.J. Montell, (2011).

[2] K. Badeker, Ann Phys. (Leipzig), 22 (1907) 749.

[3] L. Castañeda, Materials Sciencesand Applications, 2 (2011) 1233–1242.

[4] T. Minami, Semicond. Sci. Technol., 20 (2005) 35-44.

[5] Y. M. Guo, L. P. Zhu, J. Jiang, Y. G. Li, L. Hu, H. B. Xu and Z. Z. Ye, J. Alloy. Compd., 602 (2014) 294-299.

[6] S. M. A. Durrani, E. E. Khawaja, A. M. Al-Shukri and M. F. Al-Kuhaili, Energ. Buildings, 36 (2004) 891-898.

[7] H. Kawazoe, N. Ueda, H. Un'no, T. Omata,H. Hosono, H. Tanoue, J. Appl. Phys, 76 (1994) 7935.

[8] M. Hiramatsu, K. Imaeda, N. Horio, and M.Nawata, J. Vac. Sci. Technol., 16 (1998) 669.

[9] H. Agura and H. Suzuki, T. Matsushita, T. Aoki, and M. Okuda, Thin Solid Films, 445 (2003) 263.

[10] E. Fortunato, D. Ginley, H. Hosono, D.C. Paine, MRS Bulletin, 32 (2007) 242–247.

[11] C. Jagadish and S. J. Pearton, Oxford: Elsevier, (2006) 589.

[12] Z. L. Wang, Journal of Physics: Condensed Matter, 16 (2004) 829–858.

[13] R.W. Whatmore. Reports on Progress in Physics, 49 (1986) 1335–1386.

[14] E. Kisi and M. M. Elcombe, Acta Crystallogr., Sect. C: Cryst. Struct, (1989) 1867.

[15] D.C. Reynolds, D.C. Look and Jogai B Solid State Commun. 99 (1996) 873.

[16] D. M. Bagnall, Y.F. Chen, Z. Zhu, T. Yao, S.Koyama, M.Y. Shen and T.Goto, Appl. Phys. Lett. 70 (1997) 2230.

[17] P.Y. Yu and M. Cardona, (Berlin: Springer), (2005).

[18] A.Mang, K. Reimann and St. R¨ubenacke, Solid State Commun. 94 (1995) 251.

[19] T. Ive, T. Ben-Yaa cov, A. Murai, H . Asamizu, C .G. Van de Walle, U.Mishra, S.P. DenBaars and J.S.Speck, Physica Status Solidic 5 (2008) 3091.

[20] D.C. Look, Mater. Sci. Eng. B, 80 (2001) 383.

[21] C. Jagadish and S. J. Pearton (ed), New York: Elsevier, (2006).

[22] M.H. Huang, S.Mao, H .Feick, H. Yan, Y.Wu, H.Kind, E.Weber, R.Russo and P.Yang Science, 292 (200) 1897.

[23] H.Cao, Y.G .Zhao, S.T.Ho, E W Seelig, Q H Wang and Chang R P H, Phys. Rev. Lett. 82 (1999) 2278.

[24] Tsukazaki A et al , Nature Mater. 4 (2005) 42.

[25] Y R. Ryu, W J. Kim and J. Cryst. Growth, 219 (2000) 419.

[26] S .Chu, M .Olmedo, Z. Yang, J. Kong and J L. Liu, Appl. Phys. Lett. 93 (2008) 181106.

[27] K. Ellmer, J. Phys., D, Appl. Phys. 33 (2000) 17.

[28] K. Ellmer, J. Phys., D, Appl. Phys. 34 (2001) 3097.

[29] D. C. Look, B. Clafin, Y. I. Alivov, S. J. Park, Phys. Stat. Sol. 201 (2004) 2203.

[30] R.C. Wang et al, Appl. Phys. Lett, 88 (2006) 23111.

[31] L. Xuet al, J. Phys. Chem. B, 110 (2006) 6637.

[32] Lee, W., et al., Appl. Phys. Lett, 85 (2004) 6167.

[33] G. Shen et al, J. Phys. Chem. B, 109 (2005) 5491.

[34] Y. S. Li et al, J. Phys. D: Appl. Phys, 37 (2004) 2274.

[35] J. J.Liu et al, Appl. Phys. Lett, 87 (2005) 172505.

[36] H. Agura et al.Thin Solid Films, 263 (2003) 445.

[37] A. Suzuki, et al.Jpn. J. Appl. Phys, 56 (1996) 35.

[38] W.J. Jeong, et al.Thin Solid Films, 180 (2006) 506–507.

[39] G.G. Valle, et al.J. Eur. Ceram. Soc, 1009 (2004) 24.

[40] S.J. Henley, et al.Surf. Coat. Technol. 271 (2004) 177–178.

[41] H. Gomez, et al.Sol. Energy Mater. Sol. Cells, 107 (2005) 87.

[42] P.M.R. Kumar, et al.Semicond. Sci. Technol, 120 (2005) 20.

[43] S.J. Jiao, et al.Appl. Phys. Lett, 031911 (2006) 88.

[44] C.-C. Lin, et al.Appl. Phys. Lett, 5040 (2004) 84.

[45] Y. Coa, et al.Appl. Phys. Lett, 251116 (2006) 88.

[46] W.A. Bryant, Journal ofMaterials Science, 12 (1977) 1285-1306.

[47] R.N. Ghoshtagore, Journal of the Electrochemical Society, 125 (1978) 110-117.

[48] T. Suntola, Thin Solid Films, 216 (1992) 84-89.

[49] R.R. Chamberlin and J.S. Skarman, Journal ofthe Electrochemical Society, 113 (1966) 86-89.

[50] C.J. Brinker, A.J. Hurd, G.C. Frye, K.J. Ward and CS. Ashley, Journal ofNon-Crystalline Solids, 121 (1990) 294-302.

[51] C.C. Chen, M.M. Nasrallah and H.U. Anderson, Journal of the Electrochemical Society, 140 (1993) 3555-3560.

[52] R. G. Sharafutdinov; S. Y. Khmel; V. G. Shchukin; M. V. Ponomarev; E. A. Baranov; A. V. Volkov; O. I. Semenova; L. I. Fedina; P. P. Dobrovolsky; B. A. Kolesov, Solar Energy Materials and Solar Cells, 89 (2005) 99-111.

[53] I. Bozovic and J. N. Eckstein, MRS Bull. 20 (1995) 32–38.

[54] E. V.Pechen, A. V.Varlashkin, S. I.Krasnosvobodtsev, B.Brunner, and K. F.RenkAppl. Phys. Lett, 66 (1995) 2292–2294.

[55] A. M. B van Mol, Ph.D. thesis, Technical University of Eindhoven, The Netherlands (ISBN 90-386-2715-7).

[56] O.Lev, et al. Analytical Chemistry, 67 (1995) 22-30.

[57] C.J. Brinker and G.W. Scherer, Academic Press, Inc.: New York, (1990).

[58] K.D. Keefer, in: Silicon Based Polymer Science: A Comprehensive Resource; eds. J.M. Zeigler and F.W.G. Fearon, ACS Advances in Chemistry Ser, 224 (1990) 227-240.

[59] M. A. Aegerter; J. Puetz; G. Gasparro; N. Al-Dahoudi, Optical Materials, 26 (2004) 155-162.

[60] G. Srinivasan; N. Gopalakrishnan; Y. S. Yu; R. Kesavamoorthy; J. Kumar, Superlattices and Microstructures, 43 (2008) 112-119.

[61] S. W. Rees, CVD of Nonmetals. VCH: Weinheim, (1996) 12-18.

[62]L. Filipovic, S. Selberherr, G.C. Mutinati, E. Brunet, S. Steinhauer, A. Köck, F. Schrank A Lett, 21 (2013) 224-24

[63] S. A. Studenikin, N. Golego and M. Cocivera, J. Appl. Phys. 83 (1998) 2104.

[64] S. Major, A. Banerjee, and K. Chopra, Thin Solid Films, 108 (1983) 333-340.

[65]G. Korotcenkov,V. Brinzari,J. Schwank,M. DiBattista,andA. Vasiliev,
Sensors and Actuators B: Chemical, 77 (2001) 244-252.

[66] D. Perednis and L. J. Gauckler, Solid State Ionics, 166 (2004) 229-239.

[67] S. H. Ng, J. Wang, D. Wexler, S. Y. Chew, and H. K. Liu. . The Journal of Physical Chemistry C, 111 (2007) 11131-11138.

[68] G. Blandenet,M. Court,andY. Lagarde, Thin Solid Films, 77 (1981) 81-90.

[69] Y. Benkhetta et al Optik 127 (2016) 3005–3008.

[70] J.E. Hill and R.R. Chamberlin, US Patent 3, 148 (1964) 084.

Chapter II

Realization and Characterization

Of Thin Films

II.1.Introduction

Spray pyrolysis usually involves atomizing a precursor solution to an aerosol, which is then directed to a heated substrate where a thin film is formed. This thin film deposition method is simple, cost-effective, and a wide choice of precursors can be used. The composition of the film can be easily controlled by the precursor solution. Both, dense and porous structures can be deposited by spray pyrolysis, even on large substrates when scaling up the equipment. Different types of atomizers such as air blast, ultrasonic, or electrostatic can be part of spray pyrolysis equipment. The technique of atomization determines the droplet size and size distribution, the rate of atomization, and the spray angle, as we mention in chapter I.

Depend on the available equipment in our laboratory of thin solid films and semicoductor of university of biskra, which is able to supply suitable conditions for synthesis via Spray Pyrolysis (SP) and further treatments of the desired product. The present work is an attempt to summarize the basic types of equipment, and conditions for obtaining of thin films for various applications, via two kinds of spray pyrolysis method which are pneumatic spray pyrolysis and ultrasonic spray pyrolysis.

.

II.2.Decomposition of precursor

Thin film deposition using spray pyrolysis can be divided into four main steps: atomization of the precursor solution, transportation of the resultant aerosol and decomposition of the precursor on the substrate. However, four types of processes that may occur during deposition are shown in Figure 2.1; in the first process, the droplet reaches the substrate and thereby the solvent evaporates leaving a precipitate which is then decomposition in the solid state.

In the second process, the solvent evaporates before the droplet reaches the surface and the precipitate stubs upon the substrate where decomposition occurs. In the third process, when the droplet approaches the substrate, the solvent vaporizes, then the solid melts and sublimes and the vapor distributes to the substrate to undergo a heterogeneous reaction. In the fourth process, at high temperatures, the solution vaporizes before it reaches the substrate and the chemical reaction occurs in the vapor phase [1].

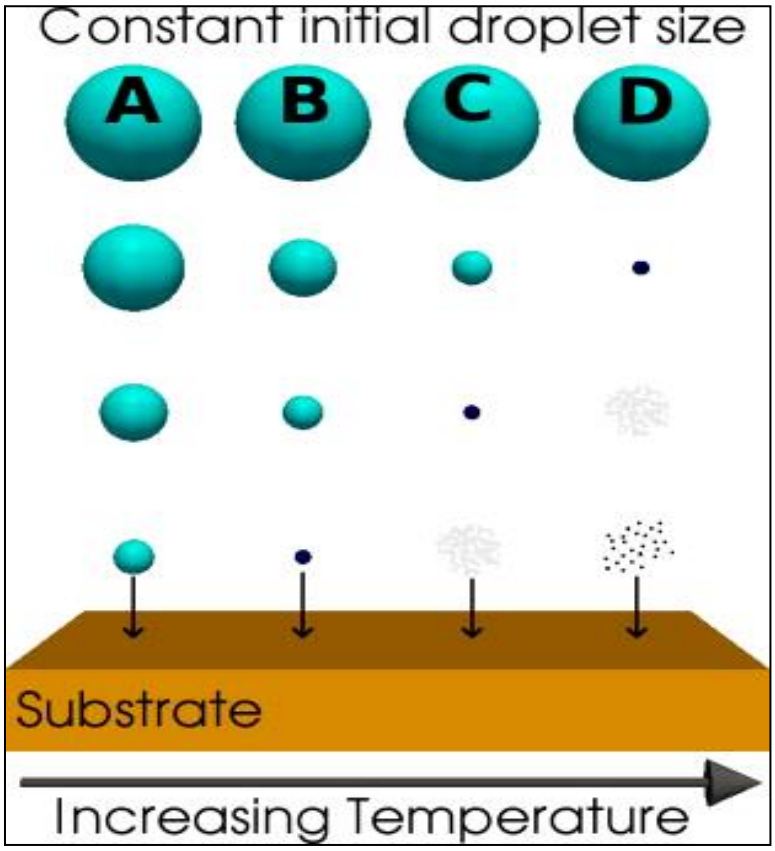

Figure 2.1: Schematic depicting different deposition processes that occur as the nozzle-to-substrate distance and deposition temperature change [2].

II.3.Spray pyrolysis system set-up

The schematic experimental set-up of our spray pyrolysis system which is built in our ((laboratory of material and physics of semiconductors and thin films)) in university of biskra, is shown below in figure 2.4, it consists of spray nozzle with two types of nozzle which are a pneumatic and ultrasonic (see figure 2.3), substrate heater, automatic temperature control unit, air compressor, pressure regulator, thermocoupl, stepper motor with controller and power supply, the heater is stainless metal block furnace electrically controlled by an automatic temperature controller unit to attain the required substrate temperature to an accuracy of ± 5 ^{0}C, the resulting temperature on the surface of the substrate is measured with a chromel-alumel thermocouple, hazardous fumes evolved during the decomposition of the precursor are driven out through an exhaut system attached to the spray pyrolysis unit, the spray nozzle in our system, having two diffrent types ultrasonic and pneumatic, the spray nozzle is fixed at an appropriate distance from the substrate for each process, in the same time the nozzle is moving toward the X and Y axis, as shown in figure 2.2 to cover the entire of the substrate, to achiave uniform diposition.

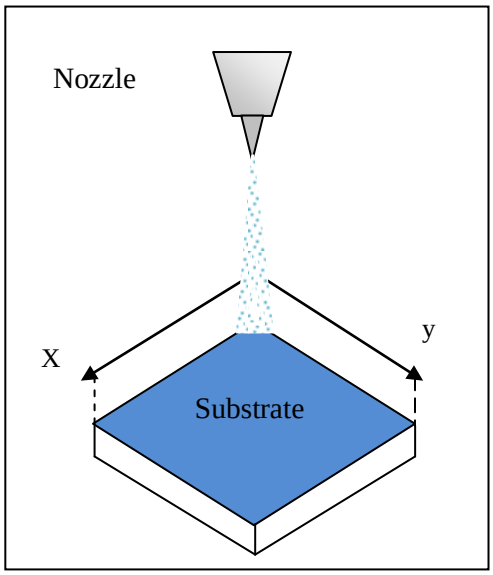

Figure 2.2: The nozzle movement toward the X and Y axis.

The X – Y movement is controlled by using a stepper motor driver, and while the spray nozzle is free the substrate is kept stationary. The precursor solution was sprayed on to the substrate in air as small droplets with a solution flow rate controlled, the processes are made closed room, i.e, around a high temperature zone where thermal decomposition and possible reaction between solutions occur, through compressed, the latest is used as carrier gas air in pneumatic case with pressure controlled.

The types of Nozzle used in this study is included two kind :

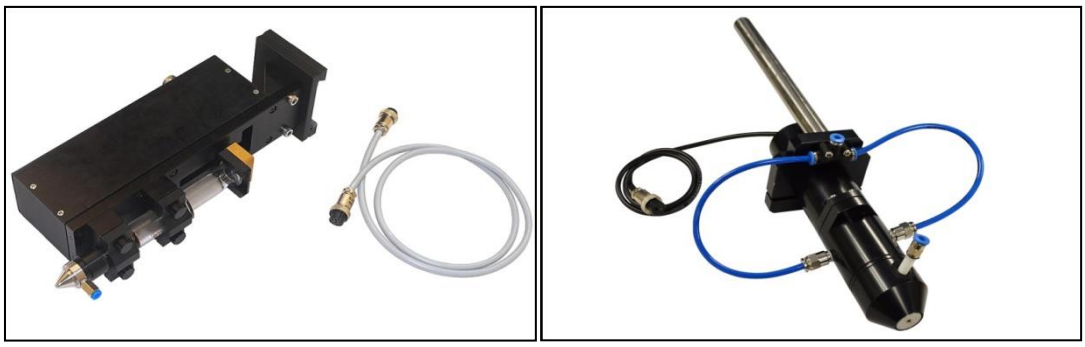

Pneumatic Nozzle Ultrasonic Nozzle

Figure 2.3: Spray nozzles with two types of pneumatic and ultrasonic.

In these processes, the precursor solution is sprayed onto a preheated substrate, each atomized droplet serves as a microreactor which is delivered by carrier gas (air) to the reaction site and undergoes solvent evaporation, decomposition and precipitations to form the final product films. The ratio of deposition temperature to solvent boiling point is found to be the most important processing parameter that determines whether a homogeneous and coherent film is obtained [3].

II.3.1.Empirical conditions

For the manufacture of thin films with different properties, and in order to custom applications, we must know the characteristics that can be changed in the approved technical, The spray pyrolysis method is an experimental process, the solution flow rate, pressure of the carrier gas (air), the substrate temperature, the properties of the precursor (doped and undoped) and percentage of the dopant in the precursor solution, in doping process is rather simple; just by varying the concentration of the dopant in the solution, one can vary the percentage of doping in the sample. A major drawback of this technique is that it cannot be used for the deposition of very thin films. Another shortcoming lies in the selection of substrate since it is a high temperature process, these parameters which mentioned befor, have different effects, and this is what we are going to study.

In the experimental study and by dividing the work into two chapters, we will see the relationship between the parameters and their effects on the thin-film structure, optical properties and electrical properties. For any deposit process, pressure, the solution flow rate, substrate temperature and the solution composition (doped, undoped), are the main parameters.

II.3.2.Empirical details

II.3.2.1.Pneumatic spray pyrolysis

ZnO films were grown on 2×2 Cm^2 glass substrates ultrasonically cleaned for five minutes also in acetone followed by deionized water for that time too, at room temperature and finally, the substrates were dried, the precursor solution were investigated using zinc chloride $ZnCl_2$ dissolved in methanol with molar concentration of 0.1 mol/l, with adding a few drops of acetic acid to the starting solution, ZnO thin films were prepared at 350 ^0C, for a deposition time of 10 min. whereas, each sample which mentioned before was located from the nozzle at 11.5 Cm, above the deposition. The x-y movement of nozzle is 30 and 5 $mm.s^{-1}$ respectively during the deposition, using pneumatic spray pyrolysis technique (HOLMARK equipment). That and in order to optime the pneumatic paramaters, we have divided the deposition process into two sections:

- **Section one**: included undoped-ZnO thin films, investigating with various values of solution flow rate from 100µl/min to 400µl/min with 100µl/min of step, at pressure 1 bar.
- **Section two**: included undoped-ZnO thin films deposited with different air pressure values from 0.5 bar to 2 bar of 0.5 step, at solution flow rate of 300 µl/min.

These parameters and their variations are reported on the following Table 2.1:

Table 2.1: Experimental conditions for pneumatic process.

Pneumatic spray pyrolysis						
Solution concentration 0.1mol/l	Pressure (Bar)	Solution flow rate ($\mu l.min^{-1}$)	Substrate temperature (^{o}C)	Deposition time (min)	Movement X – Y ($mm.s^{-1}$)	Distance Nozzle-substrate (Cm)
Section one	1	100	350	10	30 - 5	11.5
	1	200				
	1	300				
	1	400				
Section two	0.5	300				
	1	300				
	1.5	300				
	2	300				

II.3.2.2.Ultrasonic spray pyrolysis

In this technique, we investigate undoped ZnO and ZnO doped thin films by ultrasonic spray pyrolysis, and to reveal the effect of substrate temperature and the dopant, on Zinc Oxide thin films properties, we divided our work into two parts :

In the first one we have an undoped ZnO thin film, which basically for appearing the effect of substrate temperature and the sconde one is for studying the effect of fluorine and aluminum as dopants on Zinc oxide thin films.

- **Part one:** In this study and for investigating in the effect of substrate temperature on undoped ZnO thin films properties, the ZnO solution was prepared by dissolving 0.1mol/l of Zn $(CH_3COO)_2$, $2H_2O$ in the solvent containing equal volumes absolute ethanol solution (99.995%) purity, then we have added drops of mono ethanolamine solution as a stabilizer, the mixture solution was stirred at 70 ^{o}C for 2 hours to yield a clear and transparent solution.

The resulting solutions were sprayed on the heated glass substrates by ultrasonic spray pyrolysis system, which transforms the liquid to a stream formed with uniform and fine droplets of 35µm average diameter (given by the manufacturer) with solution flow rate 0,5

ml/min . The deposition was performed at different substrate temperatures of 250, 300, 350, 400, 450 and 500 ^{o}C with 10 min of deposition time. Whole of experimentale factors are shown the following table:

Table 2.2: Experimental conditions for undoped ZnO thin films.

Ultrasonic spray pyrolysis method					
Solution concentration 0.1 mol/l	Solution flow rate ($ml.min^{-1}$)	Substrate temperature (^{o}C)	Deposition time (min)	Speed movement X – Y ($mm.s^{-1}$)	Distance Nozzle-substrate (Cm)
	0,5	250	10	30 – 5	4
	0,5	300	10	30 – 5	4
	0,5	350	10	30 – 5	4
	0,5	400	10	30 – 5	4
	0,5	450	10	30 – 5	4
	0,5	500	10	30 – 5	4

- **Part two :** In the second section of studying and in order to know the effect of two types of dopants, on zinc oxide thin films, which are aluminum and fluorine, on ZnO thin films properties. To achieve our doped ZnO thin films, aluminum chloride (Al Cl_3) and zinc acetate Zn $(CH_3COO)_2$ $2H_2O$, were used as the precursor for AZO deposition, also ammonium floride (NH_4F) with zinc acetate were used as precursor for FZO deposition. Both of deposition precursors were investigated by dissolving in methanol with a few droplets of acetic acid as a stabilizing agent [4].

The concentration of the solution precursor is 0.1 mol/l, to obtain the optimum deposition rate and material quality.

Also, the doping ratio was varied from 0 (undoped ZnO) to 5% for FZO thin films and to 8% for AZO thin films, by altering the atomic percent of aluminum and fluorine relative to zinc for each diposition. The zinc oxide thin films was deposited on clean 2×2 Cm^2 soda lime glass substrates heated at 350 ^{0}C for AZO thin films, and at 420 ^{0}C for FZO thin films, with solution flow rate 0,5 ml/min in both dipositions the glass substrates were ultrasonically

cleaned, and stationary at fixed distance during each deposite from the ultrasonic nozzle, the latest is moveing towards x and y axis for speed 30 and 5 $mm.s^{-1}$ respectively during the deposition processes.

Table 2.3: Experimental conditions for ZnO doped with fluorine and aluminum.

Ultrasonic spray pyrolysis method							
Solution concentration 0.1 mol/l	Dopant Type	Doping percentage (at%)	Distance Nozzle-substrate (Cm)	Substrate temperature (^{o}C)	Deposition time (min)	Speed movement X – Y ($mm.s^{-1}$)	Solution flow rate ($ml.min^{-1}$)
	Aluminum chloride ($Al Cl_3$)	0	5	350	10	30 – 5	0.5
		1	5	350			
		2	5	350			
		3	5	350			
		4	5	350			
		5	5	350			
		6	5	350			
		7	5	350			
		8	5	350			
	Ammonium fluorine (NH_4F)	0	9	420			
		1	9	420			
		2	9	420			
		3	9	420			
		4	9	420			
		5	9	420			

In these techniques, effects of solution flow rate and air pressure, substrate temperature and dopant on the structural, optical properties and electrical of ZnO films, prepared using Chemical spray pyrolysis technique had been studied.

II.4.Characterization methods

This section aims to introduce the techniques by which deposited thin films were analysed. Further experimental details will be given in this Chapter. The two methods of film characterisation most widely used were, scanning electron microscopy and X-ray diffraction spectroscopy. A large proportion of films were also examined by UV-VIS spectroscopy, Hall effect, and four point probe for electrical measurements.

II.4.1.Microstructural and Phase Characterization

II.4.1.1.Scanning electron microscope SEM

This method is commonly used to characterise thin films, since inspection of SEM micrographs provides valuable information on the topology of the diamond films. Generally two views of the film are examined:

- Top View: gives an indication of the surface crystallinity (and therefore quality) of the diamond film.
- Cross-section: used to measure the thickness (and therefore growth rate) of the thin films.

The morphology of the films were studied using, scanning electron microscopy (SEM), this technique is useful for monitoring the surfaces with grain size above about 10 nm, Electrons have very short wavelengths, the resolution of a scanning electron microscope can be ~ 0.1 nm. In electron microscopy magnetic fields are used to focus the electron beam, but in an optical microscope lenses are used to focus the light. The Figure 2.5 shows how a SEM works, in scanning electron microscopy; the substrate is analyzed using a finely focused electron beam [5].

The primary reflected electron beam and the low energy secondary electrons which are emitted by the sample because of the initial electron beam are the detected, as shown in figure 2.4.

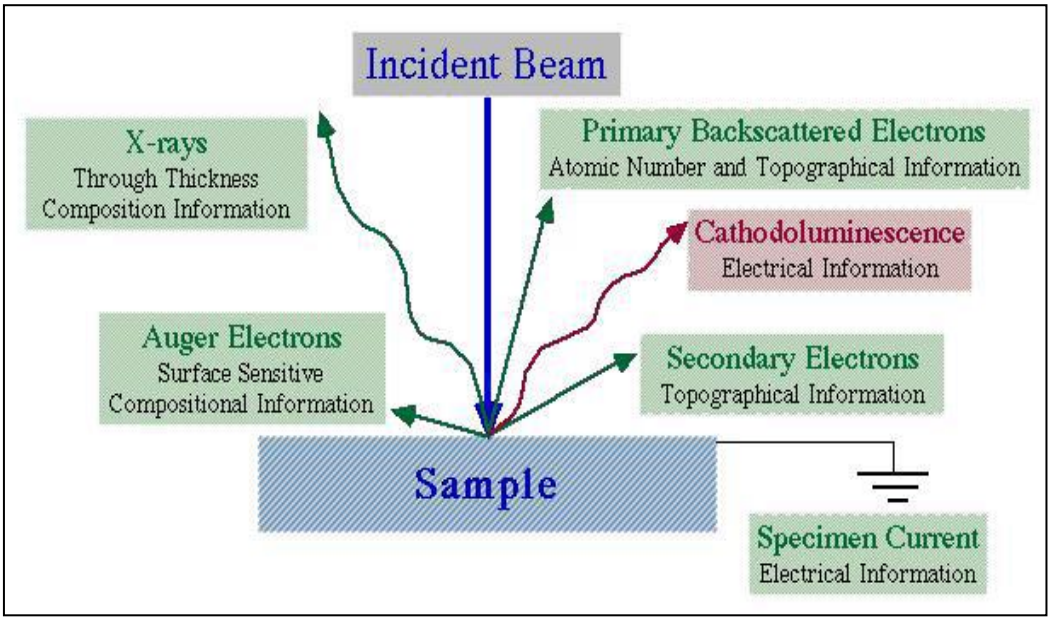

Figure 2.4: SEM setup, Electron/Specimen interactions. When electron beam strikes the sample, both phonon and electron signals are emitted [5].

After that it maps the sample topography is mapped according to those detected beams (as shown in figure 2.5) from Samples for the traditional scanning electron microscopy should be conductive.

Furthermore charging can occur on the substrate and can be causes a reduce in the intensity of electrons thereby the surface resolution. For getting an image of sample with high resolution, there should be more backscattered electrons and secondary electrons near the surface. By this manner the morphology of the surface, crystal size, surface defects... become clear [6].

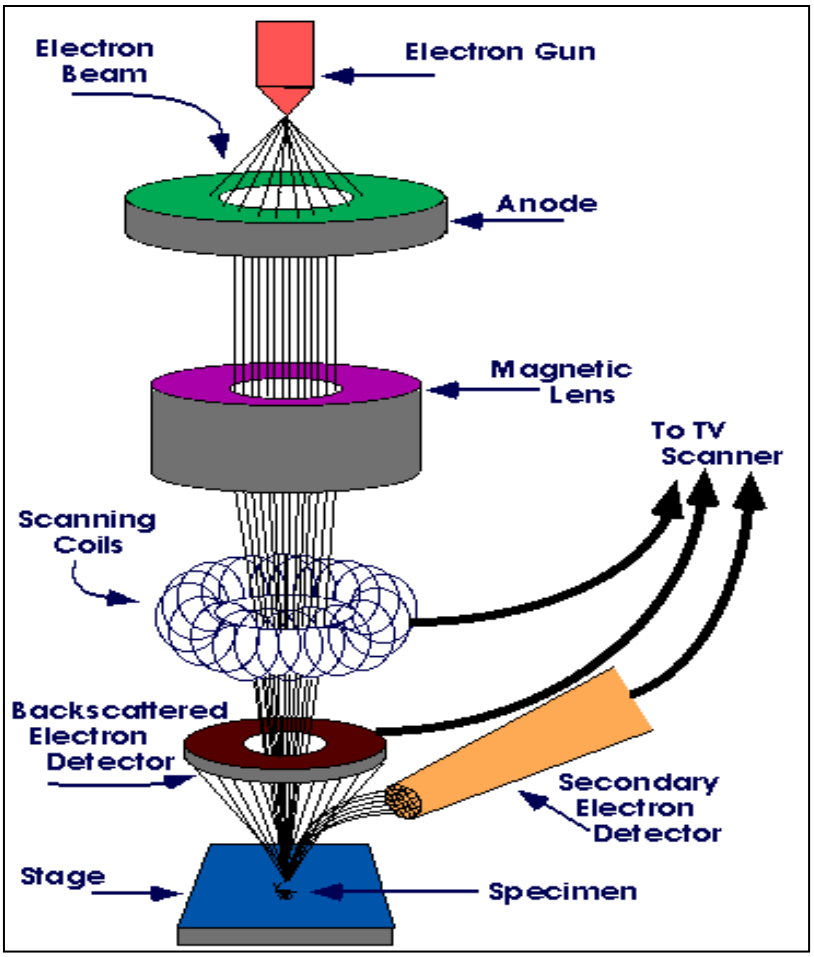

Figure 2.5: Shematic of Scanning electron mictoscope [7].

II.4.1.2.Energy dispersive X ray-spectroscopy

Energy Dispersive X-ray Spectroscopy (EDS) is an analytical capability that can be coupled with several applications including Scanning Electron Microscopy, Transmission Electron Microscopy (TEM) and Scanning Transmission Electron Microscopy.

EDS makes use of the X-ray spectrum emitted by a solid sample bombarded with a focused beam of electrons to obtain a localized chemical analysis, all elements atomic number can be detected in principle. Figure 2.6 shows e.g. for EDS equipment.

Figure 2.6: Exemple of energy despersive X-ray spectroscopy.

Accuracy of EDS spectrum can be affected by various factors. Many elements will have overlapping peaks (e.g., Ti K_β and V K_α, Mn K_β and Fe K_α), see figure 2.7; the accuracy of the spectrum can also be affected by the nature of the sample. X-rays can be generated by any atom in the sample that is sufficiently excited by the incoming beam. These X-rays are emitted in any direction, and so they may not all escape the sample. The likelihood of an X-ray escaping the specimen, and thus being available to detect and measure depends on the energy of the X-ray and the amount and density of material it has to pass through. This can result in reduced accuracy in inhomogeneous and rough samples.

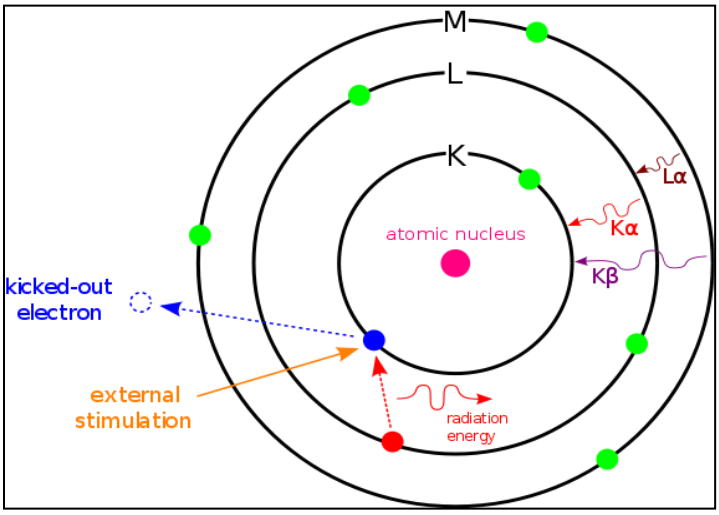

Figure 2.7: X-rays generation by the incoming beam and their emitting direction .

Energy Dispersive X-ray Spectroscopy can provide elemental analysis on areas as small as nanometers in diameter. The impact ofthe electron beam on the sample produces X-rays that are characteristic of the elements present on the sample. EDS Analysis can be used to determine the elemental composition of individual points or to map out the lateral distribution of elements from the imaged area.

II.4.1.3.X-ray diffraction

X-ray diffraction equipment that we used is shown in figure 2.8, X rays are a radiation source with wavelengths which interact with crystals containing symmetrical arrays of atoms within rows or planes to form constructive and destructive interference, i.e. diffraction results. This occurs when X-rays of a specified frequency hit an atom, leading to an interaction with its electrons causing them to vibrate with the same frequency as the incident X-ray beam. This results in the vibrated electron radiating the X-ray with no change in its frequency, in all directions as shown in figure 2.9.

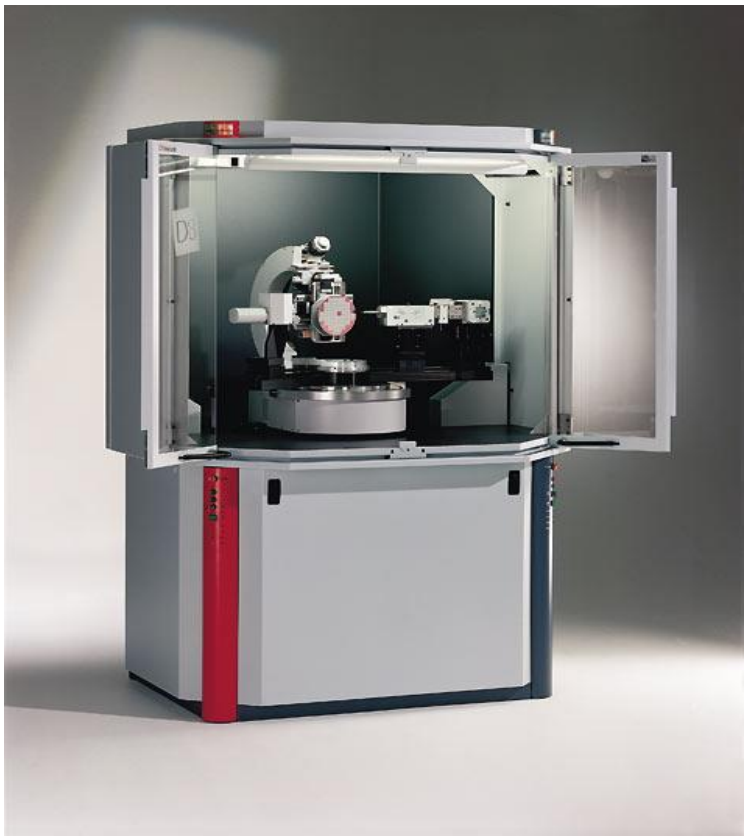

Figure 2.8: X-ray diffraction equipment.

Diffraction occurs within favourable orientated planes of atoms according to Bragg's law [8]:

$$n\lambda = 2d \sin\theta \qquad (2.2)$$

Where d is the vertical spacing between planes of atoms, λ is the wavelength of the source, n is an integer and θ is the angle of the incident radiation.

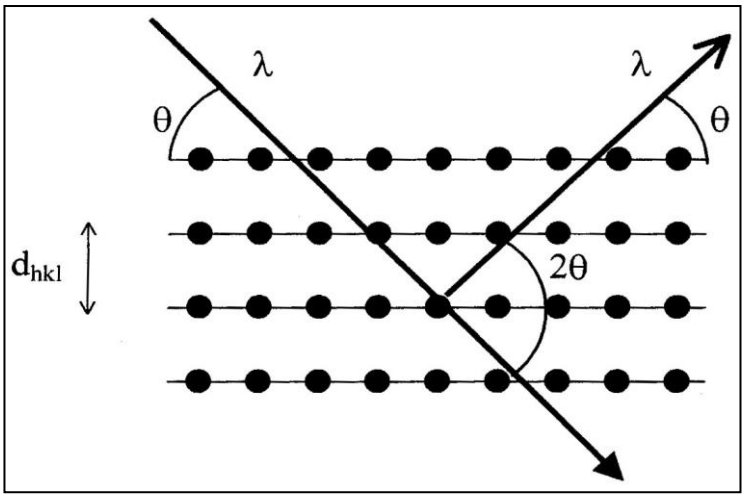

Figure 2.9 Interaction of x-rays with planes of atoms.

Using monochromatic Cu-Kα of wavelength 1.54 Å, diffraction patterns for each sample were measured by X-ray diffraction. A tube current of 40 mA was utilized, with a tube voltage of 40 kV. Rocking curve of each sample was obtained from the 2θ scan (2θ =20-100˚) with scan step size of 0.02˚ using a Philips Xpert set for 2θ scan.

The average sizes of crystallites (D) were calculated from the full width at half maximum (FWHM) of the diffraction peaks from the (002) plane of the films with the help of Scherrer formula [9].

$$D = \frac{0.94\ \lambda}{\beta \cos\theta} \qquad (2.3)$$

Where D is the crystallite size, λ is the wavelength of X-ray (λ= 1.5406 A˚), β is the full width at half-maximum (FWHM), and θ is the half diffraction angle of the centroid of the peak, as shown in figure 2.10.

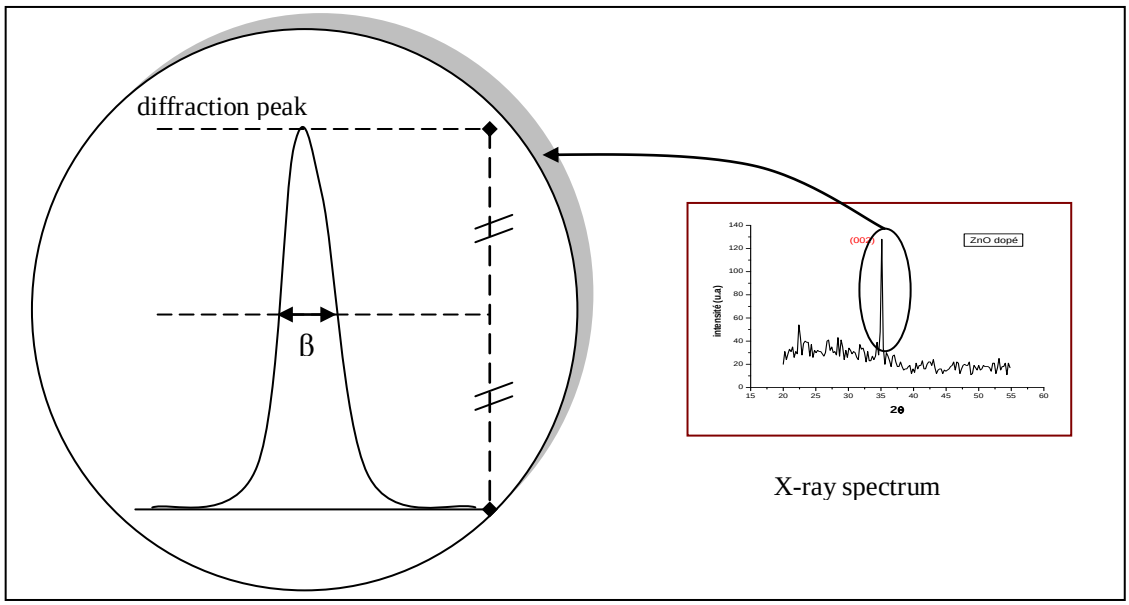

Figure 2.10: The exraction of the full width at half maximum (β) from X-ray diffraction peak.

II.4.2.Thickness measurements

II.4.2.1. Measurement by scanning electron microscopy

Indeed, knowledge of thin film thickness in semiconductores is very useful. That because provide us some informations about the structural and optical properties. In this step, the thickness was determined from scaning electron microscopy image, which is used to calculate the thickness with computer assisted by a visiometer programme, which is help to select the scale of SEM image for measureing the thickness by visiometer Ruler, by the latter we take the average of thickess measurements at different places from the films, in order to find an accuracy values, the following figure 2.11 shows the manner of thickness measurement:

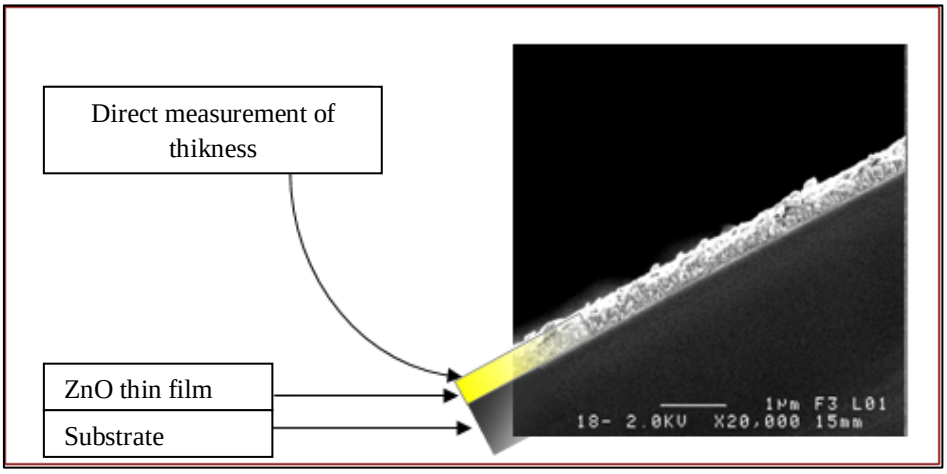

Figure 2.11: The method of thickness measurement by SEM.

II.4.2.2. Optical interference

In this method, the ditermination of thickness, is by using the optical curves that became so easy when our thin films have an uniform surface, However, the thin films with thickness (D) which has a refraction index n, where the air index is $n_0 = 1$, and the glass substrate with thickness so bigger than D and with refraction index (s) and absorption coefficient ($\alpha_s = 0$), the figure 2.12 shows form apears how does the optical radiation pass the sample:

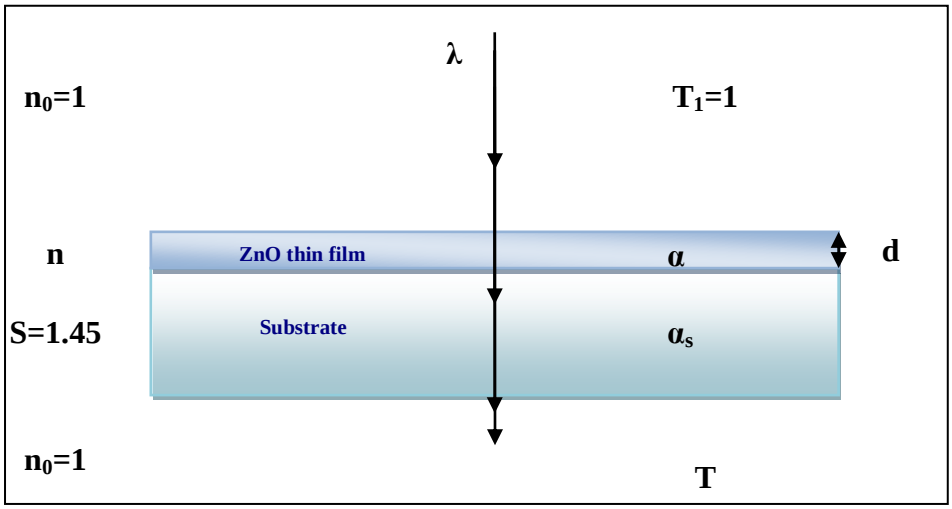

Figure 2.12: Appearing form of radiation pass through the sample.

As we see in the following figure 2.13, T is the transmission coefficient, α is the absorption coefficient of the film, λ is the wavelength of the incident light.

N_1 and n_2 are the refractive index of the layer for two adjacent maxima, T_{M1} and T_{M2}, corresponding to the wavelengths λ_1 and λ_2, the minimum transmission and T_m which lies between the two.

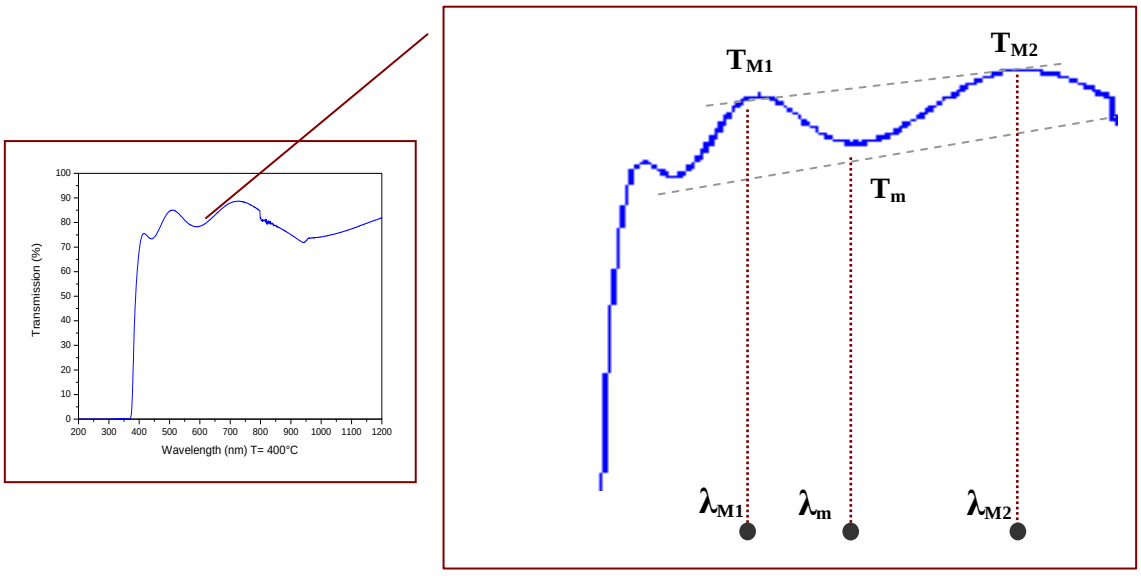

Figure 2.13: The ditermination of thickness using Optical interference curves.

From the curve, the thickness is given by [10]:

$$d = \lambda_1.\lambda_2 / 2(\lambda_1.n_2 - \lambda_2.n_1) \quad (2.4)$$

Where the n_1 and n_2 , which are corresponding to the wavelengths λ_1 and λ_2 , are determined by following relation :

$$n_{1,2} = \left(N_{1,2} + (N_{1,2}{}^2 - S^2)^{1/2}\right)^{1/2} \quad (2.5)$$

N_1 and N_2 are calculated by relation :

$$N1,2 = 2S.\frac{(T_M - T_m)}{T_M.T_m} + \frac{S^2 + 1}{2} \quad (2.6)$$

II.4.2.3.Weight difference method

In this method the film thickness was calculated using following the steps, the first : measure mass of the film before and after deposition process. The second : the difference will give the mass of the film (m) , the area of the film (A) and density (d) of the film material. By using following relation we can find out thickness (t): t = m/Ad , the estimated thickness will be not be accurate as density of the material in bulk and thin film is different.

II.4.2.4. Profilometry

For films thickness measurements, above to the deposition process a platinum strip was placed across the centre of a substrate (figure 2.14).

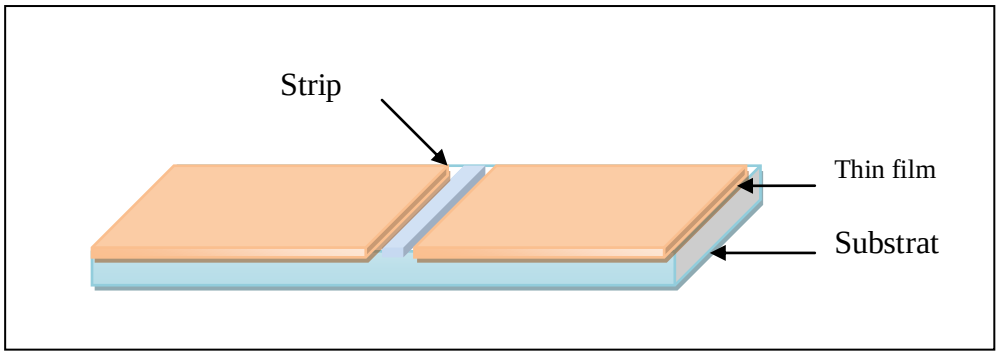

Figure 2.14: Schematic representation of the thickness monitor.

The platinum strip was removed, leaving a step in the film. The step height gives a measure of the thinckness of the films, determined using a profilometer. The profilometer consists of a diamond tip that travels across the sample along its length, and vertical downward movement of the tip at the step gives a measure of the step height which represents

the thickness of thin film. The sensitivity of the profilometer was approximately10 nm (figure 2.15).

Figure 2.15: Dektak XT stylus profiler (Bruker).

II.4.3.Stress measurement

There are intrinsic and extrinsic stresses in a thin film. Intrinsic stress comes from defects such as dislocations in the film. The origin of extrinsic stress in a thin film comes mainly from adhesion to its substrate. The differential thermal extension between the film and its substrate, and chemical reaction with its substrate when the intermitallic compound formed is coherent to the film, can be introduced extrinsic Stress in a thin film. It has also been suggested that the elimination of grain boundaries and hence the reduction of the excess volume in the grain boundaries will induce stress in the film when it is obliged by the substrate, that may be causes.

The stresses which are resulting by the deflection or curvature that the film induces to the substrate can be measured by a Profilometer.

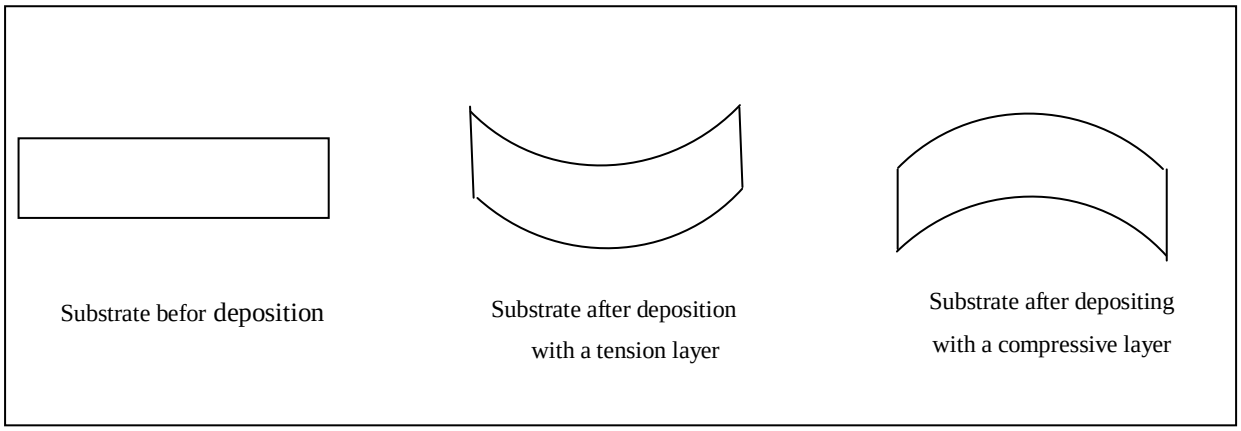

Figure 2.16: Representation of the deformation of the substrate and films due to the deposition of a thin film under stress, and associated conventions [11].

This measurement has to be before the stress inducing process and after the process to find the change in curvature due to the stress (see figure 2.16).

The calculation of the mean film stress C_{film} is based on the biaxial strain model. The strain e_{zz} in the *C*-axis, i.e., perpendicular to the substrate surface (our case), the following formula is used, which is valid for a hexagonal lattice [12]:

$$\sigma_{film} = \left(2C_{13} - \frac{\left((C_{11}+C_{12})\times C_{33}^{film}\right)}{C_{13}}\right) \times e_{zz} \qquad (2.7)$$

With

$C_{33}^{film} = \frac{0.99\times C_{33}}{(1-e_{zz})^4}$ [13], $e_{zz} = \frac{C_{film}-C_{bulk}}{C_{bulk}}$ and C_{11} = 209.7 GPa, C_{12} = 121.1 GPa, C_{13} =105.1 GPa, and C_{33} = 210.9 GPa are the elastic stiffness constants of the ZnO [14].

With C_{bulk} and C_{film} are the constants of the strain-free bulk ZnO and the lattice constant of ZnO film, respectively.

II.4.3.Optical transmittance

Optical transmission measurement of the undoped and doped ZnO on glass substrates were carried out using a UV-VIS (UV-3101 PC -SHIMADZU) spectrophotometer (see figure 2.17). Ultraviolet and visible light can cause electronic transitions.

When a molecule absorbs energy, it excites an electron into a higher empty orbital. Therefore energy absorbance can be plotted versus the wavelength to obtain a UV-Visible spectrum. Both the shape of the peak and the wavelength of the maximum absorbance (λ max) give information about the structure of the sample. UV light has a wavelength of 200~400 nm and visible light has wavelengths of 400~800 nm. Also the optical band gap can also be ascertained from the spectra graph. The wavelength was varied between 300-1000 nm at 0.5 nm intervals.

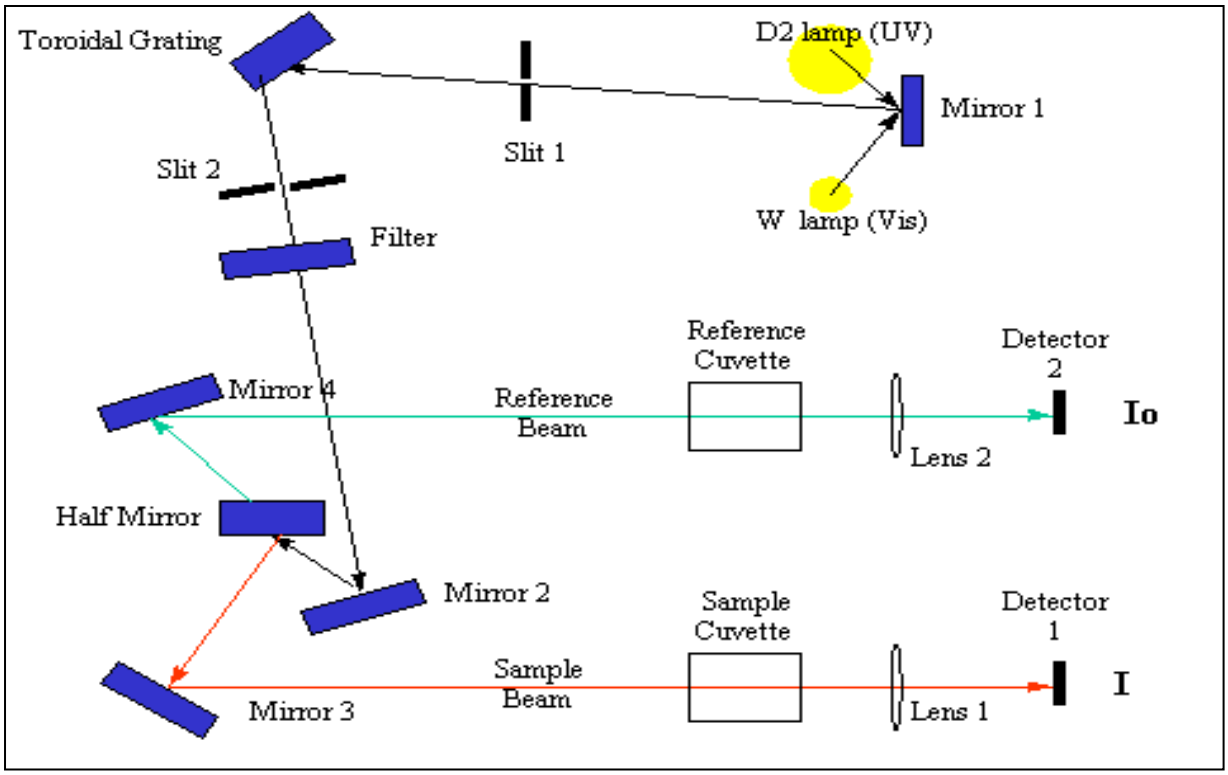

Figure 2.17: Principle spectrophotometer UV-VIS.

In the past, the determination of the optical band gap (E_g) was often necessary to develop the electronic band structure of a thin-film material. However, using extrapolation methods, the E_g values of thin films can be determined from the absorption edge for direct interband transition. The absorption coefficient α was calculated using Lambert's law as follows:

$$\alpha = ln\ (1/T)/d \qquad (2.8)$$

Where T and d are the thin film's transmittance ratio and thickness. The absorption has a maximum at a high energy and decreases with optical energy in a manner similar to the absorption edge of semiconductors. Assuming that transition becomes constant at the absorption edge, the absorption coefficient α for simple parabolic scheme can be ascribed as a function of incident photon energy as [15].

$$\alpha h\nu \propto \left(h\nu - E_g\right)^n \qquad (2.9)$$

Where n is a constant, $n = 1/2$ is the allowed direct transition and $n = 2$ is the allowed indirect transition, $h\nu$ is the photon energy, and E_g is the optical band gap. Figure 2.18 shows

the typical $(\alpha hv)^2$ versus hv plots of the AZO thin films at 3at% of aliminum concentration. the linear dependence of $(\alpha hv)^2$ on hv indicates that the doped ZnO thin films are direct transition type semiconductor.

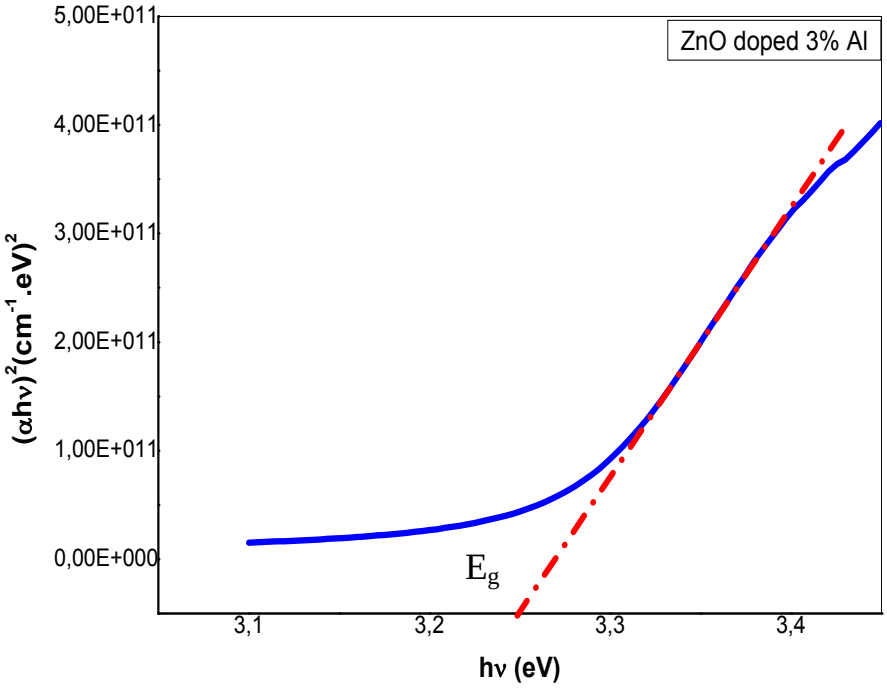

Figure 2.18: The energy gap by extrapolation from the variation $(\alpha h\nu)^2$ depending on $(h\nu)$ for ZnO thin film.

II.4.4.Electrical characterization techniques

II.4.4.1.Four probes technique

For electrical resistance measurement for thin films, the four -probe method is the most extensively used in thin films. This technique forces a fixed current through the sample, using two outer probes as shown in the figure, and measures the resulting voltage between the two inner probes.

Method is used when the specimen is in parellelopiped form of a thin wafer, such as a thin semiconductor material deposited on a glass substrate. The sample is millimeter in size and having a thickness (w). At similar distance (S) between of four probes arranged linearly in a straight line.

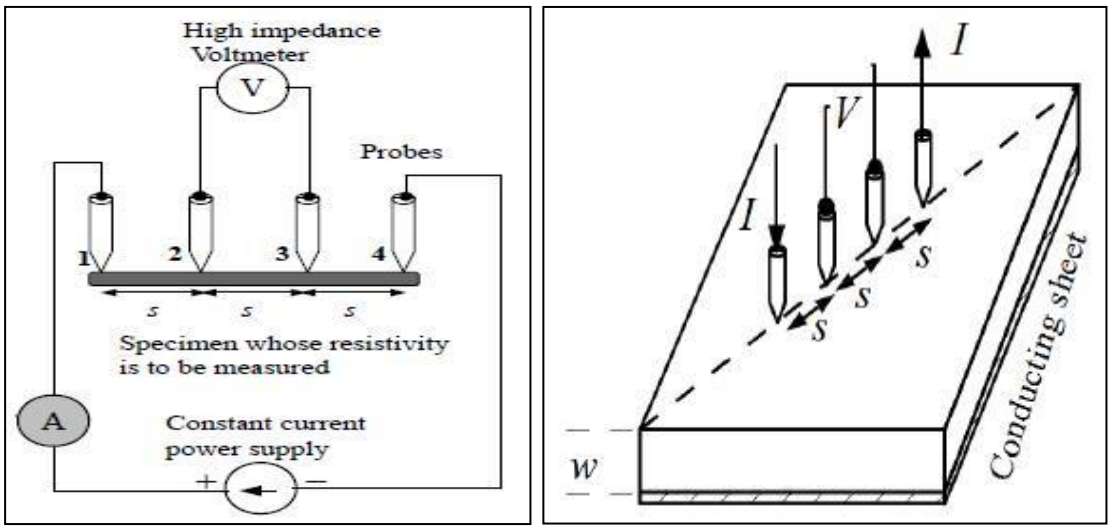

Figure 2.19: The arrangements of four probes that measure voltage (V) and supply current (A) to the surface of the crystal.

The advantage of such an arrangement over two probe experiments is that the effect of any contact resistance between the sample and probes is cancelled out. As a result of the electrical contacts being made to the surface of the film, such measurements are prone to give results more representative of the surface, rather than the bulk of the sample [16]. When this technique is applied to polycrystalline films as the surface electrical conduction is controlled by factors, there are particular problems, such as surface termination and grain boundary content, which can vary from film to film.

However, the four brope technique does give an impression of how the electrical properties of films change with deposition conditions.

- At a constant temperature, the resistance, R of a conductor is proportional to its length L and inversely proportional to its area of cross section A [16].

$$R = \rho \frac{L}{A} \qquad (2.10)$$

Where ρ is the resistivity of the conductor and its unit is ohmmeter.

If the side boundaries are adequately far from the probes, the die may be considered to be identical to a slice [17].

For this case of a slice of thickness w and the resistivity is given as

$$\rho = \frac{\rho_0}{f\left(\frac{w}{s}\right)} \qquad (2.11)$$

Where f(w/S) is a divisor for computing resistivity which depends on the value of w and S if the size of the metal tip is infinitesimal and sample thickness is bigger than the distance between the probes, according the following relation.

$$\rho_0 = \frac{V}{I} \times 2\pi S \qquad (2.12)$$

Where V is the potential difference between inner probes in volts, I is the Current through the outer pair of probes in ampere, S is the Spacing between the probes in meter.

- At temperature varied the resistivity and its dependence with Temperature of semiconductors, rises exponentially on decreasing the temperature. Where, the electrical conductivity is the whole of the conductivities of the valence band (E_v) and conduction band (E_c) carriers [18]. Resistivity is the reciprocal of conductivity and its temperature dependence is given by:

$$\rho = A\ exp\left(\frac{E_g}{2KT}\right) \qquad (2.13)$$

Where Eg is the band gap of the material, T is the Temperature in kelvin, K is the Boltzmann constant, K =8,6.10^{-5} eV/K.

II.4.4.2.Two probes technique

For a long parellelopiped shaped sample of uniform cross-section, the resistivity ρ can be measuring voltage drop across the sample due to passage of known (constant) current through the sample, as shown in figure 2.20 the generator E supplies current in through probe 1 and out through probe 2.

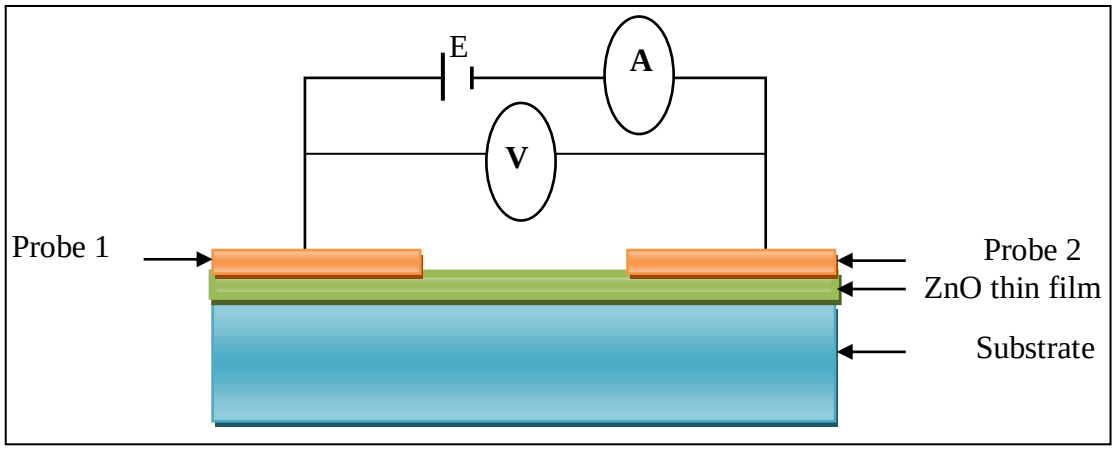

Figure 2.20: Two probes technique.

Let the current in the specimen is I (ampere). It is measured by the ammeter A.the potential difference between the two contacts (probe 1 and probe 2) at the ends of the sample is V (volt). It is measured by the Voltmeter V. let L is length of the specimen between the two probes and S its area of cross-section, then, the resistivity of the specimen is:

$$\rho = \frac{V\,S}{I\,L} \qquad (2.14)$$

II.4.5.Hall measurement

Hall effect measurements are important to semiconductor material characterization The designed automatic measuring system can be used to determine several material parameters: Hall coefficient (R_H), type (n or p), carrier concentration (n), the Hall voltage (V_H) and the conductivity are all extracted from the Hall voltage measurement. In order to obtained carrier mobility (μ) it is needful to measure also the resistivity of the sample (ρ). Due to the required contact node arrangement shown in Figure 2.21.a, a contact configuration gives current and voltage perpendicular to each other.

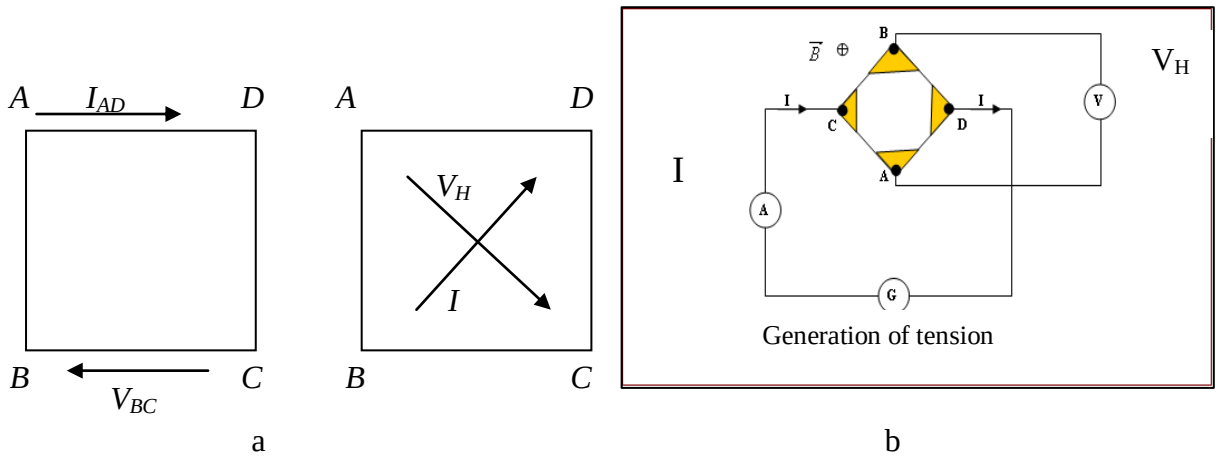

Figure 2.21: a-contact node arrangement, b-schemat shows hall volage measurement,

The van der Pauw method has been extensively used, to calculate the sample resistivity in the Hall measurement apparatus, the Hall voltage can be measured using the configurations shown in figure 2.21.b.

For ideal square symmetry samples the measured voltage at zero magnetic field should be 0 independently of the used current [19,20].

For Hall effect measurements, a voltage is applied between the contacts placed at diagonally opposite corners and the current I flowing between them is measured.

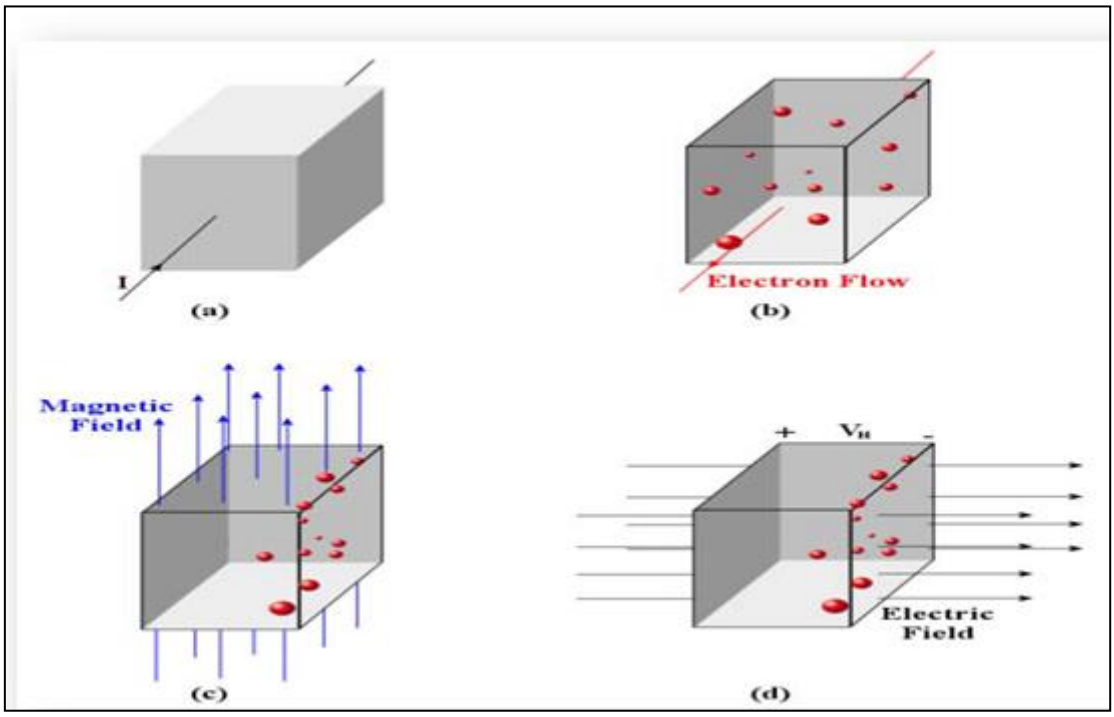

Figure 2.22 : The Hall effect (a) - a current flowing through a piece of semiconductor material, (b) - the electrons flowing due to the current, (c) - the electrons accumulating at one edge due to the magnetic field, and (d) - the resulting electric field and Hall voltage VH.

In addition, a magnetic field B is applied in the direction perpendicular to the sample and the change in Hall voltage V_H between the contacts in opposite corners is measured. Resistivity ρ, carrier density n, and mobility μ are calculated from the measured values, applied magnetic field B and the film thickness d of the measured sample [21]. The Hall effect systeme is shown in figure 2.23.

From the Hall voltage measurements it is possible to determine Hall coefficient using equation :

$$R_H = \frac{V_H \ d}{I \ B} \qquad (15)$$

Also we can specify the type of semiconductor (n or p) by the sign of the ($B \cdot R_H$),

where:

B . $R_H < 0$.....we have P-type semiconductor

B . $R_H > 0$.....we have N-type semiconductor

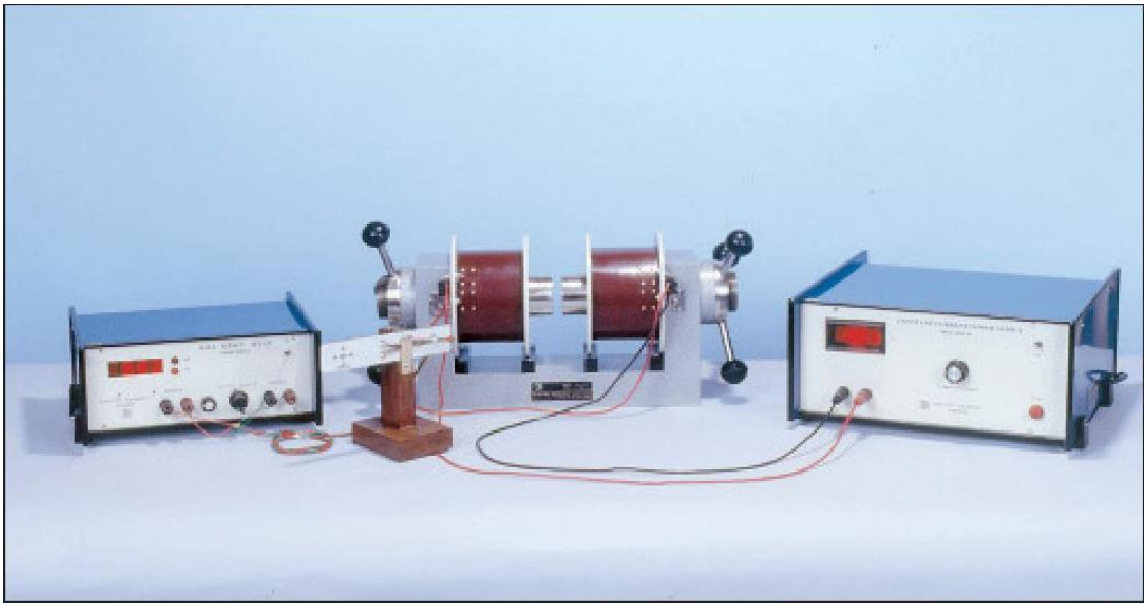

Figure2.23: The hall effect system.

And consequently carrier concentration can be determined.

$$n = \frac{1}{R_H q} \qquad (16)$$

Where q is the elementary charge. Finally, Hall coefficient and resistivity are used to determine hall mobility.

$$\mu = \frac{R_H}{\rho} \qquad (17)$$

For getting a well accuracy of obtained parameters it is necessary to ensure some basic conditions during the measurement. The most crucial one is to have good ohmic contacts.

Very important is also to ensure negligible heating of the sample during the measurements, sensitive current measurement, and good symmetry and homogeneity of the sample.

II.5.References

[1] J.C.Viguie, J.Spitz, Journal of The Electrochemical Society , 122 (1975) 585-8.

[2]L. Filipovic, S. Selberherr, G.C. Mutinati, E. Brunet, S. Steinhauer, A. Köck, F. SchrankA Lett, 21 (2013) 224-240

[3] D.Beckel, A.Dubach, R.Studart, LJ.Gauckler. Journal of electroceramics, 16 (2006) 221-8.

[4] F.Caillaud, A. Smith, and J. Baumard, Journal of the American Ceramic Society vol. 76, no. 4 (1993) 998–1002.

[5] M.Andersson, Course: Nanomaterials Chemistry, Chalmers University of Technology. (2009).

[6] L. E.Smart, E. A.Moor, Solid State Chemistry: An Introduction, Third Edition, Taylor & Francis, Chapter 2, 91- 122.

[7] mateus vieira carlesso, Thesis of Engenheiro de Materiais.University of Bremen, (2008)

[8] A. Bouhdjer, Doctorate Thesis, University of Biskra, (2016).

[9] HP. Klug, LE. Alexaander, X-ray diffraction procedure for crystalline and amorphous materials. New York: Wiley; (1974) 662.

[10] J. Basic. Appl. Sci. Res., 3(2013)597-600.

[11] S.Rahmane,Thesis of Doctorate, University of Mohamed Kheider – Biskra, (2008).

[12] A. Segmuller and M. Murakami, in Analytical Techniques for Thin Films, eds. K. N. Tu and R. Rosenberg (1988) 143.

[13]Q. Zhenxing, Z. Xiaozhong, Z. Mingzhou, W. Xizhang, and L. Yujin, IEEE Trans. Sonics Ultrason. 32 (1985) 630.

[14]T. B. Bateman, Appl. Phys. 33 (1962) 3309.

[15] A.Ables, Amsterdam: North Holland, (1992).

[16] M.S Thyagi, Publisher John Wiley& Sons, (2008).

[17] S.M.Sze, Kwok K .Ng, Publisher John Wiley& Sons, (2008).

[18] D. K. Schroder , Publisher John Wiley& Sons, (2008).

[19] VAN DER PAUW, Philips Research Reports, 13 (1958) 1.

[20] R.GREEN, Keithley Instruments, Inc., Keithley Instruments, Inc. (2011).

[21] Schematic illustrations of (a) resistivity and (b) Hall effect measurements by the van der Pauw method.

Chapter III

Effect of solution flow rate and deposition air pressure on ZnO properties deposited using pneumatic spray pyrolysis

III.1.Pneumatic spray pyrolysis

In this part of the study, we will discuss the deposition of undoped zinc oxide thin films, by the pneumatic spray pyrolysis technique, to study the effect of solution flow rate and the air pressure on the structural, optical and electrical properties.

III.1.1.Section one - Effect of solution flow rate

In order to find out the impact of solution flow rate, we have deposited undoped-ZnO samples on glass substrates by pneumatic spray technique, the effects of solution flow rate on the structural, optical and electrical characteristics of undoped ZnO thin films were obtained among this section. However, in other context, which value of solution flow rate is appropriate to that pressure, on undoped ZnO properties, whole of thin films have analyzed and discussed.

II.1.1.1.Thickness calculation

A series of undoped ZnO thin films were prepared with various solution flow rate on glass substrate at 1 bar of deposition air pressure by pneumatic spray pyrolysis deposition. As seen in figure 3.1, it's clear that the film thickness increasing from 214 nm to 336 nm when the solution flow rate increased from 100 µl/min to 300 µl/min.

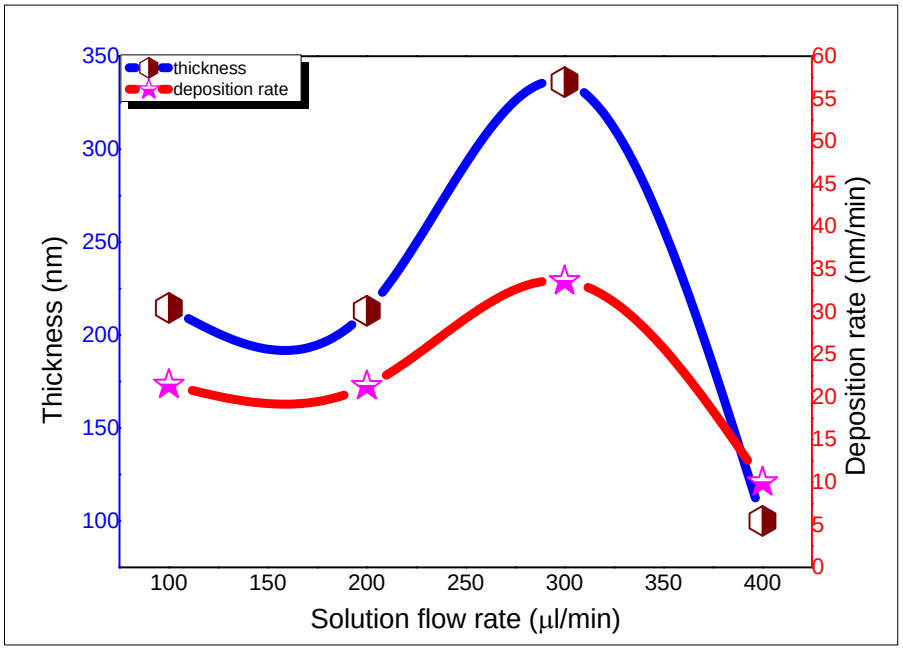

Figure 3.1: The variation of thickness of ZnO thin films deposited at different solution flow rates.

where It can be explained by amount of solution deposited was sufficient for having a good deposition on the substrate surface as the figure of deposition rate described, in other context the rise in the solution flow rate lead for increasing the solution volume sprayed onto substrate surface [1]. In addition to that, from figure 3.1 we illustrated also if the amount of the deposition solution (Solution flow rate) more than 300μl/min the film thickness decrease to lowest value 100 nm, what means that there is deterioration in film thickness may be associated with the kinetics of atomic arrangements during deposition process; caused by rapid surface diffusion process of the solution from the strained surface regions at the grain centers to the grain boundary areas [2].

III.1.1.2.Structural properties

In general, from the X-ray diffraction patterns by exploiting the peak position we can estimate that the properties of our cristallographies films, are depending on the experimental conditions for the deposition. When in the crystal case, the layers show a preferential orientation along *c*-axis (002) - Wurtzite structure, figure 3.2 show the diffraction spectra of X-rays of our samples.

The X -ray diffraction spectrum of our glass substrate glass, indicated the presence of bumps located almost between the two values 2θ = 20 ° and 2θ = 30 °, which describe the amorphous structure of the glass [3].

XRD measurements indicated that the films were crystalline with a hexagonal structure and a preferred orientation with the c-axis perpendicular to the substrate. The only diffraction peak observed was the (002) peak at a location of $2\theta \sim 34{,}60^0$ for the whole thin films , instead of the unstressed position of $3.37\ ^0$, this small difference is due to the diffraction angle corresponding to the peak of the (002) plane, and this is owing to the stress arising between the joints of grains of the sample to each other, that notice by the difference the flow rate value, However, when the flow rate increases the (002) peak intensity is increased, this means that a large number of atoms move towards the (002) plane which corresponds to the favorable energy for the formation or the crystal growth of zinc oxide (ZnO). except the point of 400 ul/min, we have observed that the intensity of the peak was decreased which means that the crystallite has a weakness.

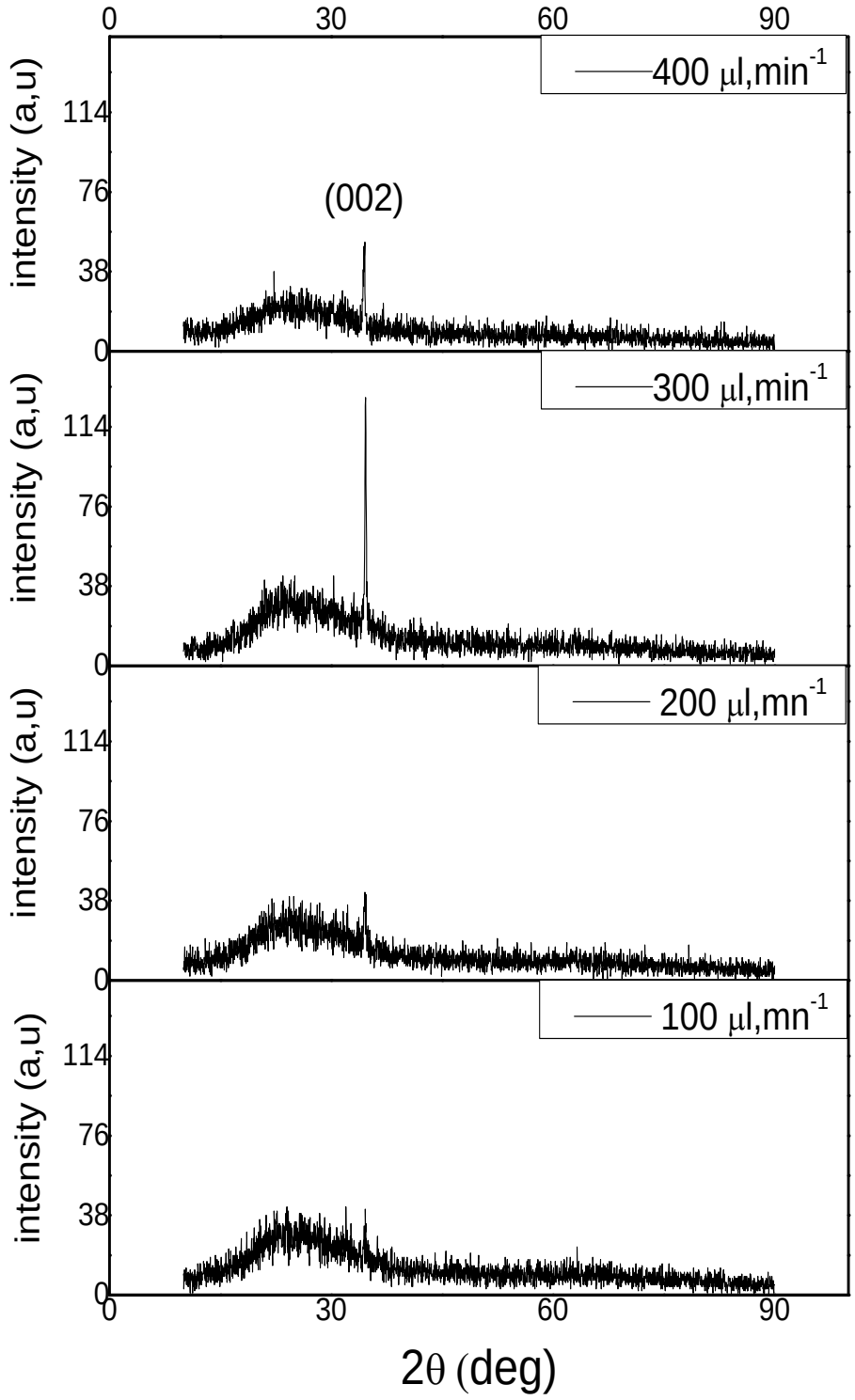

Figure 3.2: Diffraction spectra X-ray obtained from the films deposited at deposition air pressure 1 bar with different solution flow rates.

this behavior can be explained by the amount of solution flow rate (400µl/min) does not allow ZnO atoms to choose orientation [002] which corresponds to favorable energy to the formation or growth of crystals Zinc Oxide, then the increased number of the solution particles, which cause the random deposition of zinc oxide molecules (ZnO).

So when increasing the solution flow rate of 400 µl/min or more, we can predict that the (002) peak intensity decrease to the amorphous state. Therefore our thin layers consist of two phases, the first poly-crystalline and this was a hexagonal structure (Wurtzite) and the second is amorphous with intensity was varied from sample to another, due to the difference in the solution flow rate with deposition air pressure.

The following figure 3.3 shows the variation of the crystallite size as a function of solution flow rate.

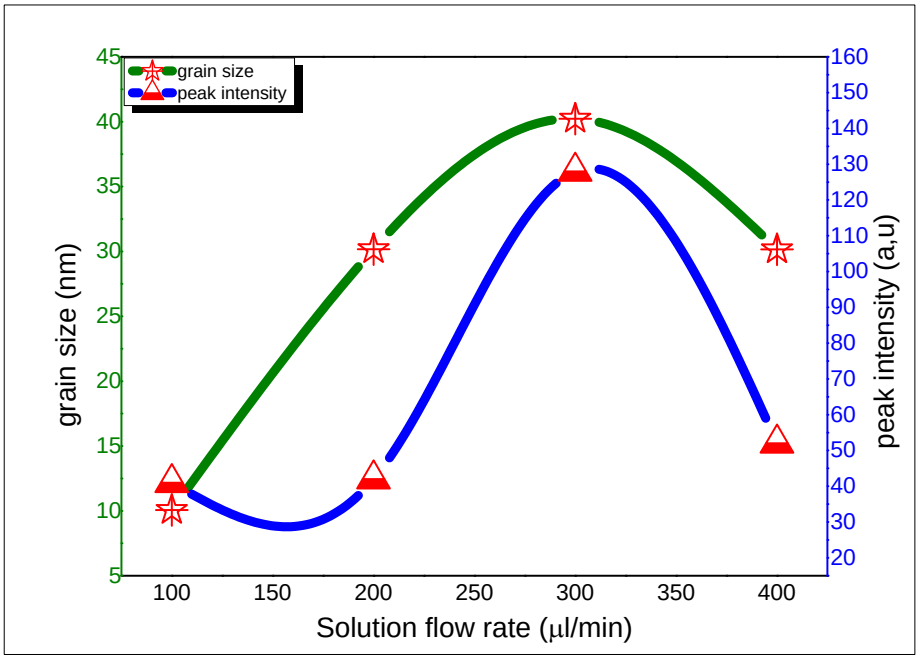

Figure 3.3: The variation of the grain size and peak intensity as a function of solution flow rate deposited at 1 bar.

The average crystallite size is between 10 nm and 40 nm were calculated form the full width at half maximum, where we can show that the increment of crystal size related to increasing of the spraying flow rate, the similar behavior described in the figure of peak intensity, in addition to that we can note that the amount of the solution deposited at substrate surface, was appropriateness for crystal growth process, once the solution flow rate is more than 300µl /min, the speed spreading process of the solution affect is the main reason the decreas of grains size [2], as shown on the following Table 3.1:

Table 3.1 Results of undoped ZnO deposited with different solution flow rates.

Solution flow rate (µl/min)	Deposition air pressure (bar)	$2\theta_{hkl}$ (°)	FWHM (°)	Plane (hkl)	Grain size (nm)	Stress (GPa)
100	1	34.669	0.864	(002)	10.060	-2.522
200	1	34.565	0.288	(002)	30.172	-1.283
300	1	34.646	0.216	(002)	40.238	-2.252
400	1	34.464	0.288	(002)	30.163	-0.031

All the samples have a negative stresses which indicated a compressive stresses in the films. Basically, and from the figure 3.4 this stress included a thermal stress originating from thermal mismatch between films and heated substrates, and another intrinsic stress originating from the film structure defects, this is attributed to a variation in the lattice parameters in the ZnO crystalline structure [4], that obviously from the shifting of the preffered peak from $2\theta = 34.54°$ to 34.66^{o}, which clearly showed in the figure of peak position.

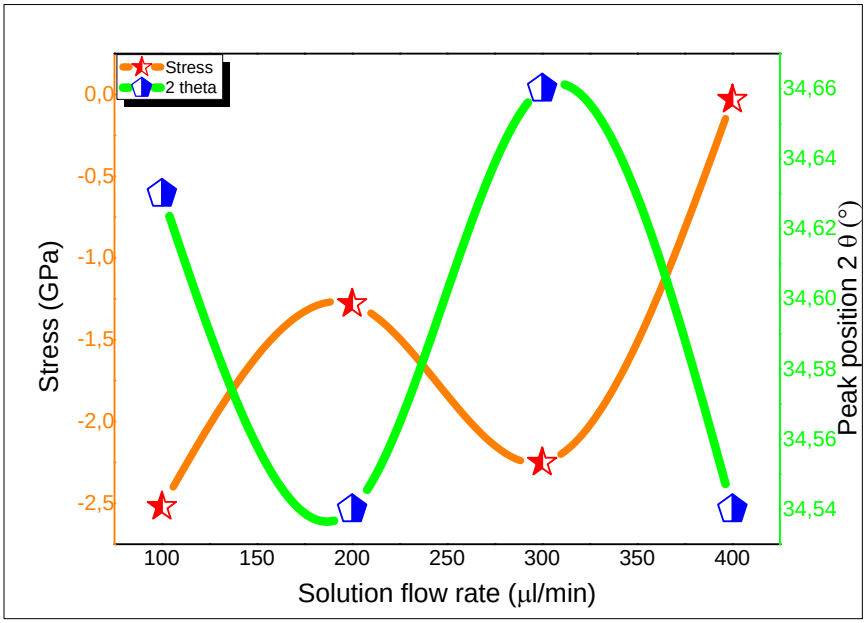

Figure 3.4: The variation of the Stress and peak position as a function of solution flow rate deposited at 1 bar.

We calculated the strains in various undoped-ZnO films, where we observed that the grain size was increased when the solution flow rate was increasing. But at 100 µl/min of solution flow rate value, the crystal size takes the lowest value, that because the grain size is created a high negative stress due to grain boundaries and their impact on defects increasing, on parallel, as we seen, that there is an increase in the value of stresses depending on the solution flow rate of the solution, this can be due to increasing the crystal size (grain size) by the growth mechanism, and the larger grain size means a decrease in the number of grain boundaries [5], and thus a reduction in the creation of crystal defects leads to decrease the value of compressive stresses between the grains [6].

III.1.1.3.Optical properties

Transmission spectra obtained for the films indicated that all films were highly transparent in the 280-900 nm wavelength range. Figure 3.5 shows a typical optical transmission (T %) spectrum of a 2×2 cm^2 ZnO films. The spectra were taken using air as the optical reference. The average of transmittance in the visible range for all the films is about 90 %. Then, and from the spectra of our films, we observed that all spectra apears a bump (bosse) between wavelength 290 nm to 350 nm, which means that our films have included a porosity, the latter due to, two or may be three phenomena:

- The thickness effects.
- The light scattering due to the difference of the quality of the layer surface.
- Grain size.

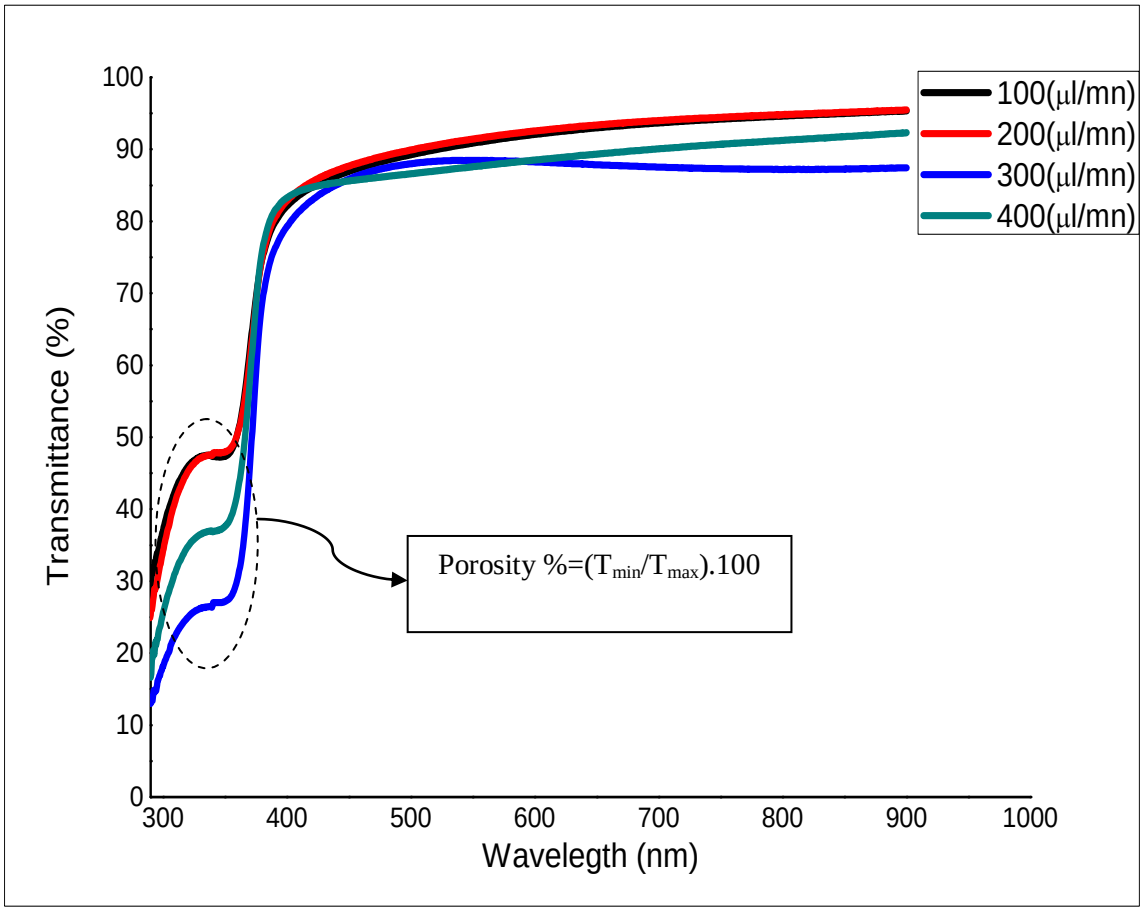

Figure 3.5: Transmittance spectra of ZnO thin films prepared at pressure of 1 bar with different solution flow rates.

We also note that the intensity of the transmittance bump has different values, which explain that the thickness of thin layers of our samples, and the number of pores exist vary from sample to another, according to the following equation [7]:

$$\text{Porosity\%} = (T_{min}/T_{max})\times 100 \qquad (3.1)$$

The optical transmission spectrum shows that the porosity increases in the visible range with solution flow rate. Where the deposited with solution flow rate 200 µl/min is too porous, this is linked with the reduction in the thickness of the deposits, because the pressure forced the zinc oxide molecules to deposition randomly.

The direct optical gap was determined from the α^2 versus photon energy graphs. For which the variation in the absorption coefficient with the photon energy hν is given by:

$$(\alpha h\nu) = A(h\nu - E_{gap})^{1/2} \qquad (3.2)$$

E_{gap} denotes the optical energy gap between the valence and the conduction band. Plots of α^2 versus hν were given by extrapolation of the linear region of the resulting curve.

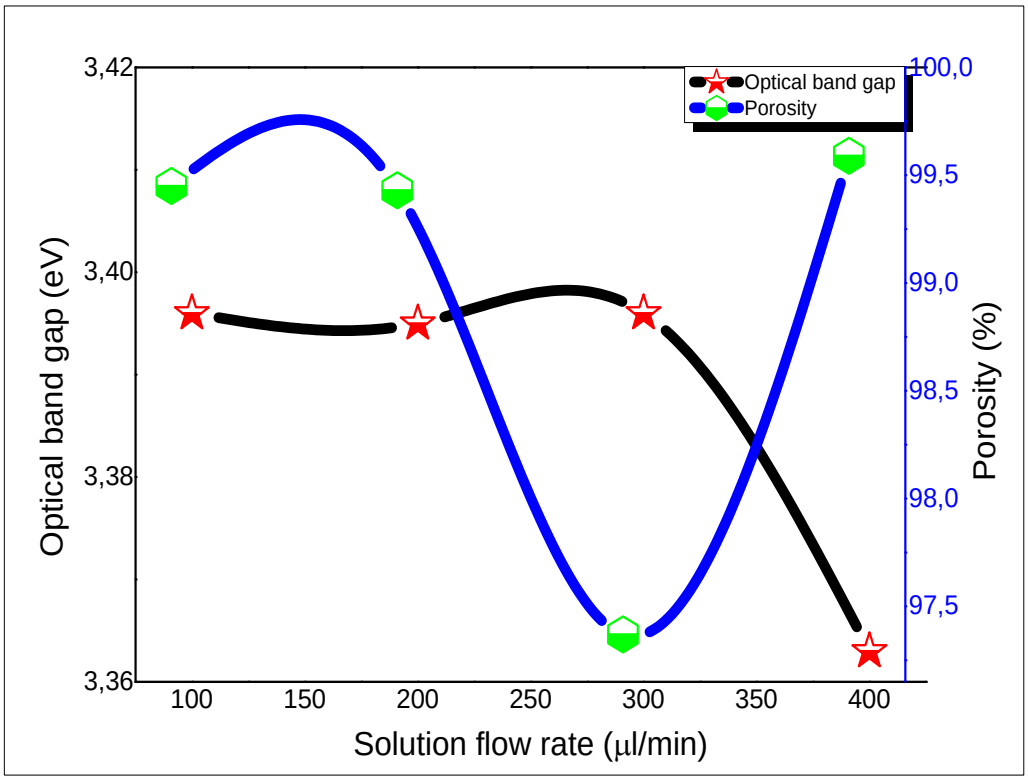

Figure 3.6: The variation of optical band gap and porosity of thin films as a function of solution flow rate deposited at 1 bar.

The optical band gap value E_{gap} is shown in figure 3.6. The variations of the optical energy gap could be attributed to changes in the deposition air pressure.

Generally, it can be stated that the reduced band gap energy of ZnO may be due to the extent of non-stoichiometry of the deposited layers. Which may be due to the various lattice associated atomic interaction phenomena come into play from its ionic crystalline lattice nature [8]. ZnO thin films deposited at 1 bar of deposition air pressure have a variations of the optical energy gap could be from 3.36 eV to 3.39 eV with increasing solution flow rate. those variations can be explained by the increased concentration of free electrons and probably due to the occupation of interstitial zinc atoms because these native latter represent the main

donors in the ZnO films [9]. In addition to that, we can show reduction in the porosity which can be returned to presence of oxygen on the film-substrate related to solution flow rate, furthermore it is evident that for the highest solution flow rate, the most dense ZnO structures of highest porosity were obtained containing the grains with a dimension of 30 nm, it was related to the fact that only for the highest O_2 caused by solution flow rate does the highest amount of oxygen prevent the growth mechanism and coalescence of Zn crystallites by raiseing new nucleation centers at the crystalit growth front in the presence of oxygen atoms. This leads to a decrease in the crystallite size (see figure 3.3) [10].

III.1.1.4.The electrical conductivity of ZnO thin films

The variation of the electrical conductivity of ZnO films deposited at 1bar of deposition air pressure with varied solution flow rate value, is shown in figure 3.7, revealed an decearing in electrical conductivity with increasing solution flow rate values, up to 300 µl/min where took a lowest value 0.12×10^3 $(\Omega.cm)^{-1}$ and then going toward the highest value which is 0.46×10^3 $(\Omega.cm)^{-1}$ at 400 µl/min of solution flow rate, that decreasing in condutivity may be due to an increase in the grain size; therefore decrease in the number of grains which leads to decrease of number of the grain boundaries which operate as a trap for free carriers by created barriers prevent the transport of free charge [11].

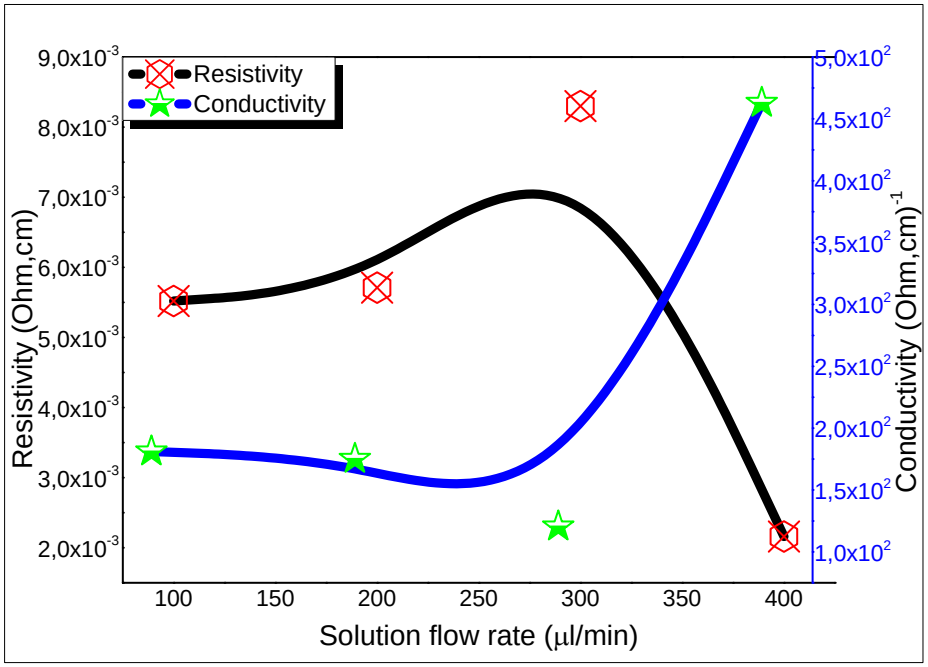

Figure 3.7: The variation of electrical conductivity of undoped ZnO films deposited at 1 bar.

That increase of the electrical conductivity with increasing of solution flow rate is explained by decreasing grain numder which increases the probability of grain boundary scattering, the latter causes increasing of the disorder in the films hence the potential barriers increased [12]. That means an increase in the carrier concentration, the similar results has been explaining by displacement of the electrons or may be due to the interstitial defect of zinc atoms which provide the free carriers, so the reduction in electrical resistivity occur. Where the maximum resistivity value was 8.3×10^{-3} Ω.cm, which obtained at 300 µl/min [13].

III.1.2.Section two - Effect of deposition air pressure

Pressure carrier gaz (air) or air pressure is an important factor in the pneumatic spray pyrolysis process, that because, as we listed in the preceded chapter, the pneumatic nozzle employed as a reactor to create aerosol from the precursor solution, and droplets size is relating strongly with air pressure from side, and the nozzle rediu from other side, where, we have to use a nozzle with 2.5×10^{-3} m Diameter given by manufactory, in this study and in physical mechanism, we can just playing in the air pressure to improve the aerosol, hence a good properties of ZnO thin film. So in this deposition all parameters are remaining constant, as well the solution flow rate at 300µl/min, except the deposition air pressure which is varied from 0.5 bar to 2 bar with 0.5 bar as step, and as mentioned above, for checking on the effect of air pressure on growth of ZnO thin films, the undoped ZnO films are deposited and characterized below.

II.1.2.1.Thickness calculation

The undoped Zinc oxide film thickness increased from 100 nm to 336 nm when deposition air pressure varied from 0.5 to 2 bar. the calculation film thickness was also investigated from the transmittance spectrum as shown in figure 3.8:

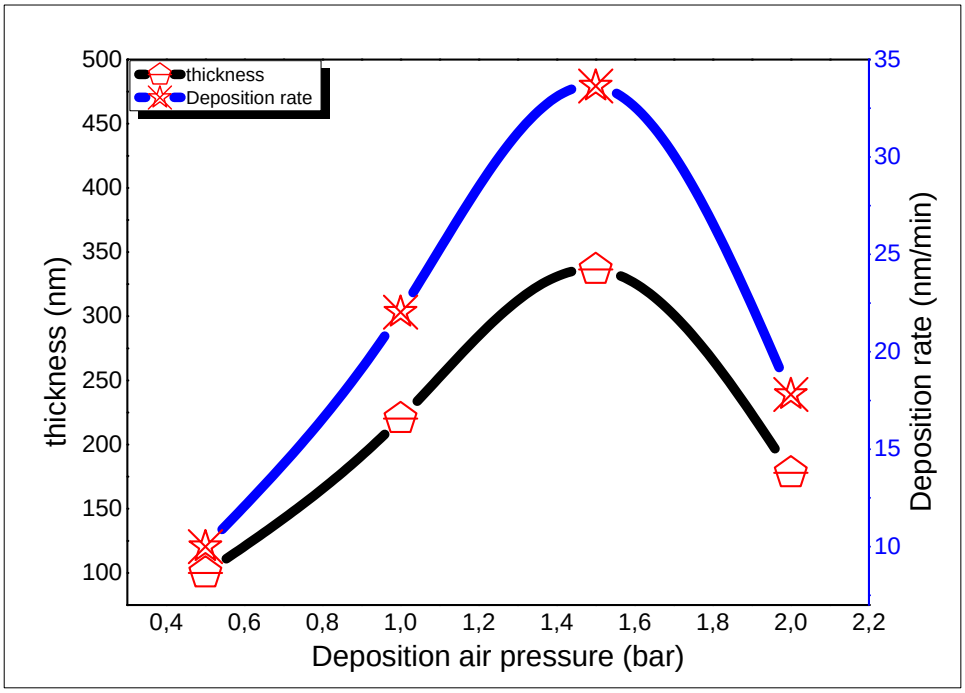

Figure 3.8: The variation of film thickness and deposition rate of ZnO thin films deposited at different deposition air pressures

from the figure 3.8 It can be observed that the films deposited for various deposition air pressure show an increment of thickness from 100 to 336 nm as the pressure increase from 0.5 bar to 1.5bar, this can be explained by the grain size distribution on the substrate surface, where we observed that the increment of the thickness extend to take the highest value of 336nm at1.5bar of deposition air pressure then come back to 178nm value at 2 bar [2].

However, according to deposition rate curve and the film thickness results we observe that, there is an appropriate deposition air pressure value for improving the characteristic of ZnO thin films deposited using pneumatic spray pyrolysis.

III.1.2.2.Structural properties

Figure 3.9 presents the XRD patterns obtained for the undoped ZnO samples, the characteristic diffraction peaks of the hexagonal ZnO structure can be observed opviously, evidencing a strong orientation in the [0 0 2] direction. all of crystalline planes appears at the positions corresponding to the wurtzite phase on whole of ZnO samples, but with different relative intensities with respect to the air pressure variation, where we can estimate that peak intensity (002) increases to the highest value 128 (u.a) with increasing the deposition air

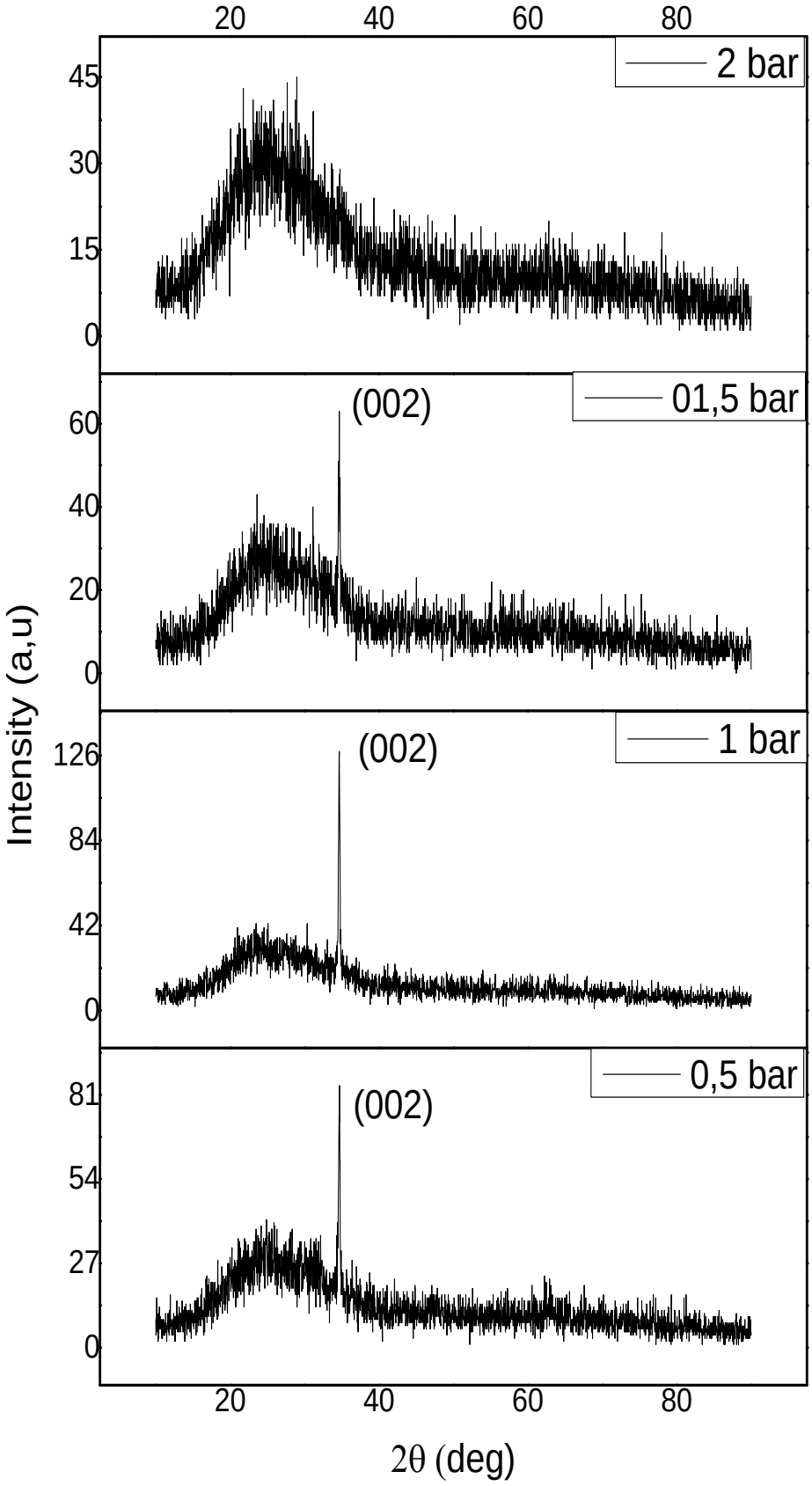

Figure 3.9: Diffraction spectra X-ray obtained from the films prepared at solution flow rate of 300µl/min with different deposition air pessures.

pressure, where was increasing to the highest in 1 bar of depoition air pressure, which indicates that the ZnO thin film prepared with air pressure of 1 bar is monocrystaline, then return to decrease, where the intensity of the diffraction peak becomes valueless, moreover no peak shown, and thereby the layer becomes amorphous in the pressure value of 2 bar.

As result and from the patterner of X-ray diffraction we can say, that the structure of ZnO thin films deposited with pressure 1 bar, have good structural quality.

Whole of The X -ray diffraction spectrum shown a boss (thoroughly as been disscused in the section one), located almost between the two values 2θ = 20 ° and 2θ = 30 °, however, we can say that the boss in each patterner evidences a change in the ZnO structure, At the same time, a shifting of the (0 0 2) peak from 2θ = 34.69° to 34.66°, respectively with increasing of deposition air pressure.

This is attributed to a variation of the lattice parameters in the ZnO crystalline structure[14]. This analysis proceeds by means of the equation:

$$\frac{1}{d_{hkl}^2} = \frac{4}{3}\frac{h^2+hk+k^2}{a^2} + \frac{l^2}{c^2} \qquad (3.3)$$

Where (h k l) are the Miller indices of the respective crystalline planes, $a = b$ and c stand for the lattice parameters of the hexagonal ZnO structure and d(hkl) is the distance between (hkl) planes. In this way, we found that the parameter *c* increases from 5,171 Å to 5,176 Å. This change was attributed to Zn vacancies formed in the ZnO crystalline structure; means the increase in the formation of Zn vacancies influences the *c* lattice parameter [15]. Therefore, the presence of Zinc vacancies tends to make the structure more randomly into the ZnO crystalline structure, yielding an increasing of the *c* lattice parameter [14].

In figure 3.10 we show the variation of crystallite size for the [2 0 0] orientation, obtained for all undoped ZnO films. As can be seen, the increment of deposition air pessure results in an increase of the cyrstallite size from 39,70 nm to 89,19 nm.

That, at higher deposition air pressure (1.5 bar) the droplet becomes more fine which makes the reaction droplets-substrate occur, thereby film growth efficiency.

In addition to that, we ca estimate, that 1.5 bar of deposition air pressure, is appropriate to achieve a thin films of Zinc Oxide with crystalline structure.

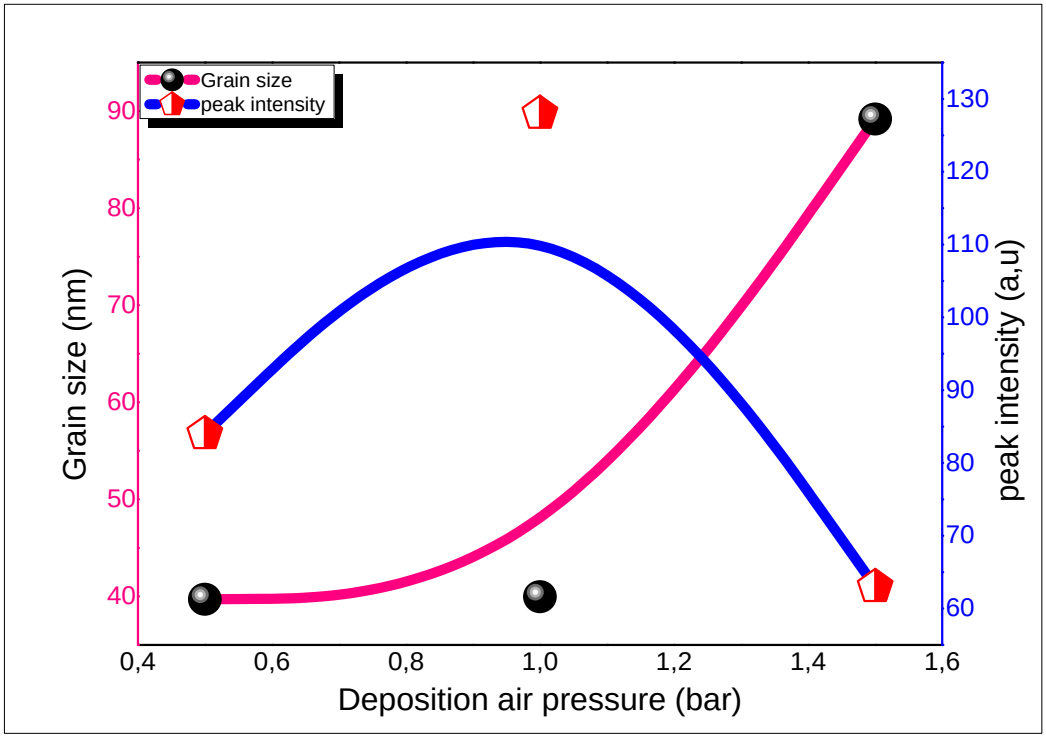

Figure 3.10: The variation of the grain size and peak position as a function of deposition air pressure.

The figure 3.10 shows the increment of crystallite size as the air pressure increases. As we metion before, a shifting of the (002) peak from 2θ = 34.69° to 34.66° (see the peak position figure), this is attributed to a variation in the lattice parameters in the ZnO crystalline structure, due to intrinsic stresses, which are created fundamentally from the grain boundaries which exhibit strong participation on defects. [15].

All measurements of the stresses and grain size are appearing on the following table.

Table 3.2 Results of undoped ZnO deposited with different deposition air pressures.

Air pressure (bar)	Solution flow rate (µl/min)	$2\theta_{hkl}$ (°)	FWHM (°)	Plane (hkl)	Grain size (nm)	stress (GPa)
0.5	300	34,69	0,213	(002)	39,702	-2,978
1		34.66	0,211	(002)	39,976	-2,564
1.5		34.66	0,095	(002)	89,180	-2,564
2		-	-	-	-	-

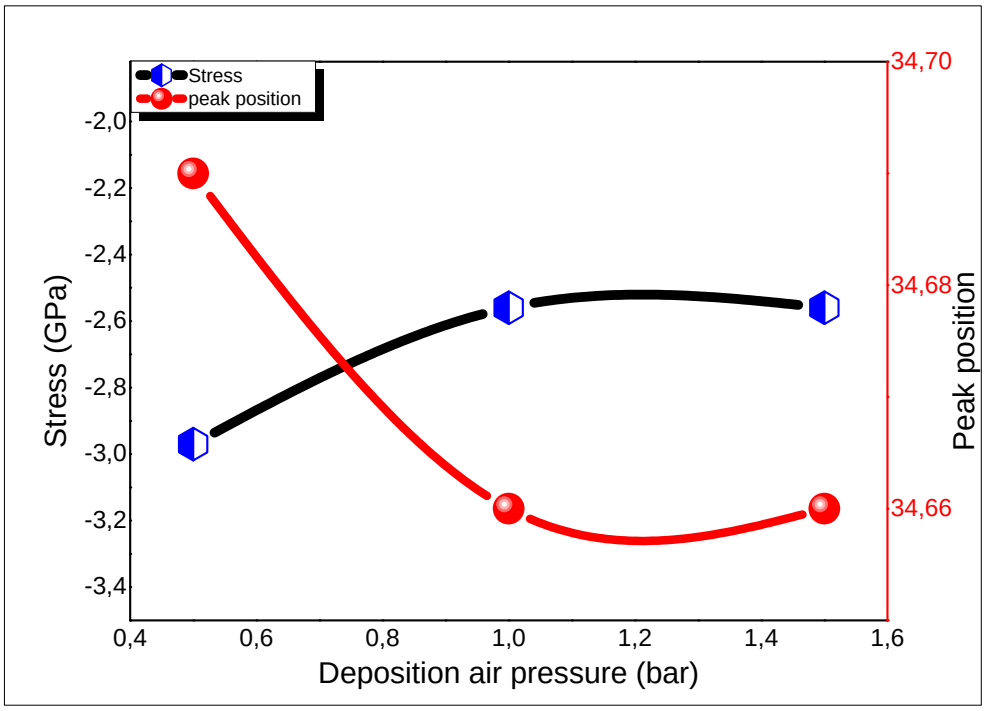

Figure 3.11: The variation of the stress and peak position as a function of deposition air pressure.

However, from the figure 3.11, is obviously that, whole of stresses have a negative signal that means compressive stresses occur; as the peak position described. Whereas, the stresses in increment as the deposition air pressure increases, where the decrease of grain boundaries means the increment grain size, and stress becomes less [6].

III.1.2.3.Optical properties

Figure 3.12 shows the optical transmittance at room temperature. The transmittance spectrum indicates a high degree of optical transparency close to 95% in the visible region with steps due to the band-edge absorptions by undoped-ZnO prepared at diffrent air peassure. From the transmittance spectra of ZnO films, we note that all spectra have a bosse between wavelength 290 nm to 360 nm, as we have seen in the section one.

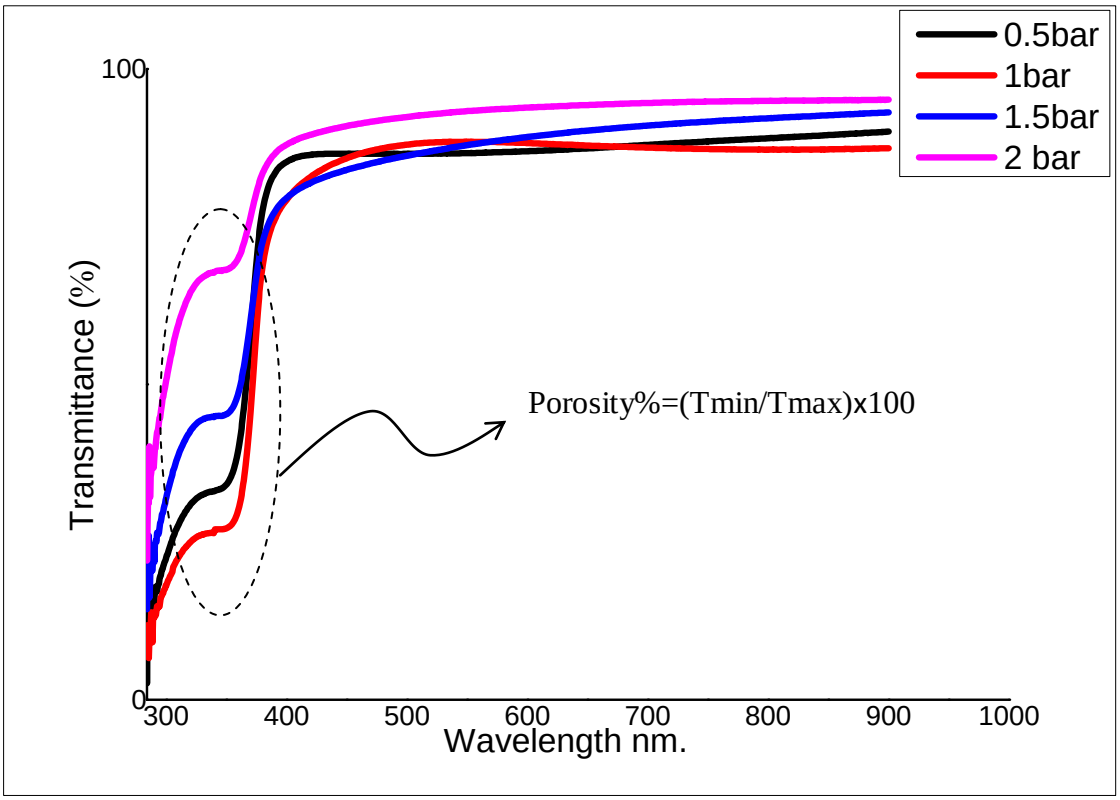

Figure 3.12: Transmittance spectra of ZnO thin films prepared with different deposition air pressures.

The optical transmission spectrum shows, that there is an increment in the porosity as air presuure increases. Where the ZnO film deposited at air pressure of 2 bar is too porous compare the other films at lower pressure, this is explained the state of thickness and its reduction of the deposits, because the pressure forced the zinc oxide molecules to deposition randomly, the latter, is affected on the trends of grains and their growth, thereby leaving a relative porosity.

We applied the $(\alpha h\nu)^2$ vs $h\nu$ plot for the transmittance curve in the staircase regions, and The optical energy gap value E_{gap} for the undoped ZnO, is shown in figure 3.13.
From the curve it is clear that the E_g of ZnO thin films varied from one deposition air pressure to another. Where the behavior of the optical band gap could be attributed by changes in the deposition air pressure.

In other context, there is a diminish in the optical gap as the deposition air pressure varied from 0.5 bar to 2 bar, this results can be explain by physical mechanism of the solution reaction at substrate surface; which has an important affect [16].

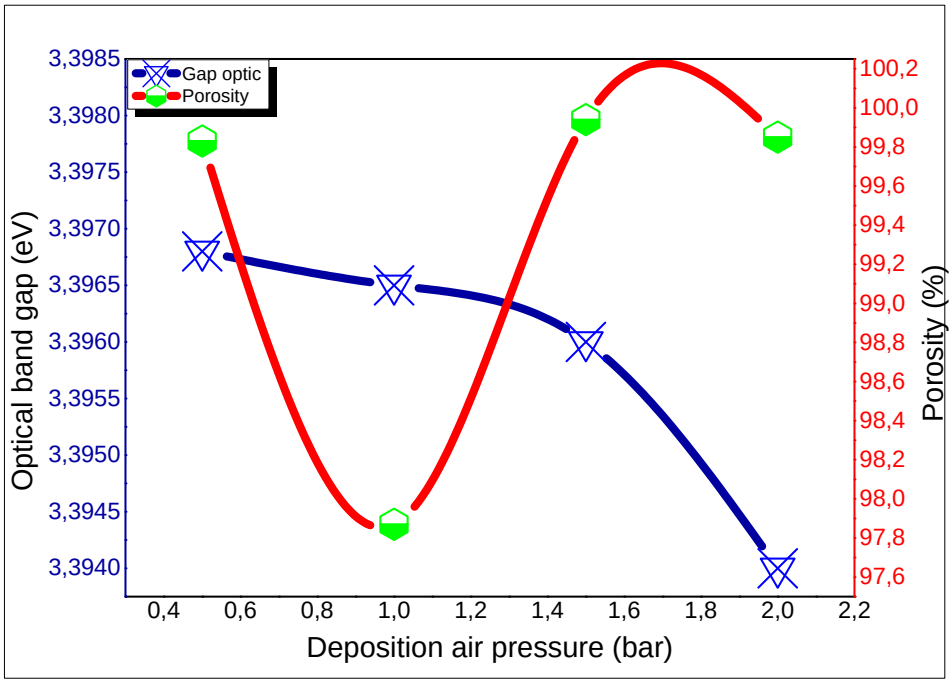

Figure 3.13: The variation of optical band gap and porosity of thin films as a function of deposition air pressure.

Where in the lower pressure the size of droplets is may be bigger than what happen in higher pressure. However, the function of air pressure (as mentioned befor in chapter II) is the generate of droplets, the size of the droplets is strongly related with air pressure, when the aerosol as fine the interaction between aerosol- substrate well occur [17].

But in the same time, the aerosol undergo of the air pressure (as carrier gaz), in this case the function of the pressure is unfavorable for getting an uniforme optical options. on other hand and in thermal mechanism, the effect of air pressure compare to substrate temperature is slightly small, and as we have mentioned in the decomposition of precursor, that when the droplet approaches the substrate, the solvent vaporizes, then the solid melts and sublimes and the vapor distributes to the substrate to undergo a heterogeneous reaction, the latter provides defects interstitial of Zin Oxide, these native latter represent the main donors in the ZnO films, that defects, diminish in the optical gap from side, also from another side to be cause to random structure or amorph phase [18].

However, ZnO thin films deposited with diffrent air pressures shown variations of the optical energy gap could be from 3.36 to 3.39 eV.

III.1.2.4.The electrical conductivity of ZnO thin films

From the figure 3.14, we can estimate that the conductivity affected with variation of deposition air pressure, where it is obvious that there is a reduce in the conductivity up to the lowest value of 0.18×10^{3} $(\Omega.cm)^{-1}$ at deposition air pressure of 1 bar, then has a increment after 1 bar, towards the highest value of 0.9×10^{3} $(\Omega.cm)^{-1}$.

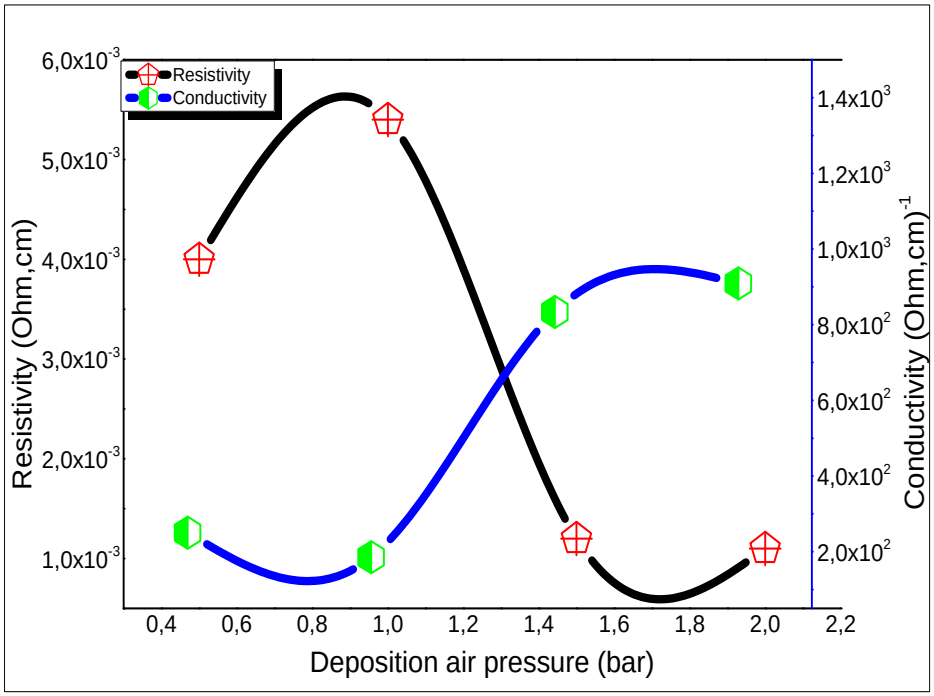

Figure 3.14: The variation of electrical conductivity of ZnO films deposited at different deposition air pressures.

that reduction in the resistivity can be for two or may be three reasons, the extent of the grain size, the interstitial ZnO, or free carriers concentration, the first one means that the structre is trends to be monocrystaline, furthere a decreasing of deffects, the second exhibit more randomly in the distribution of ZnO films, so the potential barriers increased the same phenomena with similar results was observed [12]; or there is an increasing in the carriers concentration by electron displacement [13].

III.2.Conclusion

Dedova et al studied the effect of the solution flow rate on the growth of undoped ZnO films prepared from $ZnCl_2$ solution and reported that the solution flow rate influences the surface topology. Concluded that the solution spray rate affects the surface morphology and roughness of undoped ZnO thin films produced by spraying Zn acetate solutions [18].

In conclusion, we have studied the effect of pressure and its relation with the variation of solution flow rate on Structural, optical and electrical properties of ZnO thin films deposited using pneumatic spray pyrolysis. The structural and optical properties become worse when the flow rate value is above 200 µl/min.

In our study and when the solution flow rate is bigger than 200 µl/min, we have observed that the solution flow rate value is more effective during low pressure and The X-ray diffraction spectrum indicated that the films were crystalline with hexagonal structure with the only diffraction peak. However, in lower pressure we estimate that the (002) diffraction peak was going to high intensity, with low solution flow rate, compare with higher pressure value. So the impact of the solution flow rate has weak effect on the optical, structural and electrical properties at lower and higher pressure. Then, we observed that the optical band gap value E_g has less variation with solution flow rate increasing, whereas, the films processed at 0.5 up to 1.5 bar the optical band gap were remained about 3.3965 to 3.3968 eV, and has been decreasing at 2 bat, to 3.394 with 300µl/min of solution flow rate. We conclude that there is a very important factor to get the best properties between pressure and solution flow rate , affect directly on the structural , optical and electrical characteristics, this brings us to choose an appropriateness solution flow rate value having an agreement to the deposition air pressure.

III.3.References

[1] C.M. Mahajan, M.G. Takwale, , Alloys Comp. 584 (2014) 128–135.

[2] S. Zargou, S.M. Chabane Sari , A.R. Senoudi1 , M. Aida , N. Attaf , I.F. Hakem, J. Mater. Environ. Sci. 7 (2016) 3134-3147.

[3] S. Laghrib et al, Revue des Energies Renouvelables , 10 (2007) 357 – 366.

[4] G.Anil Kumar, M.V.Ramana Reddy, Katta Narasimha Reddy, Materials Science and Engineering. 73 (2015) 012133.

[5] M. Mazilu, N. Tigau, V. Musat, Optical Materials. 34 (2012) 1833–1838.

[6] Lin Zhu Bai, Zhong Zhao Xing, Xu Sheng, Fu Hai Su, Guo Hua Li, Xiao Guang Wu. Jpn J Appl Phys, 47 (2008) 2225–9.

[7] Ishak Afs¸in Karipur, j mater res technol ,5(2016) 77–83.

[8] Gonioakowski and C. Noguera, Surf. Sci. 340 (1995) 191.

[9].J.Mattila, Nieminen, R.M. Phys. Rev. *B* , *55 (*1997) 9571–9576.

[10] M.Masłyk, M.A.Borysiewicz, M. Wzorek, T. Wojciechowski, M.Kwoka, E. Kaminska, Appl. Surf. Sci., 389 (2016) 287–293.

[11]F.Bouaichi,H.Saidi,A.Attaf,M.Othmane,N.Lehraki,M.Nouadji, M.Poulain, S.Benramache ,Main Group Chemistry,15 (2016) 57–66.

[12]Y. Benkhetta, A. Attaf, H. Saidi, A. Bouhdjar, H. Benjdidi, I.B. Kherchachi,M. Nouadji, N. Lehraki, Optik 127 (2016) 3005–3008.

[13] Z. Zhang, C. Bao, W. Yao, S. Ma, L. Zhang, S. Hou, Superlattices Microstruct. 49 (2011) 644–653.

[14]F.A.Garcés,N.Budini,R.R. Koropecki,R.D. Arce, Procedia Materials Science 8 (2015) 551 – 560

[15]R. Revel, D. Bazin, A. M. Flank, J. Synchrotron Rad. 6 (1999) 717-718

[16]D. L. Roberts, L. Chan, and C. L. Griffin

[17] Viguie JC, Spitz J. Journal of The Electrochemical Society, 122 (1975) 585-8.

[18] T. Dedova, J. Klauson, C. Badre et al, Physica Status Solidi A, 205 (2008) 2355–2359.

Chapter IV

Effect of substrate temperature and dopants on ZnO properties deposited using utrasonic spray pyrolysis

IV.1 Ultrasonic spray pyrolysis

In this chapter of the study, we will deposit of zinc oxide thin films using the ultrasonic spray pyrolysis technique; in order to find out the impact of two diffrent doping of fluorine and aluminum and their concentrations and the influence of substrate temperature on the structural, optical and electrical properties.

IV.1.1. Part one- Effect of substrate temperature

IV.1.1.1.The growth rate calculation

ZnO thin films with various thicknesses were deposited by varying the deposition temperature of spraying solution on glass substrates. Thicknesses of the ZnO thin films are computed from transmission data (see chapter II).

The calculation of growth rate of the film were from the thickness values for 10 min of time of deposition process, where its variations with substrate temperature is shown in figure 4.1, from which it is seen that film growth of these films are between 4 nm and 8 nm.

The expected reason for such behavior is the supply of more number of ingredient ions with increase in substrate temperature.

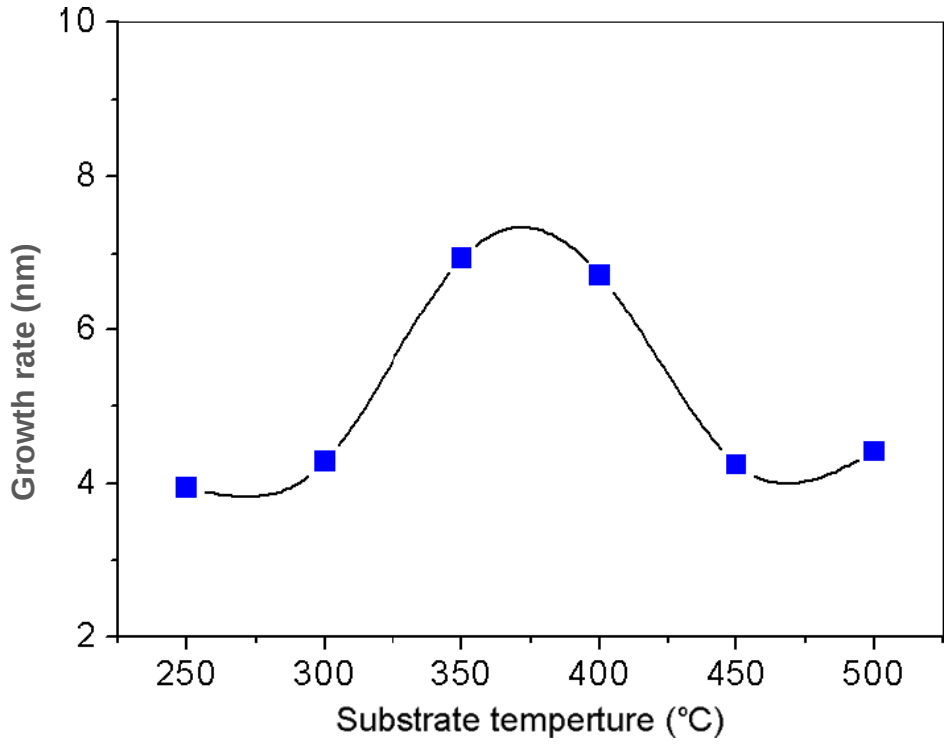

Figure 4.1: The variation of growth rate of ZnO thin films deposited at different substrate temperatures.

IV.1.1.2.The crystalline structure of ZnO thin films

The XRD patterns of ZnO thin films are presented in figure 4.2, Here the films were deposited on glass substrates at different substrate temperatures.

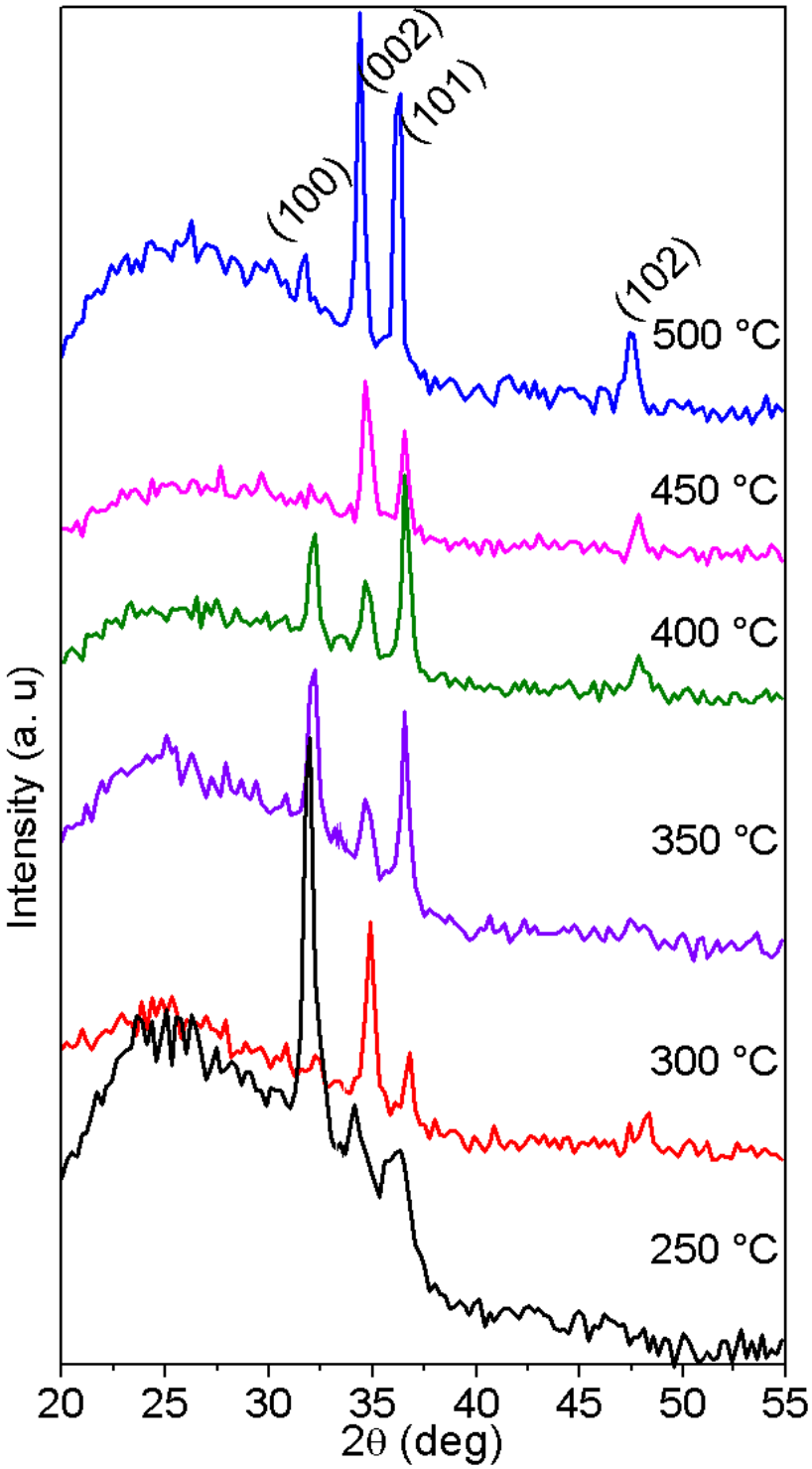

Figure 4.2: XRD spectra of ZnO thin films deposited at different substrate temperatures.

Ranging between 250 °C and 500 °C in the scale of 50 °C. As can be seen, the diffraction peaks were observed at 2θ =32.0°, 34.6°, 36.5° and 47.3° which are related to the following plans (100), (002), (101) and (102), respectively. The obtained XRD spectra matched well with the space group P63mc (186) (No. 36–1451) of the wurtzite ZnO structure [1].

From analysis data, all deposited films have different orientations of ZnO films, which were related to the higher and sharper diffraction peaks. Moreover, single significant (100) diffraction peak, with height intensity, was observed for deposited film at 250 °C, which indicates that the film has preferential a-axis orientation along the (100) plane.

Whereas for other films, it was observed that (002) and (101) planes are prominent. So the films exhibit polycrystalline structure it is hexagonal wurtzite structure from these spectra [2].

In order to evaluate the preferred orientation of the ZnO films, we use the texture coefficient TC(hkl) which represents the texture of the particular plane, deviation of which from unity implies the preferred growth. The texture coefficient TC(hkl) can be calculated from the X-ray data using the well-known formula of the intensity peaks corresponding to the (100), (002), (101) and (102) planes [3]:

$$TC(hkl) = \frac{I(hkl)/I_0(hkl)}{N^{-1}\sum_n I(hkl)/I_0(hkl)} \qquad (4.1)$$

where I(hkl) is the measured relative intensity of a plane (hkl), I_0(hkl) is the standard intensity of the plane (hkl) taken from the JCPDS data card 36–1451, N is the reflection number and n is the number of diffraction peaks. The texture coefficient related to the atomic densities corresponds to that plane as X-ray intensities, which correspond to planar densities.

The evolution of TC(hkl) values of the four major peaks of the films is shown in figure 4.3 and Table 4.1.

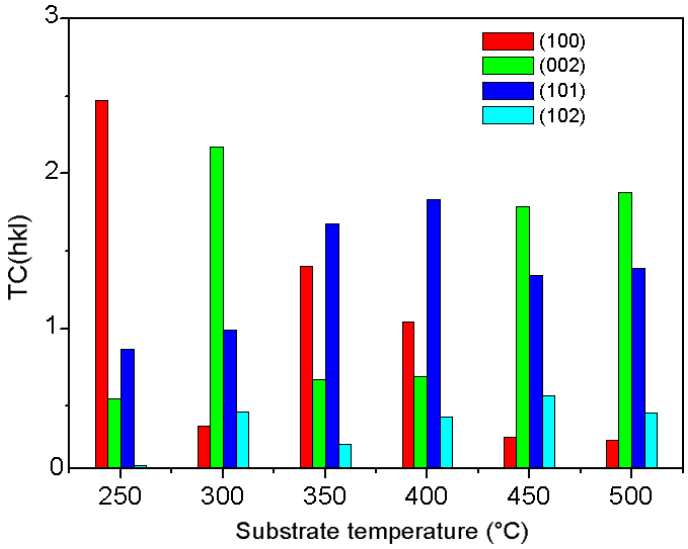

Figure 4.3: The texture coefficient TC(hkl) variation of (100),(002), (101) and (100) peaks with substrate temperatures of ZnO thin films.

One can observe that the texture coefficient of (100) peak decreases with increasing substrate temperature, whereas the texture coefficient of (002) and (101) peaks is highest in each temperature variation from 300 °C to 500 °C. The growth at 350 °C and 400 °C indicates that the films have preferential orientation along the (101) plane, the films deposited at 300 °C, 450 °C and 500 °C show that the texture coefficient of (002) is the highest one, which indicates that the films have preferential c-axis orientation along the (002) plane.

Table 4.1: The evolution of TC(hkl) values of the four major peaks.

Average						G(nm)				TC(hkl)				
$\sigma(\Omega.cm)^{-1}$	E_u (meV)	ΔE_g (eV)	E_g (eV)	c-c_o (A^o)	G (nm)	(102)	(101)	(002)	(100)	(102)	(101)	(002)	(100)	T(°C)
0.00137	0.11311		3.245	0.03937	8.777	5.931	6.084	9.072	14.023	0.12	0.86	0.55	2.47	250
0.00387	0.08785	0.017	3.262	-0.06565	10.287	5.931	11.481	14.283	9.453	0.46	0.99	2.17	0.37	300
0.00137	0.08297	0.006	3.268	-0.03113	12.724	5.952	18.267	12.491	14.186	0.25	1.67	0.67	1.39	350
6.2618	0.06135	-0.003	3.265	-0.03113	13.164	7.454	16.743	14.275	14.184	0.43	1.83	0.69	1.05	400
11.72831	0.05455	0.013	3.278	-0.03113	13.573	12.258	18.291	16.653	7.088	0.57	1.34	1.79	0.29	450
41.57901	0.04974	0.003	3.281	0.00387	16.630	11.904	18.255	22.194	14.167	0.45	1.38	1.88	0.28	500

This observation shows that the films have a high crystallinity with high temperature. The crystalline quality of thin films enhanced with increasing substrate temperature.

The exact reason for this behavior of texture coefficient is decrease at (100) peak and increase at (002) and (101) peaks at 300 – 500 ^{o}C which could be understood as follows; it is a well-known fact that the various factors such as crystallinity and morphology, increase the texture coefficient of (002) and (101) which results in reduced planar densities on (100), as discussed with Othmane et all [4] this is an increase in film thickness of ZnO thin films.

The variation of the crystallite size of the ZnO thin films with substrate temperature was calculated from the four diffraction peaks, using the full width at half maximum (FWHM) in conjunction with the Debye–Scherer formula.

According to the hexagonal symmetry, the lattice constant can be calculated by the following formula:

$$d_{hkl} = \left(\frac{4}{3}\frac{h^2+hk+k^2}{a^2} + \frac{l^2}{c^2}\right)^{-\frac{1}{2}} \qquad (4.2)$$

Where a, c are the lattice parameters, (h, k, l) are the Miller indices of the planes and d_{hkl} is the interplanar spacing.

Figure 4.4 presents the variation of crystallite size as a function of substrate temperatures. As can be seen, the crystallite sizes were varied in the range of 5.93–22.19nm (see Table 4.1).

Upon approximation, the crystallite sizes of (100) and (102) plans are smaller than the others. It can be seen, that the crystallite sizes of (002) and (101) plans increase with increasing substrate temperature.

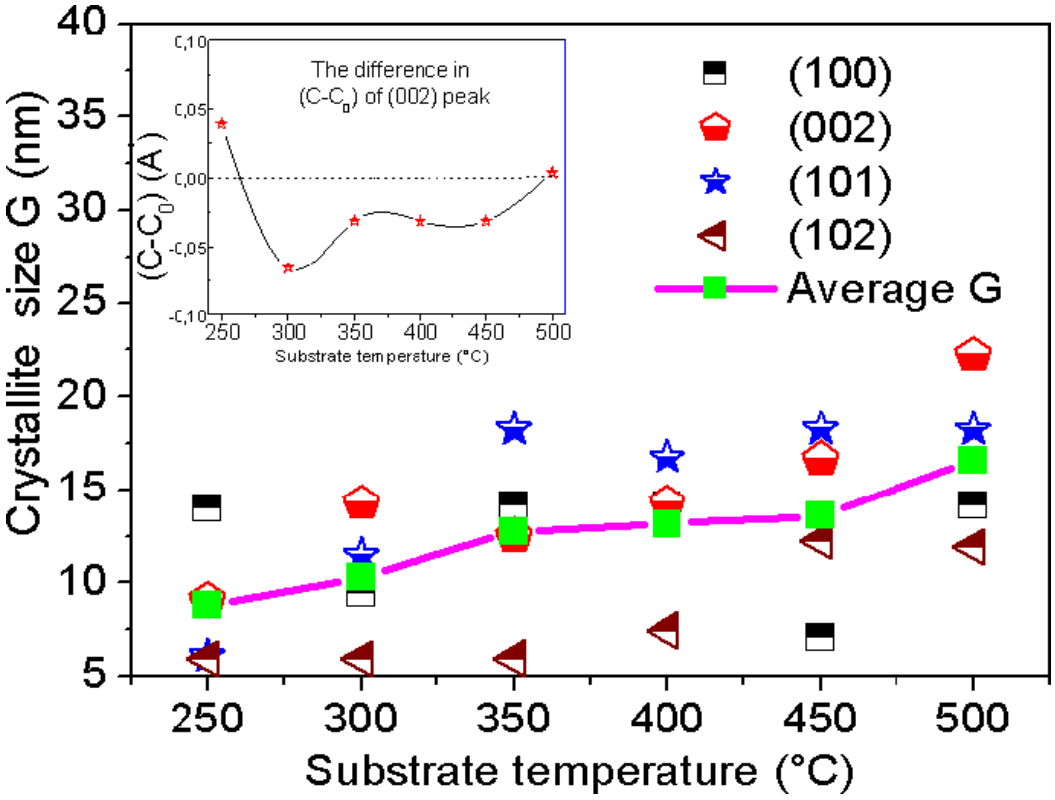

Figure 4.4: The variation of crystallite size G as a function of substrate temperatures, in the inset the variation of c - c_0 of (002) peak.

On the other hand, it can be noted that the optimal values of the average crystallite size of the ZnO films were obtained after increase of substrate temperature 350 ^{o}C. The inset of figure 4.4 shows that the lattice constant c of ZnO thin films was approached to the lattice constant of bulk c_0 indicating the strain is along the c-axis. The increase of the crystallite size has been indicated by the enhancement of the crystallinity and c-axis orientation of ZnO thin films, these phenomena were observed with [5].

IV.1.1.3.The microstructural and morphology properties

Scanning electron microscopy analysis revealed that the structural properties of the ZnO thin films were found polycrystalline with a hexagonal wurtzite-type structure, as we can see from the images.

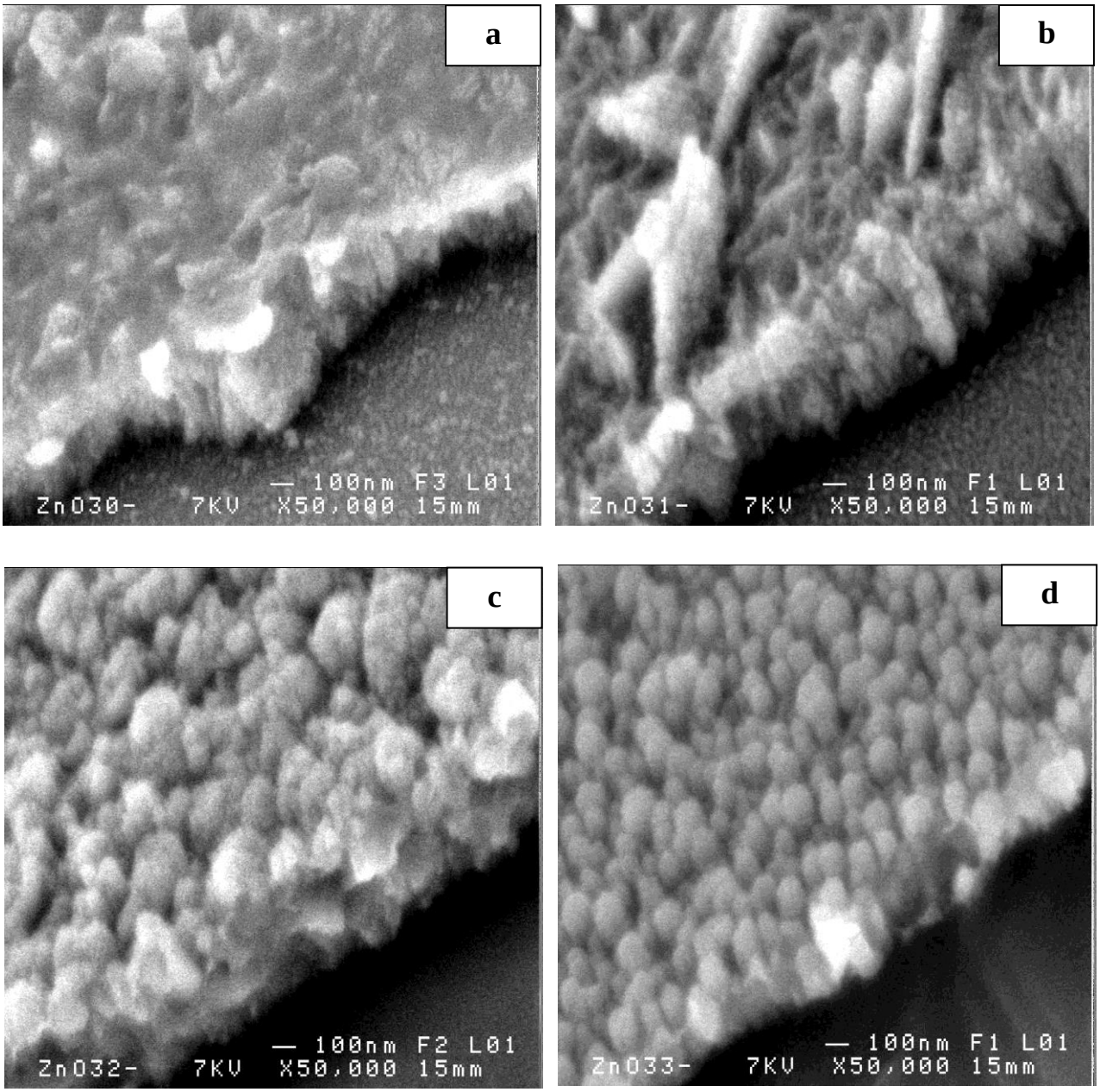

Figure 4.5 : The SEM micrograph of crystalline undoped ZnO thin film deposited at differente substrate temperatures a : T=250°c, b : T=300°c, c : T=400°c, d : T=500°c.

The accurate particle size and morphology of undoped ZnO were confirmed by Scanning electron microscopy SEM, where we can observe the morphology of highly crystalline of undoped ZnO nanoparticles. The SEM micrograph clearly showed nanostructural homogeneities and remarkably different morphologies of the undoped ZnO nanoparticles prepared by the ultrasonic spray pyrolysis technique.

The Scaning electron microscopy result showed the presence of conglomerate nanospheres with an average diameter of 10 –20 nm. Therefore, from these results we can only observe the rough morphology was found**.**

IV.1.1.4.The optical properties of ZnO thin films

The optical transmission of ZnO films was determined from the transmission measurement in the range of 300–1300 nm. Figure 4.6 shows the optical transmission of the ZnO thin films deposited at different substrate temperatures, where for the longer wavelengths (λ > 400 nm) all the films become transparent. It is found that all the films show a high optical transmission, around 85%, in the visible region. Where the film exhibits significant oscillations in long wavelength, such oscillation may be due to the roughness of the top surface of ZnO film. Which can generate interference phenomenon, even with naked eye one can see that the ZnO lattice is very smooth. Then the transmission decreased because of the onset of fundamental absorption in the region between 370nm and 390nm as shown in the inset of figure 4.6, which shows a plot of $(Ah\nu)^2$ versus photon energy hν.

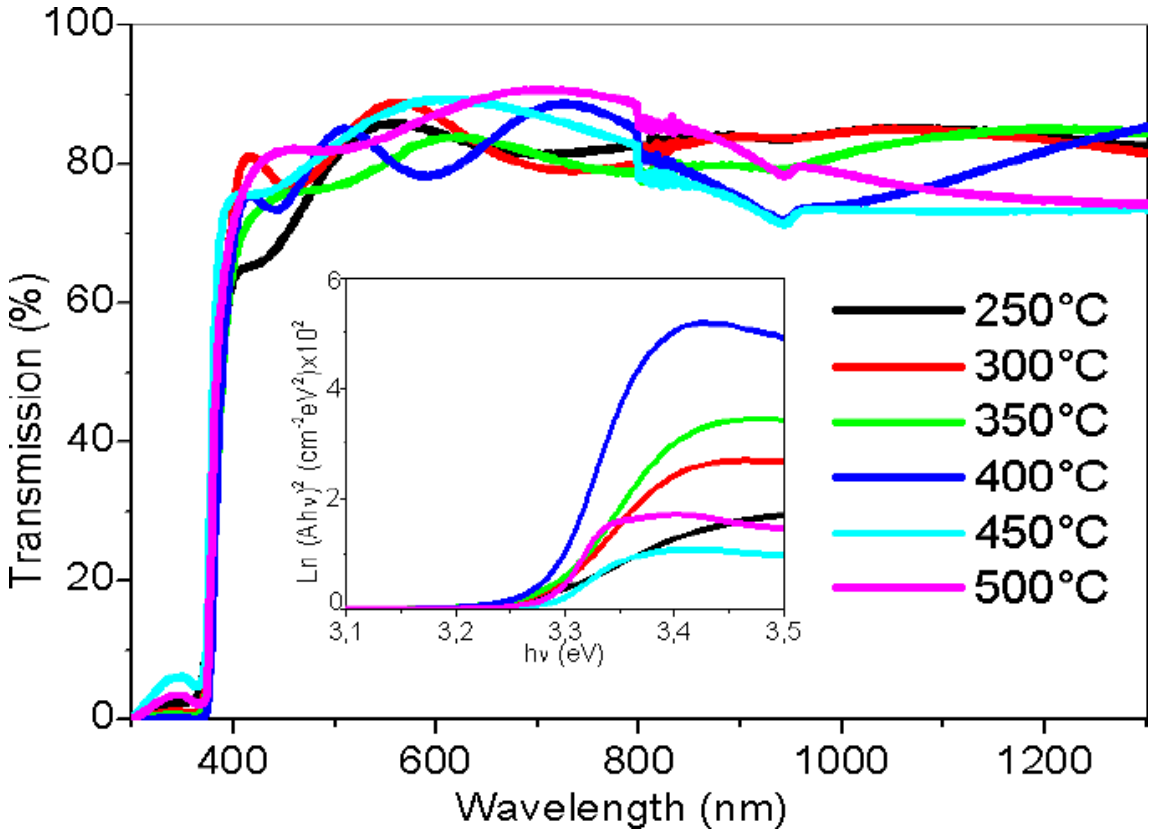

Figure 4.6: Transmission spectra of ZnO thin films for different substrate temperatures, in the inset the typical variation of $(Ah\nu)^2$ as a function of photon energy.

One can note that the effect of substrate temperatures is clearly observed in the layer quality such as in the average between 370 nm and 390 nm; a blue shift of the absorption edge was observed revealing Burstein–Moss [6]. As mentioned in the inset of figure 4.6, it was demonstrated by the decrease in the curve tendency with increasing temperatures. We can attribute this evolution to a change in the optical bandgap and the decrease in defects of the Urbach energy.

Based on the transmittance spectra in figure 4.6, the optical bandgap E_g was obtained by extrapolating the linear portion of the plot $(Ahν)^2$ versus (hν) to A =0 (see inset of figure 4.6) according to the following equation [7]:

$$A = \alpha d = -lnT \qquad (4.3)$$

$$(Ahv)^2 = C(hv - E_g) \qquad (4.4)$$

Where A is the absorbance, d is the film thickness; T is the transmission spectra of thin films; α is the absorption coeffcient values; C is a constant, hv is the photon energy and E_g the bandgap energy of the semiconductor. The values of E_g and ΔE_g are listed in table 4.1.

On the other hand, we have used the Urbach energy (E_u), which is related to the disorder in the film network, as it is expressed below [8]:

$$A = A_0\, exp\,(hv/E_u) \qquad (4.5)$$

Where A_0 is a constant hv is the photon energy and E_u is the Urbach energy, as presented in Table 4.1.

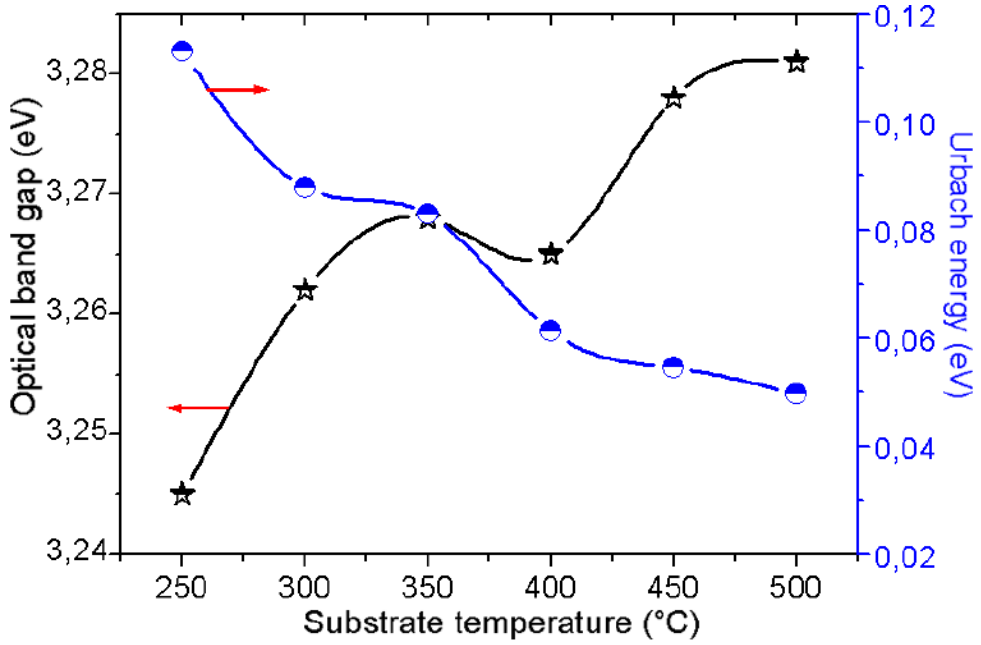

Figure 4.7. The variation as a function of substrate temperatures the optical bandgap E_g and Urbach energyE_u.

As clearly seen in figure 4.7, the optical gap energy increases as a function of substrate temperatures, which can be explained by the Burstein–Moss effect, which causes the widening of the energy band (blueshift). This is the phenomenon that the fermi level merges into the conduction band with an increase in the carrier concentration.

This can be explained by increasing the crystallite size (see figure 4.4), as reported in the literatures [1,9]. As can be seen in figure 4.7, a minimum Urbach energy was reached at longer temperatures due to the high crystallinity, which can be explained by the oxygen diffusion and is related to the approach of the lattice constant c of ZnO thin films of the lattice constant of bulk c_0 (see inset of figure 4.4) [5,10].

Oxygen vacancies in crystal have important impacts on the electronic properties of ZnO. In the synthesis of ZnO thin film, we believe that after deposition of ZnO at a higher temperature, we introduce a less concentration of oxygen vacancies into ZnO successfully. At a higher temperature, ZnO exhibits a broadening of the bandgap (see figure 4.7). The loss of lattice oxygen atoms at a higher temperature weakens the Zn–O–Zn bonds, which can be the reason for lowering of O 1S binding energies and can explain the stability of Urbach energy at 0.06meV.

In figure 4.8, we present the description of the variation of Optical bandgap energy as a function of substrate temperature, which is related by the band tail width. The decreases in the disorder lead to increase of optical gap, because of the less concentration of oxygen vacancy.

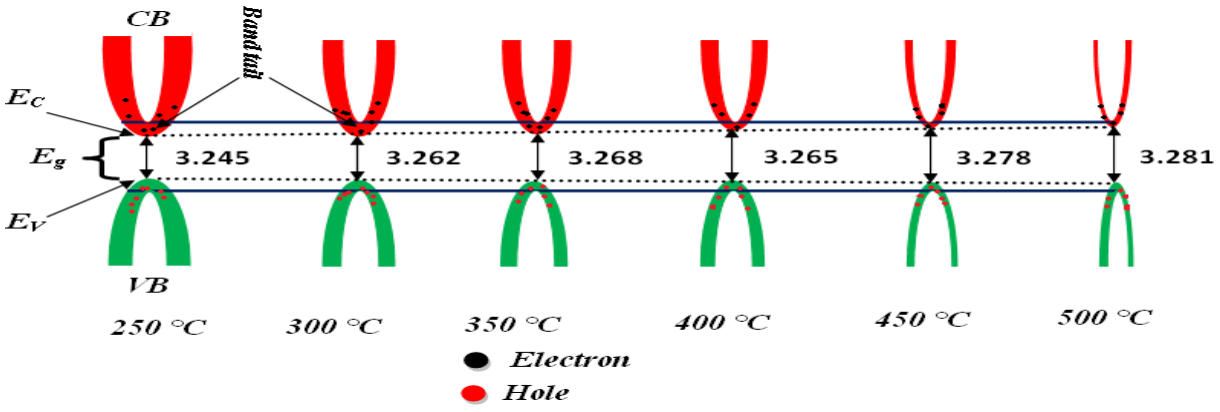

Figure 4.8: The description of the variation of optical band gap energy of ZnO thin films as a function of substrate temperature.

Bandgap broadening is important and advantageous for potential visible light photocatalytic applications involving metal oxide nanostructures. We can find a linear fitting for the proposed model to correlate the optical gap energy with Urbach energy for all substrate temperatures, the proposed model is expressed as (see Figure 4.9):

$$E_g = -0.4934E_u + 3.3034 \qquad (4.6)$$

From figure 4.9, we found that the broadening of optical bandgap should be explained by the narrowing in the conduction band E_c and the valence band E_V which causes the motion of E_c upward and E_V downward.

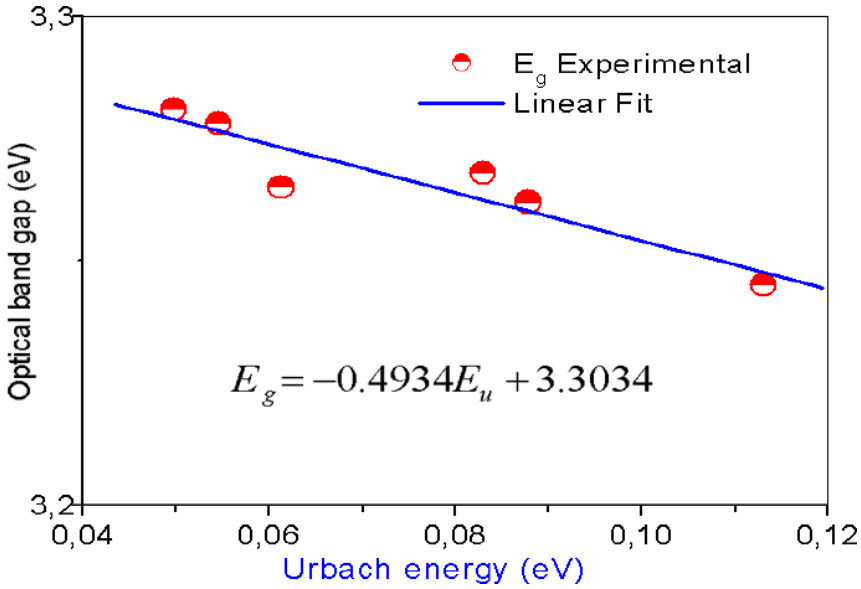

Figure 4.9: The correlation between optical band gap and Urbach energy of ZnO thin films.

IV.1.1.5.The electrical conductivity of ZnO thin films

Figure 4.10 shows the variation of electrical conductivity σ of ZnO films as a function of substrate temperatures. As it can be seen, for the small substrate temperature (T), the electrical conductivity of ZnO films was varied between 10^{-3} $(\Omega cm)^{-1}$ and 4×10^{-3} $(\Omega.cm)^{-1}$,

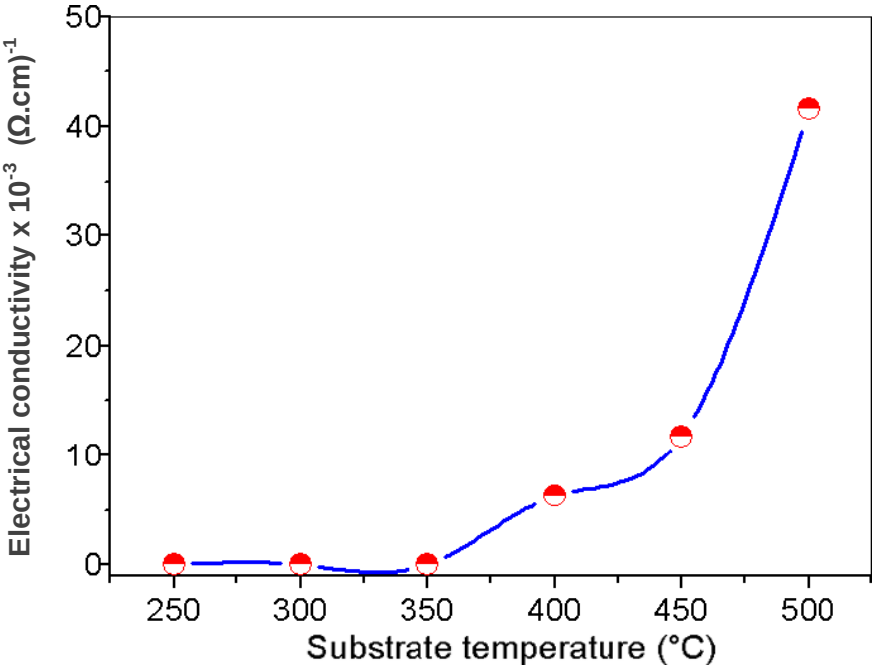

Figure 4.10: Variation of electrical conductivity σ of ZnO thin films with substrate temperature.

Then increases from 3.87 × 10^{-3} $(\Omega.cm)^{-1}$ to 41.58 $(\Omega.cm)^{-1}$ with the increasing of substrate temperature from 350 ^{o}C to 500 ^{o}C (see table 4.1).

Zaier et al [11]. studied the effect of substrate temperature on electrical and structural properties of ZnO films deposited by spray pyrolysis, and showed that the resistivity of ZnO films was decreased due to an increase in the regular sites of the Zn atoms in the film's network, which might be attributed to intrinsic donor defects such as donor vacancies and Zn interstitials and can also be due to increases in electron mobility. The increases in the electrical conductivity at longer temperatures are influenced by the oxygen diffusion with high crystallinity, which can be explained by decreasing of the potential barriers. This interpretation is consistent with the authors [12], who obtained similar results. This behavior is due to the increases of the crystallite size and less defects in the surface morphology of ZnO thin films. In order to increase the substrate temperatureto 700 ^{o}C the electrical conductivity of the film will increase until it reaches the optimum value.

IV.1.1.6.Conclusion

In conclusion, highly transparent conductive ZnO thin films has been deposited on glass substrate by Ultrasonic spray at different substrate temperatures from of 250 ^{o}C to 500 ^{o}C. The crystalline structure, conductivity and optical properties were investigated.

The DRX analyses indicated that ZnO films have polycrystalline nature and a hexagonal wurtzite structure with (100) and (002) preferential orientation corresponding to ZnO films was observed at high temperature.

The optimal values of the average crystallite size of the ZnO films under consideration are observed beginning at 350 ^{o}C of substrate temperature. All films exhibit an average optical transparency of about 85% in the visible range. The shift of optical transmittance toward higher wavelength can be shown by the increase of bandgap energy from 3.245 eV to 3.281 eV with increasing of substrate temperature of 250 ^{o}C to 500 ^{o}C. The observed Urbach energy of ZnO thin films decreases from 0.11311 eV to 0.04974 eV. At high temperature, the electrical conductivity of ZnO films was increased from 3.87×10^{-3} $(\Omega.cm)^{-1}$ to 41.58 $(\Omega.cm)^{-1}$ with the increasing of substrate temperature from 350 ^{o}C to 500 ^{o}C.

IV.1.2.Part two - Effect of dopants on ZnO thin films

Nowadays, the effect of several technological parameters (zinc source and concentration, dopant type and concentration, solvent, growth temperature, etc.) on the properties of sprayed ZnO films have been studied [13,14] to determine the optimal deposition conditions to obtain as high electrical conductivity and optical transparency as possible.

Earlier studies have shown that the preferred crystallite orientation of intrinsic ZnO and flourine and aluminum-doped ZnO is along c-axis [15, 16,17] while the preferred crystallite orientation of indium-doped ZnO film is (101) plane parallel to the substrate [18,16,19]. The use of F or Al as a dopant leads to smaller grains than the use of In as a dopant [13, 18, 16]. Additionally, the density and the optical transmittance of sprayed ZnO film is controlled by the dopant type and concentration [18]. It has been reported that an optimal growth temperature for sprayed ZnO films is in the range of 350–500°C. Independent of dopant, the optical transmittance is about 85% [18, 16, 20, 21] while the lowest resistivities of sprayed indium-doped and gallium-doped ZnO thin films are in the order of 8×10^{-4} Ω.cm [20, 22] and in the order of 10^{-3} Ωcm for aluminum-doped ZnO [21].

Among mentioned technological parameters, the solution spray rate (or solution flow rate) and its effect on ZnO thin films have received little attention. Ebothé et al. [14]. Recently, we showed that the electrical resistivity of chemically sprayed In-doped ZnO thin films grown at 400°C can be altered within an interval of 10^{-2} – 10^{-3} Ω.cm by varying the solution spray rate [19]. In this study we will not focus on obtaining the highest electrical conductivity or optical transmittance; we study the effect of the concentration rate of dopant on the structural, morphological, optical, and electrical properties of ZnO:Al and ZnO:F thin films deposited by ultrasonic spray pyrolysis. The aim is to find the optimal concentration rate to deposit transparent and conductive AZO, FZO thin films. The experimental set-up has been previously described in chapter II.

IV.1.2.1.Effect of Aluminum doping on ZnO thin films

Many factors strongly influence both the physical and chemical properties of ZnO films, such as the type of doping, film thickness, substrate type and the growth temperature.

Recently, several studies have focused on the influence of doping levels on the electrical properties of the films [23]. More recently, Doped ZnO films revealed electrical and optical properties similar to indium tin oxide (ITO) films. However, they take more advantages than ITO due to good stability at high temperatures and lower cost to manufacture [24].

In our work, ZnO: Al films have been studied for looking at the influence of the Al doping concentrations on the optical, structural and electrical properties.

IV.1.2.1.1.Thickness calculation

From transmission spectrum the thicknesses of aluminum doping ZnO thin films are observed between 160 nm and 550 nm. It is clear that the concentration of aluminum doping has a strong effect on the increment of thickness, whereas taking a highest value 554,78 nm at 5 at% of aluminum doping, due to the increment in the concentration of aluminum that leads the increasing in Al ions [25].

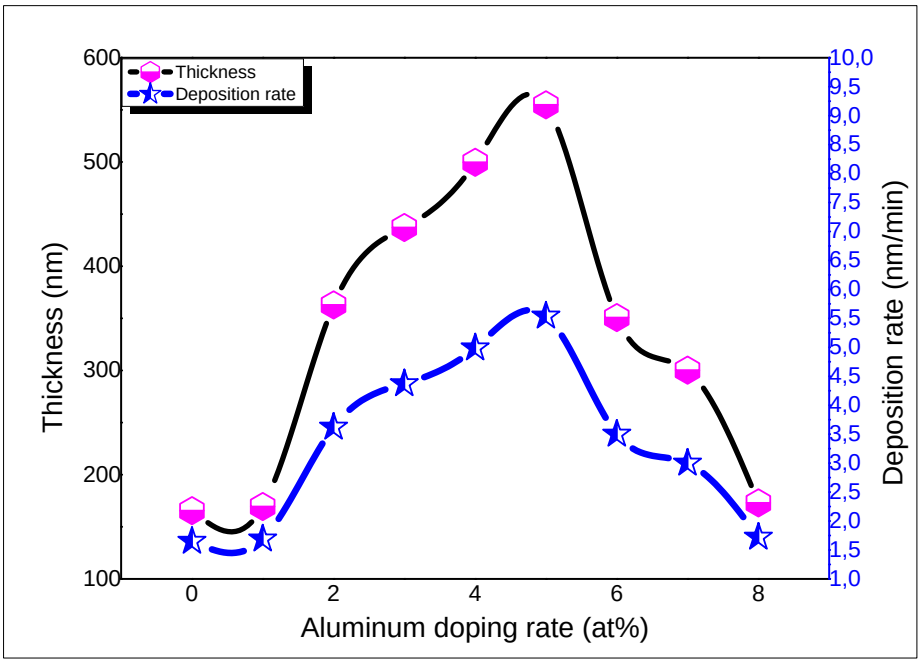

Figure 4.11: The thickness variation and deposition rate graph of ZnO: Al.

after that, the figure shows film thickness decrease as the aluminum doping increase, we can explain this by increasing the grain size obtained gradually decreased (see figure 4.11), which return into two possible reasons: the disturbance of grain growth due to the difference in ion radius between zinc and aluminum or the increasing number of nucleation leading to the formation of small grains during incorporation of the dopant into the host material [26].

IV.1.2.1.2.The crystalline structure of ZnO: Al thin films

The crystal structure and crystallinity of the prepared AZO thin films were characterized by X-ray diffraction (XRD) with CuK_α radiation (k = 0.154056 nm). Figure 4.12 shows the XRD spectra of the AZO samples at different concentrations of Al. The spectra showed very sharp diffraction peaks that indicate high crystallinity [27], The sharp diffraction peaks corresponding to (100), (002) and (101) planes indicate the crystalline ZnO with hexagonal wurtzite structure, which are in close agreement with the standard card (JCPDS Code No. 36-1451). Whole of AZO thin films exhibited an intensive hexagonal ZnO (002) plane. Though, the apearance of any secondary phase means a decrease on the diffraction peak intensity of Al doped ZnO thin films. As the Al concentration rate increases the intensity of diffraction peaks decrease profoundly and this may be attributed to the defects of the crystalline structure due to the incorporation of aluminum, However, the peaks intensity decreased with the further increase in Al doping concentrations except the (002) diffraction peack is going optimum compare the others, where It is clear from the XRD pattern that, when the Al doping level increases the orientation of ZnO thin films changes from (101) reflection peack to (002) peack, The intensive diffraction from (002) plane indicate that the growth direction of Al doped ZnO thin films is oriented along *c*-axis. The similar observation has been indicated by many authors [28, 29].

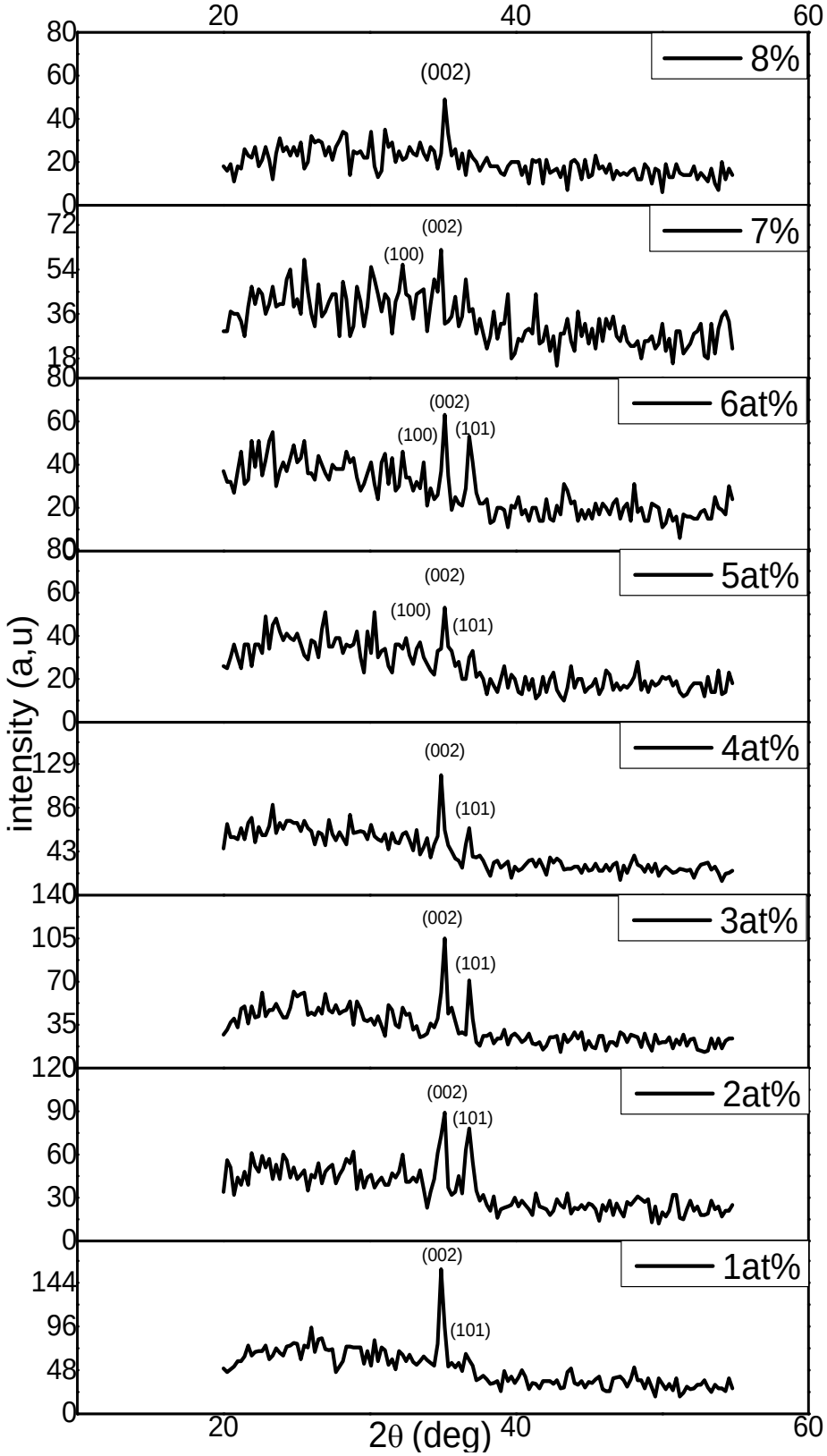

Figure 4.12: Evolution of the X-ray diffraction spectra of ZnO thin films as a function of Al doping rate.

The redirection of the reflection peak from (101) to (002) peack causes by increasing of the stress in the lattice. When we know, that the ion size differences between Al^{3+} (0.054 nm) and Zn^{2+} (0.060 nm), this phenomenon was expected [30]. As well as the formation, separation or segregation of aluminum in the grain boundaries at higher doping concentrations [31].

The average crystallite size of undoped and ZnO doped thin films is showing in figure 4.13 with Al atomic concentration from 0 at% to 8 at%, and are estimated using Scherre's formula.

Improvement of structural quality of the AZO thin film reached on the lowest value of the full width at half maximum (FWHM) of the (002) peak, the grain size of the films are increased with the increasing in doping atomic percentage of Al up to 5 at% where it take a high value of 35.80 nm, and when the Al concentrations are lower than 5 at%, we observed that the grain size decreased, indicating thereby that the number of the crystal depends on the microstress within crystallite size [32].

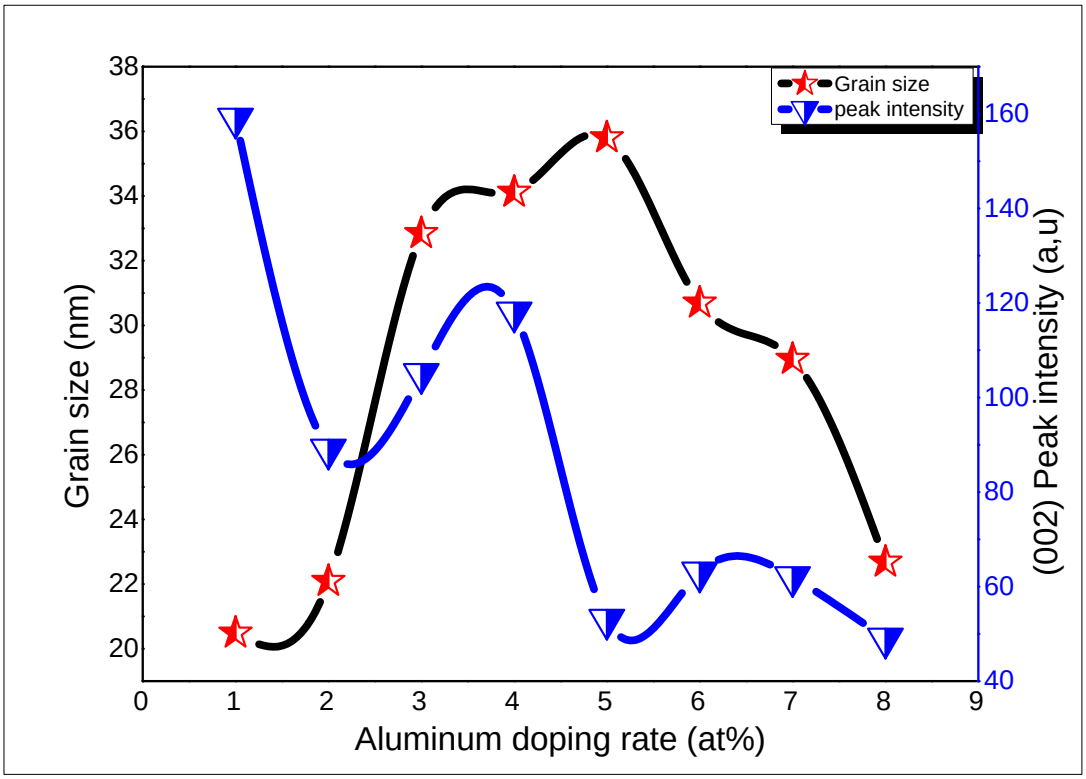

Figure 4.13: The variation of grain size and (002) peak intensity of ZnO doped Al thin films.

The corresponding (002) peak location, full width at half maximum of X-ray diffraction spectra, stress and crystallite size are listed in Table 4.2.

Table 4.2: Results of ZnO doped deposited with different Aluminum rates.

Doping Al (at%)	FWHM (°)	2 θ_{hkl} (°)	Grain size (nm)	Plane (hkl)	stress (GPa)
1	0,41373	34,88	20,490	002	-2,565
2	0,384	35,12	22,091	002	-1,33
3	0,25827	35,12	32,845	002	-1,05
4	0,2419	34,88	34.125	002	-1,565
5	0,23692	35,12	35,805	002	-1,002
6	0,27637	35,12	30,694	002	-1,03
7	0,29299	35,12	28,953	002	-1,15
8	0,37394	35,12	22,685	002	-1,036

the grain size of our AZO thin films is found to decrease due to the grain growth during processing is blocked by resistance of the motion of the grain boundaries via the secondary phases, Al_2O_3, which should have occurred at high doping of Al. When the motion of the grain boundaries are prevented by secondary phase, they give a retarding force on the boundaries and this force resist the driving force of grain growth hence the crystallite size gets decreased [33].

And this what the curve of the stress described (figure 4.14), as well from figure of X-ray diffraction we observed that there is a variation of the position of (002) peak from 34.88^o to 35.12^o.

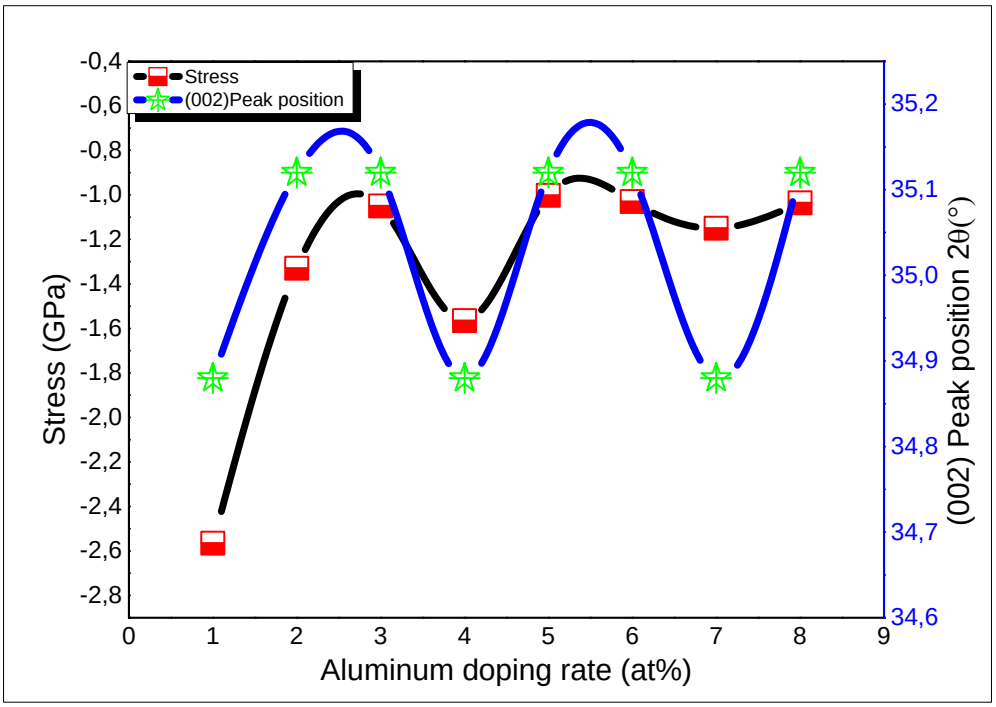

Figure 4.14: The variation of stress and (002) peak position of ZnO doped with different Al concentrations.

Which means and confirms that stresses of our Zinc oxide thin films are compressive stress, those stress are defined to be which grow through the deposition process, many mechanisms generating compressive stress result in a variation in quantity that produce stresses due to the force of the substrate or other layers [34], the latest affect directly on the grain size; where the grain edges and their increasing leading increasing compressive stress this what being clear in the Al doping rate up to 5at%. Moreover, the XRD patterns show clearly that the secondary phase of Aluminum Al_2O_3 be occur among grain edges towards the (110) orientation, which may be the cause of increase in the stresses depending on the Aluminum concentrations [5].

IV.1.2.1.3.The microstructural and morphology properties

Scanning electron microscopy analysis revealed that the structural properties of the AZO films were found polycrystalline with a hexagonal wurtzite-type structure. The

Morphologies of ZnO thin films prepared with different doping concentration of Aluminum from 1 to 8 at% aluminum are shown in Figures 4.15: A.B.

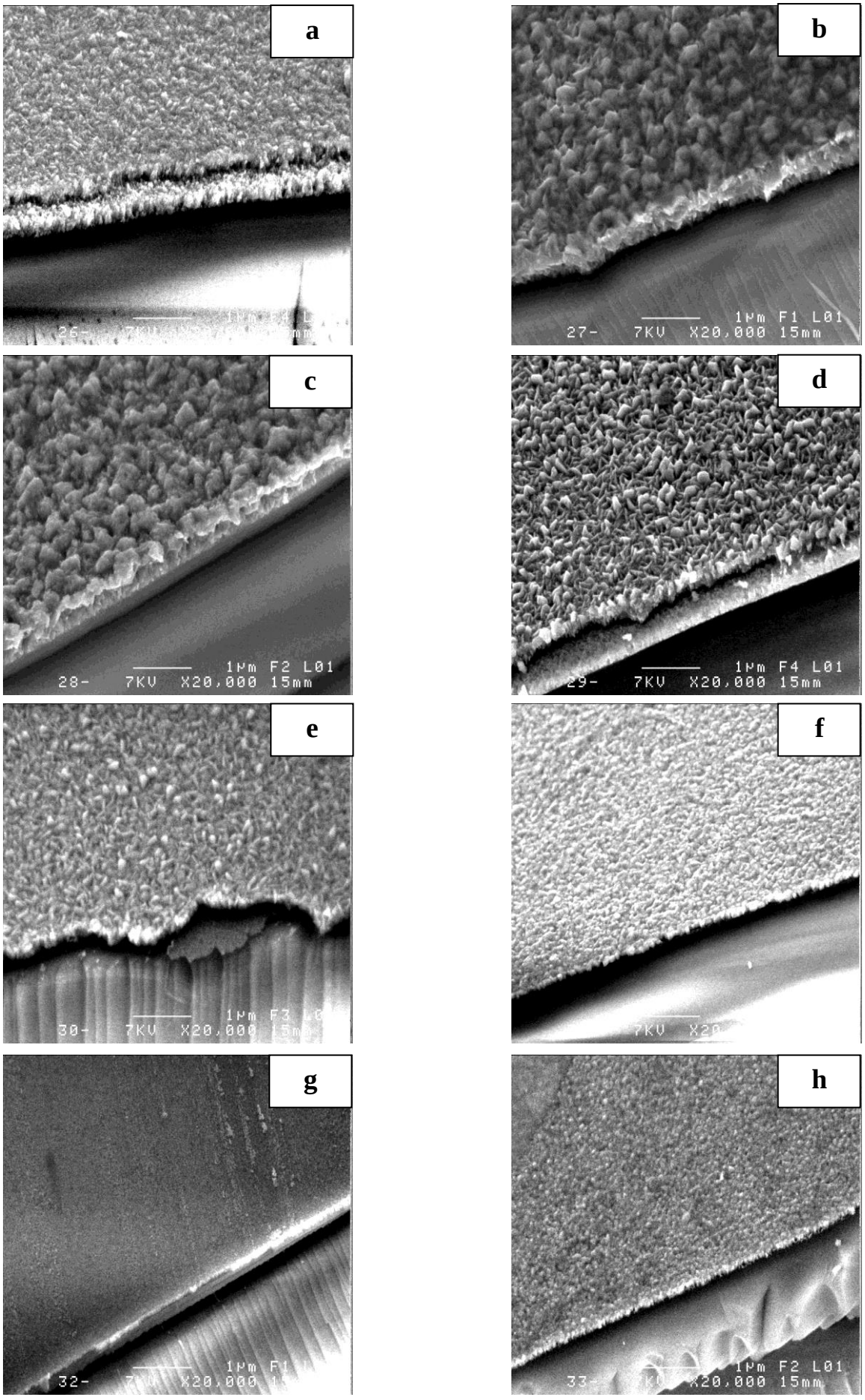

Figure 4.15.A: SEM images at level of 1 µm for ZnO doped Al from 1at% to 8at% respectively.

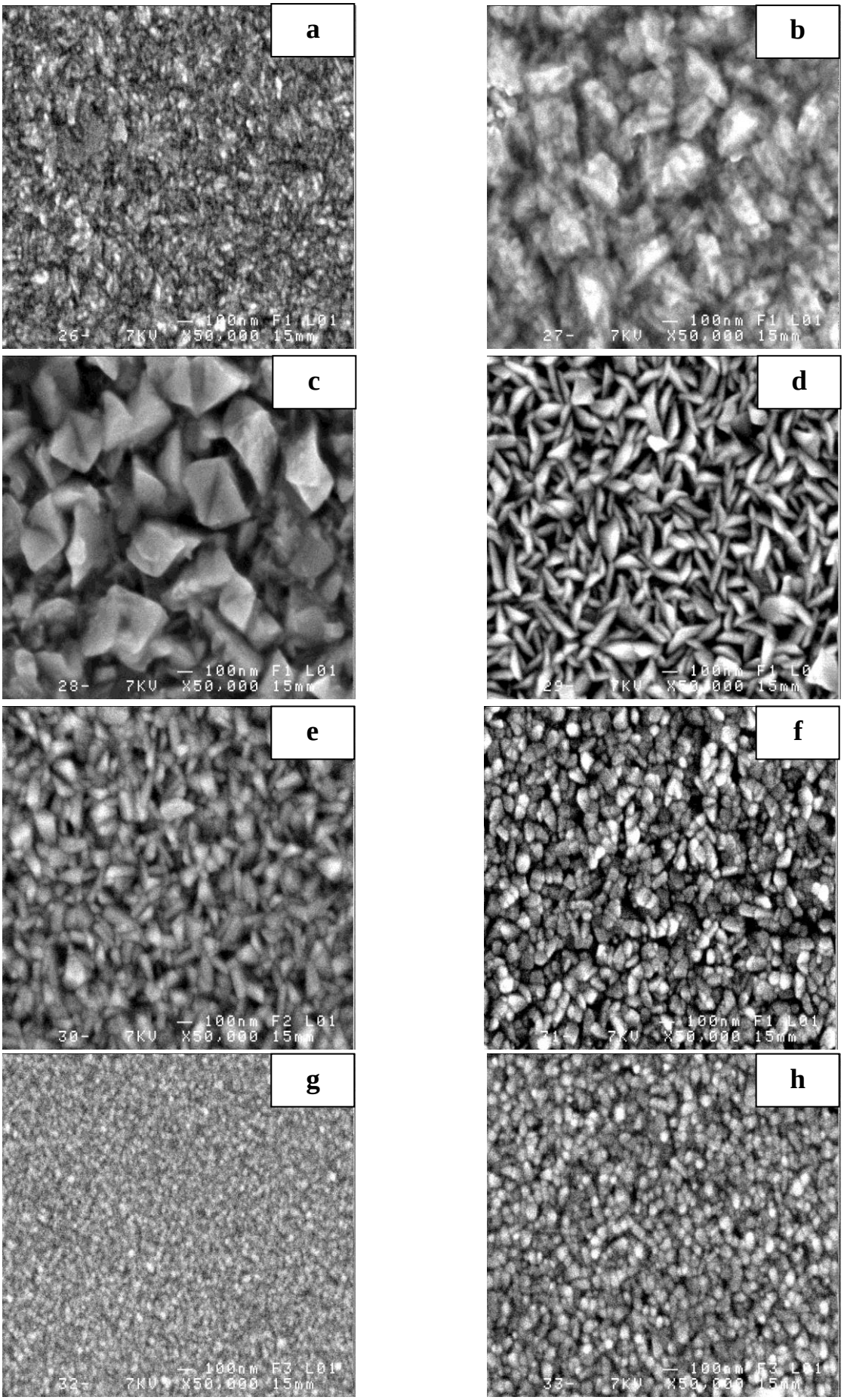

Figure 4.15.B: SEM images at level of 100nm for ZnO doped Al from 1at% to 8at% respectively.

These SEM images show that the surface morphology of the films is strongly dependent on the doping rate of aluminum.Films exhibit a granular surface morphology with a grain size notoriously increase and dense microstructure are observed in Figure.4.15(A,B) for the whole of ZnO thin films. In addition to that the pyramid-shaped grains were observed at aluminum concentration rate of 2 at% and 3at%, When the doping concentration is 1 at%, 6 at%, 7at% and 8at% the films exhibit a dense microstructure and the spherical crystalline particle size is approximately 20 nm; whereas the particle size decreases lead the films become denser. The surface morphology of 5at% and 6at% doped films are similar with average of particle size of about 30 nm, however the difference in the surface morphology may be due to a high difference in ionic radius between zinc and aluminum [35].

Nevertheless, we can see that the increase of the number of the spherical like features is obvious from 1 to 8 at% of aluminum doping rate, except at 4at%, 5at% and 6at% of aluminum doping. In the three cases, the results can be return to two reasons the first one due to the different spherical like features ZnO with different diameters have been reported [36], sconde one the increment in particle size due to the formation of stress resulting from a high difference in ionic radius between aluminum (0.057 nm) and zinc (0.074 nm) [35].

SEM micrographs of the surfaces for foursamples of AZO thin films and the Energy X-ray Dispersive Spectroscopy (EDS) spectra of their chemical composition are shown in following Figure 4.16.

The aim from using this technique (EDS) is a confirmation of the existence of Al. Where, All spectra show the presence of this element from doping, where has been an increase in the percentage of Al with increasing doping rate.

However in the surface of the films EDS analysis showed that these particles have the same composition, as well as the presence of such particles contributes to the increase of the roughness of the film surfaces.

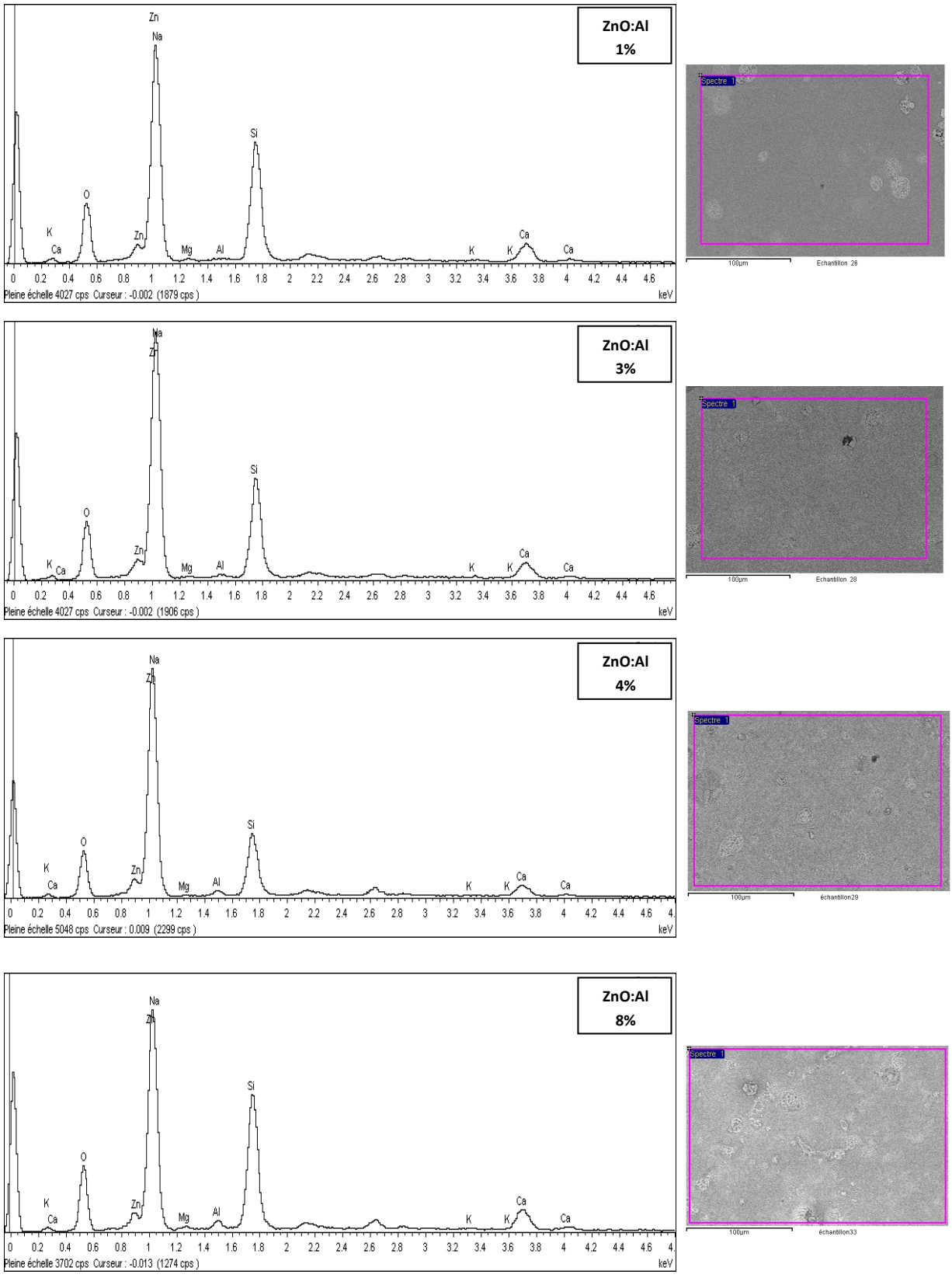

Figure 4.16: Energy X-ray Dispersive Spectroscopy spectra of four samples of AZO

IV.1.2.1.4.The optical properties of ZnO: Al thin films

The optical transparency of the ZnO: Al thin film is one of the important factors which need to be taken into consideration for a better TCO. The percentage of transmission is measured using UV-Vis Spectrophotometer.

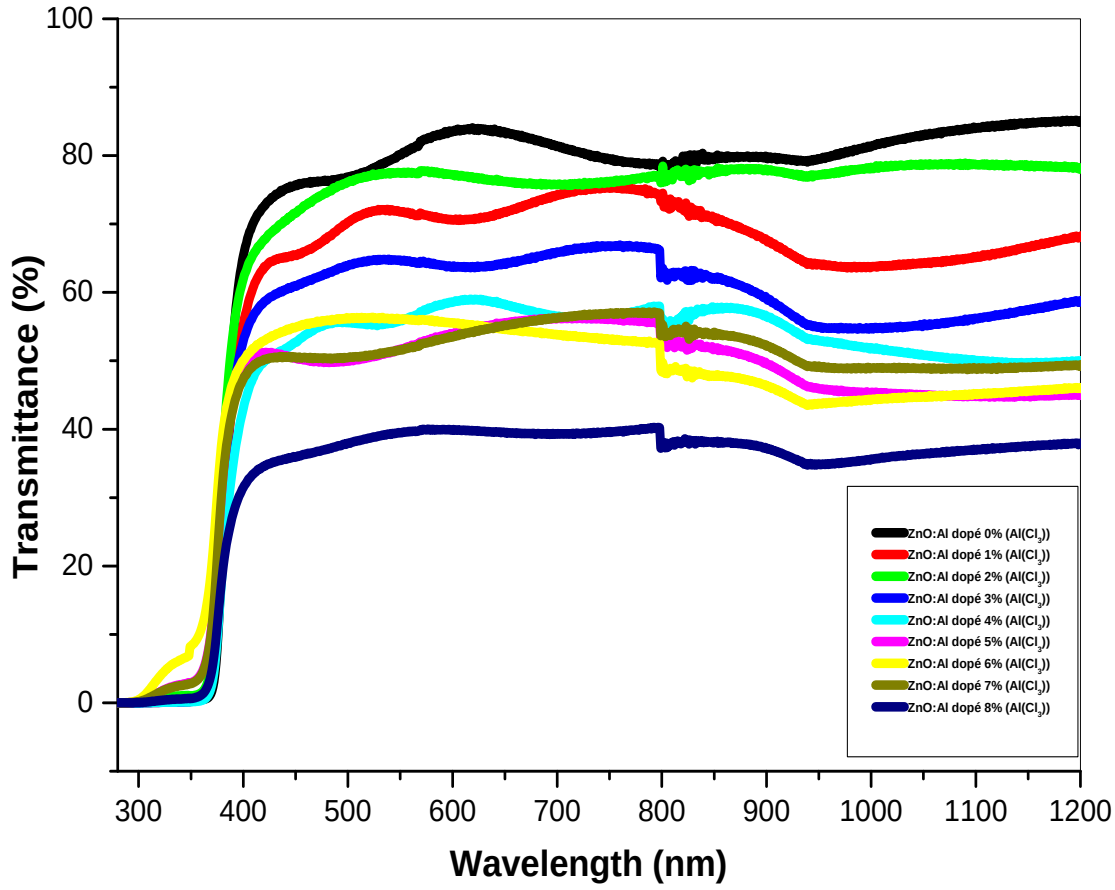

Figure 4.17: Variation of the transmittance of the ZnO films doped with Al depending on the wavelength.

The transmittance spectrum of undoped – doped ZnO thin films in the wavelength range 300-1000 nm are shown in the figure 4.17, optical properties of the zin oxide thin films were studied with the help of transmission spectrum in the UV-visible region. The spectrum shows a maximum transparency bigger than 80% at wavelength about 600 nm and 75% at wavelength about 500 nm for undoped ZnO and ZnO doped with Al percentage of 2 at%. From the transmittance spectrum we observed that the transparency of our AZO thin films

was reduced, with increaring Al doping, that can be explained by existence of Al atoms among grain boundaries, which prevent of grain growth size for extensively, that leads to diminish of the crystallinity growth [33].

Based on the location of the absorption edge of about 350 to 400 nm, the optical energy gaps appeared in the range from 3.27 to 3.38 eV for ZnO and the AZO thin films.

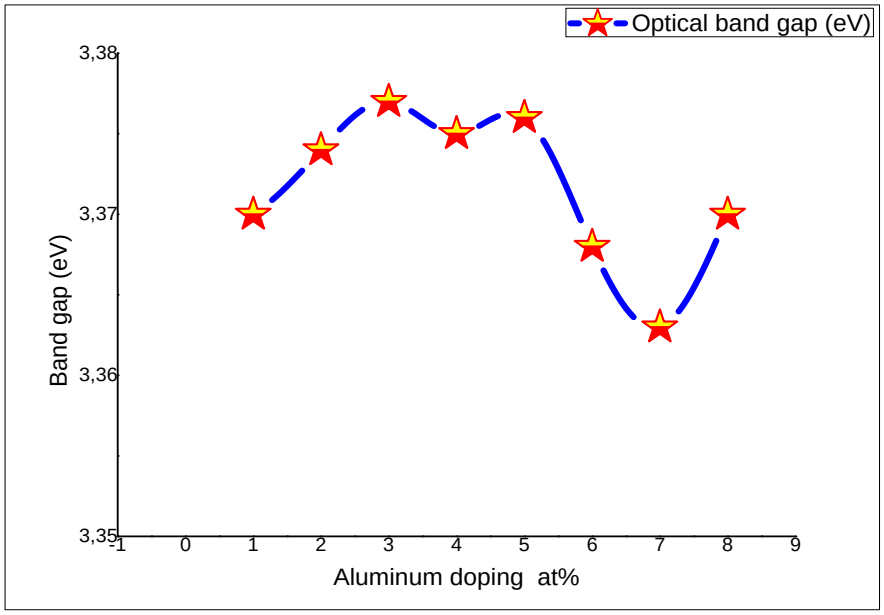

Figure 4.18: The variation of optical band gap of ZnO doped with different Al concentrations.

At first the energy gap E_g increased when the Al concentration was increased up to 5 at% then decreased when the Al doping was more than 5 at%, this result has been indicated by other authors [37, 38].

The variation of direct band gap for different Al doping concentration was shown in figure 4.18, and from the curve the increment in band gap was observed, when the concentration was changed from 1 to 5 at%, this result might be due to the effect of energy gap widening, which is apeared the shifts of the optical band gap to 3.39 eV, this can be explained by the effect of Burstein-Moss, which is occured during the Al doping of ZnO because the aluminum atoms replaced Zn in the ZnO lattice. The aluminum atoms behave as donor ions, where provide one extra electron, this electron occupied the bottom of the conduction band. Thus, the number of electrons increased as the doping concentration was increased; thereby the optical band gap become wider [39].

IV.1.2.1.5.The electrical conductivity of ZnO :Al thin films

The deposited ZnO: Al thin films as described above are measured for the sheet resistance using 4-probe measurement device. Later, the conductivity of the material is calculated.

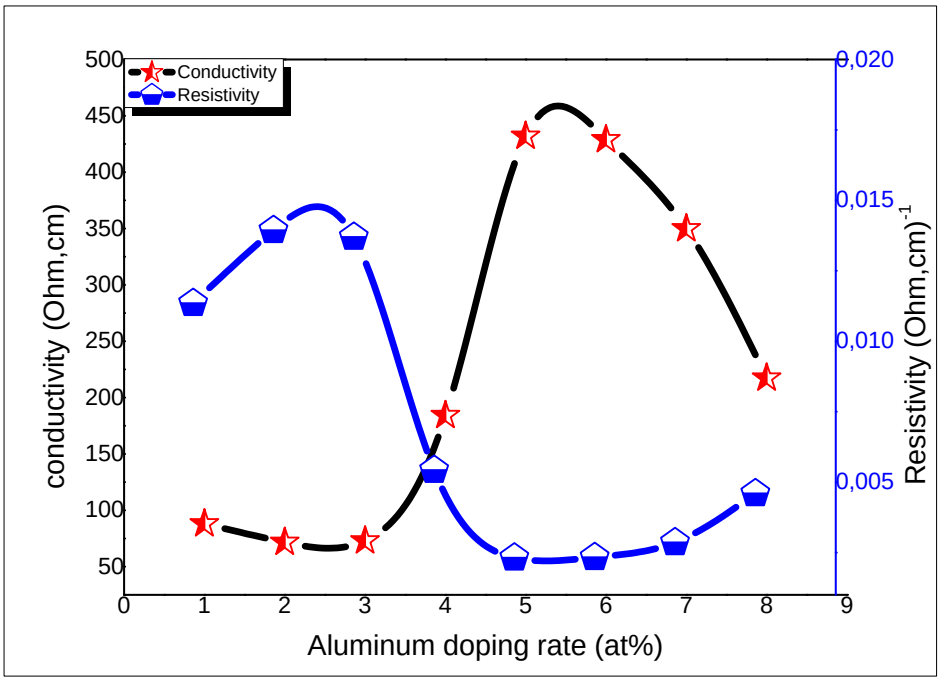

Figure 4.19: The variation of electrical conductivity of ZnO doped at different Al concentrations.

Many various applications in transparent conducting films required that electrical conductivity should be as high as possible. This is particularly important for solar cell applications because high optical transmission in the visible region enhances the photogenerated current and low sheet resistance reduces the series resistance of the cell, but in many applications of transparent conductive films either the electrical or optical properties are more critical [40].

Figure 4.19 shows the change in the electrical conductivity of undoped ZnO and doping with aluminum for (1 to 8 at%). The effect of Aluminum doping on the electrical conductivity was obtained at differents doping percentages and it was shown in figure 4.19 that doping had a significant effect of the electrical conductivity of ZnO doped with aluminum. in our experiments ZnO films showed that the electrical conductivity increase with increasing the concentration of Al in ZnO thin films, where at 5at% of Al doped ZnO showed 4.31×10^{2} $(\Omega.cm)^{-1}$.

The increase in conductivity with Al doping is due to the fact that Al^{+3} going into Zn^{+2} sites will have one extra electron and these electrons were used as conduction electrons [13,41]. where the aluminum atoms compensate the Zn locations in the Al_{zn} lattice acting as donors as shown in the following formula:

$$Al^{3+} \longrightarrow Al^{2+} + e$$

Al^{2+} occupies the locations in the ZnO lattice and (e) the free electrons that participate in electrical conductivity. When doping with aluminum from percentages of 1at% to 5at% there was an increase in the electrons with the increase in the values of mobility ; The results indicate that the increase in the percentages of Al doping to 5 at% has lead to the increase in the donor levels and which in turn led to an increase in the number of atoms that donate electrons and become ions, the value of electric conductivity of thin films is changed from 0.60×10^{2} $(\Omega\cdot cm)^{-1}$ for ZnO undoped to 4.31×10^{2} $(\Omega\cdot cm)^{-1}$; in case of ZnO doped with 5 at%. And if the percentage of Al doping is more than 6 at%, the crystallite size became smaller, with increasing Al contents, this results an increasing the grain boundaries, which makes the structure more deteriorated, and then the electrical conductivity go to the lowest values [39].

IV.1.2.1.6.Conclusion

Al-doped ZnO (AZO) thin films were deposited on glass substrates; the influence of the doping level of the ZnO: Al films were investigated. The results of X-ray diffraction and scanning electron microscopy analysis revealed that the structural properties of the AZO films were found polycrystalline with a hexagonal wurtzite-type structure along the (002) plane. The grain size of the AZO films was observed as approximately 30 nm in the film doping with 5 at% ZnO :Al concentration. The thin films also exhibited an optical transmittance as high as 85% in the wavelength range of 350 – 1000 nm. There is a diminish in the optical band gap from 3. 38 to 3. 27 eV. Based of four probes studies, the lowest resistivity (2.32×10^{-3} Ω.cm) was observed for the film doping with 5 at% ZnO: Al concentration. These results showed improvements in the properties of AZO thin films.

IV.1.2.2.Effect of fluorine doping on ZnO thin films

A renewed interest in the study of zinc oxide thin films exists due to the simultaneous properties of low resistivity and high transmittance besides chemical stability under strong reducing environments. Despite the extensive investigations on this material, there are still some unknown points related with the effect of fluorine doping in the transport, structural and electrical properties.

The case of fluorine doped ZnO thin films is an example for this. Apart from the academic interest, the fluorine doping has several potential advantages over the well-known and successful In-doping, such as low cost and abundance. More over fluorine does not introduce significant perturbation into the conduction band, due to the size compatibility of the oxygen and fluorine atoms.

IV.1.2.2.1.Thickness calculaion

The Thickness of thin films, has varied clearly, with the flourine doping concentration as shown in figure 4.20. When there is an increasing with increasing of flourine presentaion in the films up to 467,57 nm then decreasing to the lowest value 170,43 nm at maximum flourine doping rate.

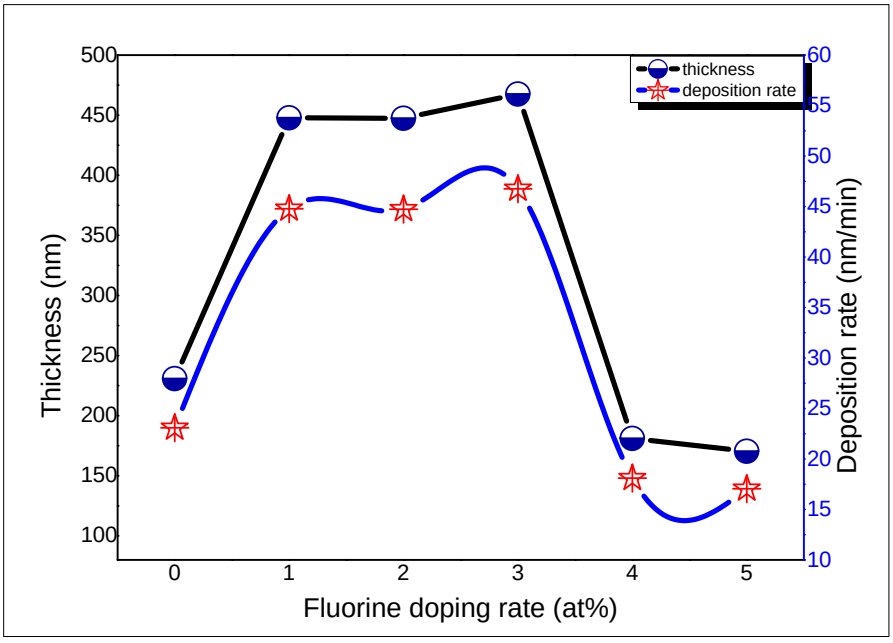

Figure 4.20: The variation of thickness and deposition rate graph of ZnO: F.

Probably, the substutation of fluorine atoms in the Zinc atoms sites initially, this leads an increase in film thickness and that means the film growth remains towards a *c*-axis perpendicular to the substrate (this obvious in the X-ray spectra), and may be the substrate temperature afficiency at substrate surface with the lowest fluorine doping percentage, and thereby favorable growth occur, then the extent of non-stoichiometry occur on the top of the films, which makes random growth of the films [42], which leading the films thickness into the lowest value (170,43 nm) when the fluorine concentration is more than 4 at%.

IV.1.2.2.2.The crystalline structure of ZnO:F thin films

X-ray diffraction patterns are used to study the crystal structure and orientation of undoped and fluorine doped ZnO thin films**.** Figure 4.21 depicts the X ray diffraction pattern for ZnO: F thin films:

All the peaks correspond to the hexagonal wurtzite structure of ZnO. For undoped ZnO and fluorine doped ZnO films, the dominant diffraction peak at around $2\theta = 34.50°$ and is very close to the standard bulk ZnO crystal, that means 2θ value is not much changed with the doping concentration of fluorine, similar struture has also observed by Maldonado et al using spray pyrolysis method [43], taking into consideration the preferential growth shown in figure 4.21, it can be concluded that fluorine incorporation in the ZnO thin films with F^{-1} are substituted at O^{-2} sites without changing the ZnO structure as also reported by A. Sanchez-Juarez et al [44] using chemical spray pyrolysis and H.Liang et all [45] by chemical vapor deposition technique.

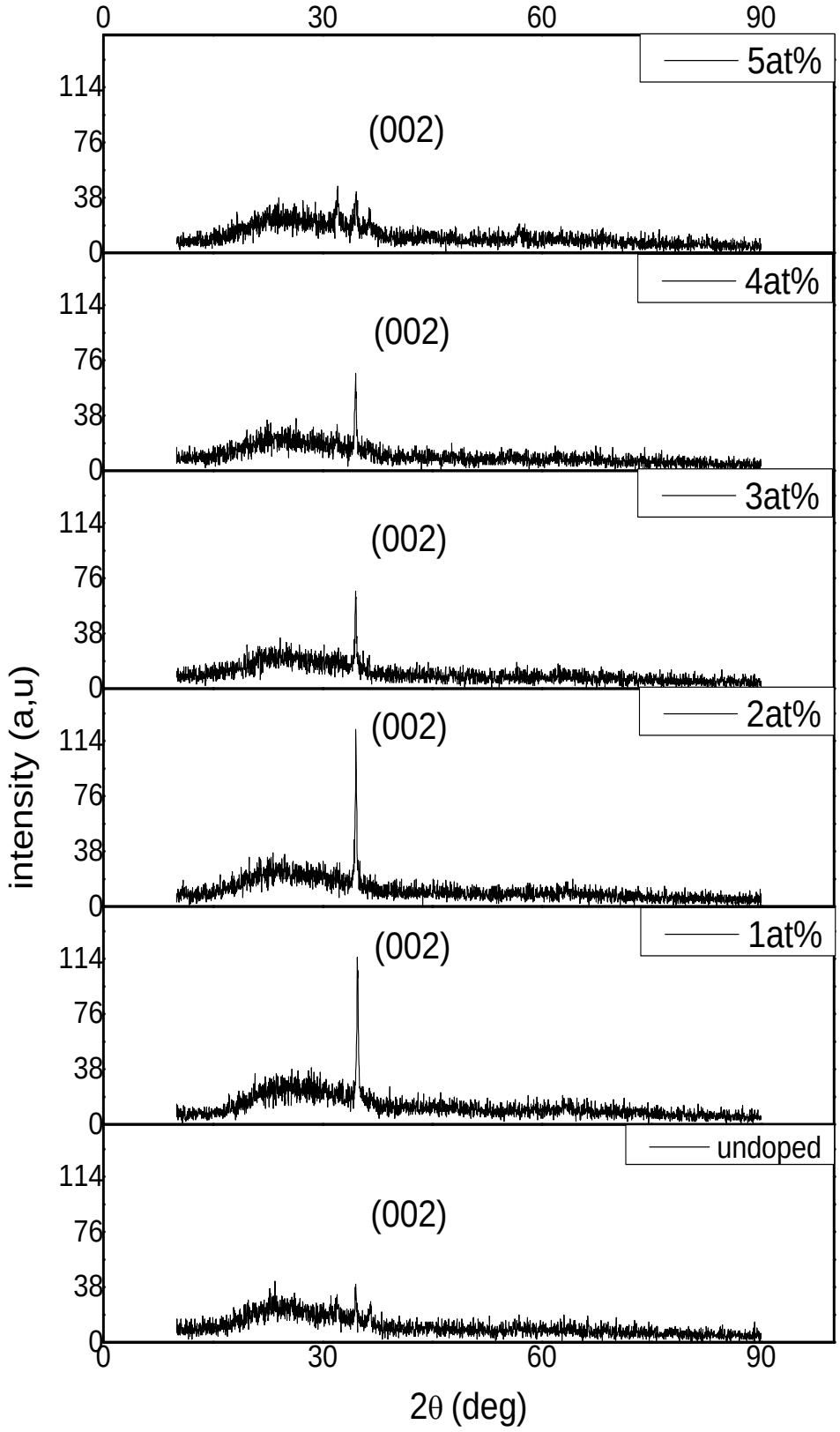

Figure 4.21: X-ray diffraction patterns for undoped ZnO and ZnO doped with different fluorine concentrations.

Whole of ZnO doped fluorine films show preferential growth along (002) diffraction plane irrespective of the doping concentration. At initial stage, the intensity of (002) peak was increased with F doping, reached to its optimum value for 2 at% and then suppressed for excess F doping, this indicates, on one hand, that fluorine doping deteriorated the crystallinity of ZnO thin films causing to be incorporated at the grain boundaries or at the film surface, the same results of deterioration in crystallinity with increase in F content observed by S. Ilican [46] above 10% of doping volume proportions prepared by sol gel method and B. N. Pawar [47] observed the similar above 4 at% doping, on the other hand, by the substitution process of O by F species and this process could only be partial leading to the formation of a specific configuration like ZnF_xO_{1-x} [48], this could be the reason for reduced intensity of XRD peak of ZnO: F thin films.

The average sizes of crystallites (G) were calculated from the full width at half maximum (FWHM) of the diffraction peaks from the (002) plane of the films with the help of Scherrer formula [49] (see chapter III).

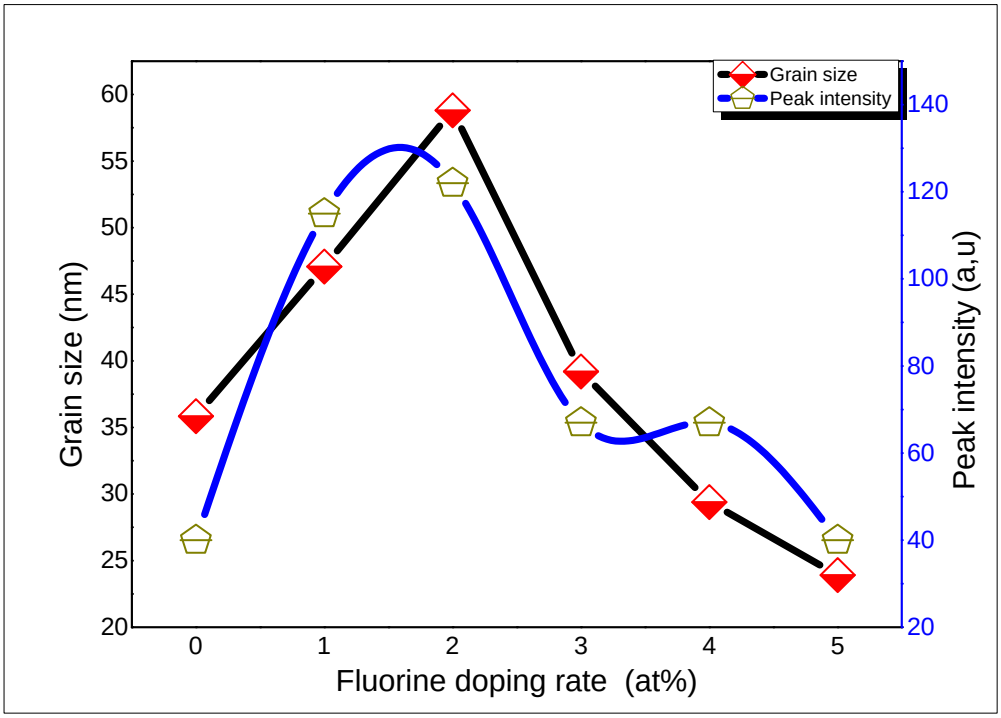

Figure 4.22: The average of crystallite size and peak intensity of FZO thin films.

The average crystallite size is between 23 and 58 nm were calculated for the fluorine doped ZnO thin films. It was found that the grain size of the FZO thin films increased with

increasing the concentration of the fluorine percentage, where take up to the highest value of 58,81 nm at 2 at%, and return to decrease this is obviously in figure 4.22.

Another important observation which is on the position corresponding of (002) peak, as we can see in the Table 4.3 where the diffraction peak was slightly shifted to lower 2θ values, 34.54 ° to 34.78° at very high doping concentrations as shown in figure 4.23, while it remained unaffected at lower concentration.

Table 4.3: Results of doped ZnO deposited with different fluorine rates.

Doping F (at%)	FWHM (°)	2 θ_{hkl} (°)	Grain size (nm)	Plane (hkl)	stress (GPa)
0	0,236	34,540	35,85	002	-0,991
1	0,18	34,785	47,08	002	-4,246
2	0,144	34,558	58,81	002	-1,234
3	0,216	34,530	39,20	002	-0,868
4	0,288	34,501	29,40	002	-0,502
5	0,3542	34,593	23,914	002	-1,686

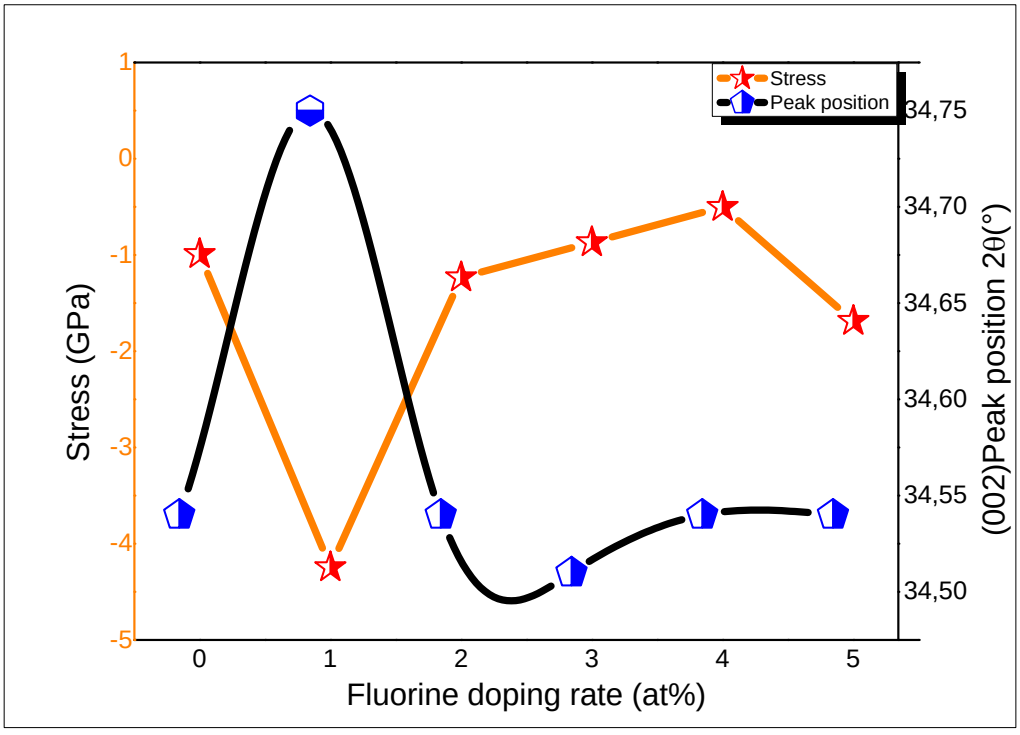

Figure 4.23: The variation of stress in ZnO thin film doped with different fluorine concentrations.

This variation of position of the diffraction peak is corresponding with increasing of lattice strain values from 0,50 to 4.24 GPa (see figure 4.23) along *c*-axis was also observed. The increase in lattice strain may be due to the increase in interstitial fluorine atoms at higher doping concentrations.

IV.1.2.2.3.The optical properties of ZnO: F thin films

Optical transmission spectra were recorded in the wavelength range 300-1000 nm from the figure 4.24, the transmission spectra as a function of the wavelength of the pure ZnO films and the ZnO films doped with (1, 2, 3, 4, 5%) fluorine, in the visible region with oscillations due to interference fringe pattern in transmission spectrum. This revealed the smooth reflecting surfaces of the film and there was not much scattering loss at the surface. Interestingly, ZnO doped fluorine 5 at% and undoped ZnO samples exhibited the highest optical transmission in the visible region, and this due to the increase in the concentration of doping fluorine which is improve the crystal structure. However, which the energy of the incident photon is low and the (ZnO:F) film is transparent to this range and the absorption is lowest.

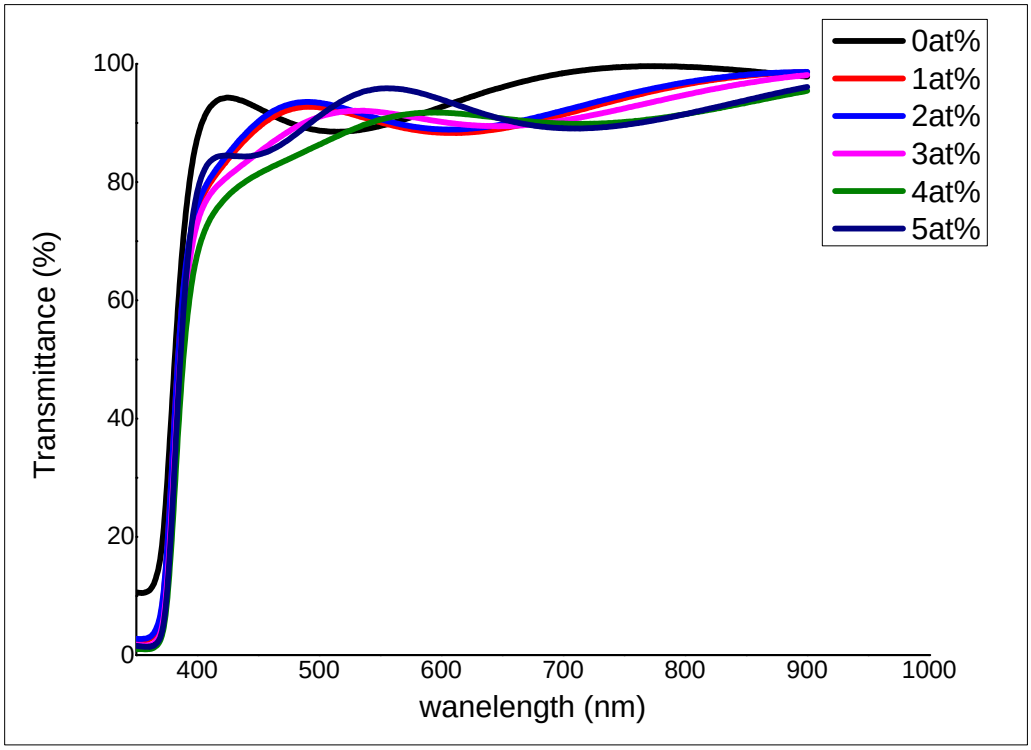

Figure 4.24: Transmission spectra of the pure ZnO thin films and the ZnO films doped with 1, 2, 3, 4 and 5% of fluorine concentrations.

We can see from the figure 4.24 that the increase in the percentage of fluorine added to the ZnO leads to the shift in the absorption towards the short wavelengths, a shift that is termed (Burstein-Moss) shift. This type of shift leads to an increase in the optical energy gap, the decrease of wave length, optical spectrum radiation, which indicates that these films have large energy gap to allow most of the visible light to pass. The results show that the transmittance is higher than 92 % in all thin films.

The optical energy gap (E_g) is defined as the lowest energy required for the electron to travel from the peak of the valence band to the peak of conduction band.

Optical band gap was determined from the plot of $(\alpha h\nu)^2$ vs $h\nu$, the following figure is showing the evaluation of energy band gap of FZO thin films:

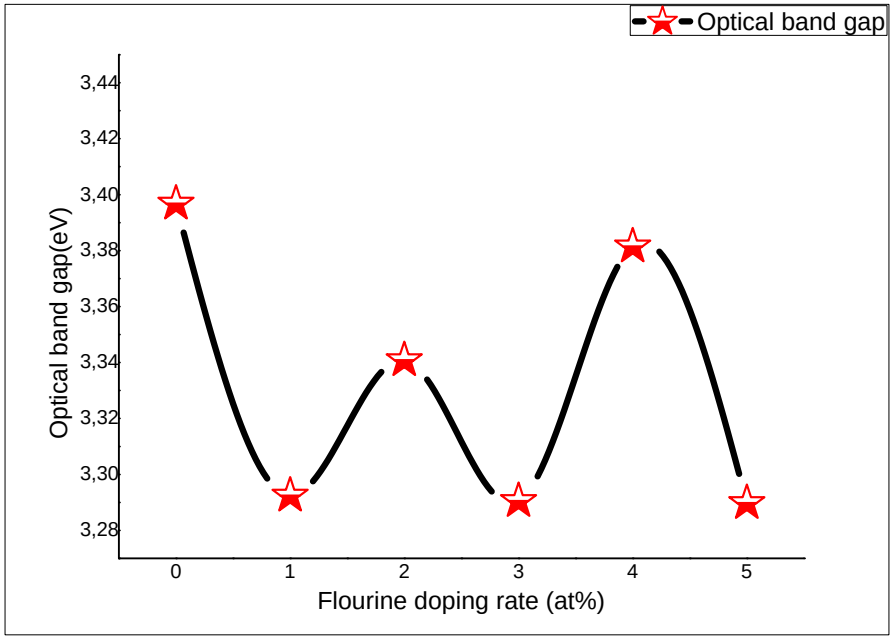

Figure 4.25: Optical band gap graph of ZnO: F

The variations of the optical energy gap the band gap energy values (E_g) slightly decreases while the concentration of doping increased from 2 to 5 at%, generally, it can be stated that the reduced band gap energy of FZO may be due to the extent of non-stoichiometry of the deposited thin films [42] .

IV.1.2.2.4.The electrical conductivity of ZnO:F thin films

To characterise the electrical properties of the thin films, at room temperature were employed, figure 4.27 presents the electrical behavior of the thin films as a function of the fluorine content, where we can observed that the highest electrical condutivity was achvieved

with the fluorine concentration of 5 at% correspoding to a resistivity of $5{,}9\times10^{-3}$ Ω.cm, The improvement in the electrical properties is attributed to the ionic radius of F (1.36 Å) is slightly lower than that of O^{2-} (1.40 Å).

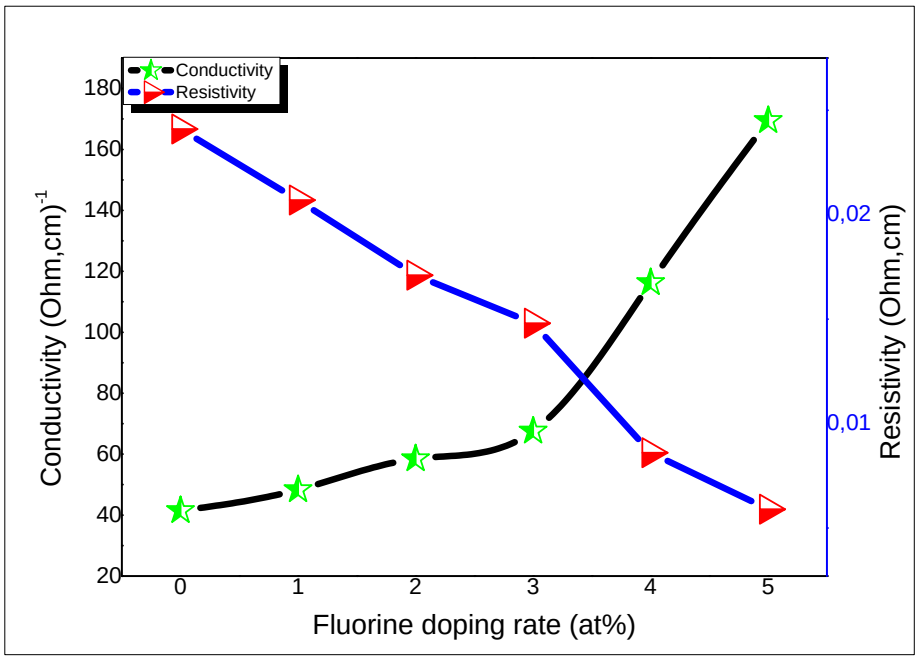

Figure 4.26: The variation of electrical conductivity with atomic doping rate of fluorine.

So when the fluorine atoms replace of oxygen provide one free electron/ molecule, therefore the hybrid orbital configuration of fluorine is $2S^2 2P^5$ and oxygen is $2S^2 2P^4$, so the fluorine atoms are more electronegative than the oxygen atoms, therefore the fluorine substitutes the oxygen sites more easily. That means a higher carrier concentration occur.
This behavior of doping in our ZnO thin films, suggesting that the electrical resistivity related inversely to the concentration of the fluorine [50].

IV.1.2.2.5.Conclusion

It is clear that, the effect of fluorine doping ZnO thin films on the structural, electrical, and optical properties is slightly obvious after our study. Where the FZO films deposited at different percentage of fluorine then characterized using a various methods.

The results of X-ray diffraction showed that FZO thin films have peaks correspond to the hexagonal wurtzite structure of ZnO. Where the intence diffraction peak is around $2\theta = 34.50°$ and is very close to the standard bulk ZnO crystal, that means 2θ value is not much

changed with the doping concentration of fluorine, after 2 at% of fluorine the grain size grows and surface becomes denser for all FZO films, the stuctural properties bring us to mentioned the electrical conductivity, we observed that, it has an increment as the fluorine doping increases, where took a highest value $1{,}68\times10^{2}$ $(\Omega.\mathrm{cm})^{-1}$ at doping with 5 at%.

IV.3.References

[1] B. Benhaoua, A. Rahal and S. Benramache, Superlattices Microstruct, 68 (2014) 38.

[2] N. A. Vorobyeva, M. N. Rumyantseva, R. B. Vasiliev, V. F. Kozlovskiy, Yu. M. Soshnikova, D. G. Filatova, V. B. Zaytsev, A. V. Zaytseva and A. M. Gaskov, 114 (2015) 198.

[3] S. Benramache, B. Benhaoua, N. Khechai and F. Chabane, Mat_er. Tech, 100 (2012) 573.

[4] M.Othmane, A.Attaf, H.Saidi, F.Bouaichi, N.Lehraki, M.Nouadji, M.Poulain, S.Benramache, International Journal of Nanoscience, 15 (2015) 1650007

[5] S. Benramache and B. Benhaoua, Superlattices Microstruct, 52 (2012) 1062.

[6] T. S. Moss, Proc. Phys. Soc. London B, 76 (1954) 775.

[7] S. Rahmane, M. S. Aida, M. A. Djouadi and N.Barreau, Superlattices Microstruct. 79 (2015) 148.

[8] S. Benramache, B. Benhaoua and O. Belahssen, Optik 125 (2014) 5864.

[9] V. Devi, M. Kumar, R. Kumar and B. C. Joshi, Ceram. Int. 41 (2015) 6269.

[10] A. Barhoumi, G. Leroy, B. Duponchel, J. Gest, L. Yang, N. Waldho® and S. Guermazi, Superlattices Microstruct. 82 (2015) 483.

[11] A. Zaier, F. Oum El az, F. Lakfif, A. Kabir, S. Boudjadar and M. S. Aida, Mater. Sci. Semicond. Process. 12 (2009) 207.

[12] K. Zhu, Y. Yang and W. Song, Mater. Lett. 145 (2015) 279.

[13] A. Hafdallah, F. Yanineb, M. S. Aida, and N. Attaf, Journal of Alloys and Compounds, 509 (2011) 7267–7270.

[14] J. Ebothé, A. El Hichou, P. Vautrot, and M. Addou, Journal of Applied Physics, 93 (2003) 632–640.

[15] M. Krunks, O. Bijakina, V. Mikli, T. Varema, and E. Mellikov, Physica Scripta, 79 (1999) 209–212.

[16] M. L. Olvera, H. Gómez, and A. Maldonado, Solar Energy Materials and Solar Cells, 91 (2007) 1449–1453.

[17] J. Wienke and A. S. Booij, Thin Solid Films, 516 (2008) 4508–4512.

[18] A. R. Babar, P. R. Deshamukh, R. J. Deokate, D. Haranath, C. H. Bhosale, and K. Y. Rajpure Journal of Physics D, 41 (2008) 135404.

[19] M. Vent, E. Kärber, T. Unt, A. Mere, and M. Krunks, Physica Status Solidi C, 9 (2012) 1604–1606.

[20] S. Major, A. Banerjee, and K. L. Chopra, Thin Solid Films, 108 (1983) 333–340.

[21] M. L. Olvera, A. Maldonado, R. Asomoza, R. Castanedo-Pérez, G. Torres-Delgado, and J. Cañetas-Ortega, Journal of Materials Science, 11 (2000) 383–387.

[22] K. T. R. Reddy, T. B. S. Reddy, I. Forbes, and R. W. Miles, Surface and Coatings Technology, 151-152 (2002) 110–113.

[23] C. A. Tseng, J. C. Lin, Y. F. Chang, S. D. Chyou and K. C. Peng, Applied Surface Science, 258 (2012) 5996-6002.

[24] H.W. Lee, S.P. Lau, Y.G. Wang, Journal of Crystal Growth, 268 (2004) 596–601.

[25] A. El Manounia, F.J. Manjón , M. Mollar , B. Marí , R. Gómez , M.C. López , J.R. Ramos-Barrado, Superlattices and Microstructures 39 (2006) 185–192.

[26] Hu J, Gordon RG: Textured aluminum-doped zinc oxide thin films from atmospheric pressure chemical-vapor deposition. J Appl Phys 72 (1992) 5381.

[27] Haller S, Rousset J, Renou G, Lincot D EPJ Photovoltaics, 2 (2011) 20401.

[28] T.V. Vimalkumar, N. Poornima, K.B. Jinesh, C. Sudha Kartha and K.P. Vijayakumar, Appl.Surface Sci. 257 (2011) 8334.

[29] S. Mandal, H. Mullick, S. Majumdar, A. Dhar and S.K Ray, J.Phys.D: Appl.Phys. 41 (2008) 025307.

[30] R. Sarvana kumar, R. Sathyamoorthy, P. Sudhagar, P.Matheswaran, C.P. Hrudhya and Yong Soo Kang, Physica E, 43 (2011) 1166.

[31] Zhou H, Yi D, Yu Z, Xiao L, Li J. Thin Solid Films 515 (2007) 6909–6914.

[32] Berginski M, Hüpkes J, Schulte M, Schöpe G, Stiebig H, Rech B . J Appl Phys. 101 (2007) 074903–079114.

[33] S. Suwanboon, P. Amornpitoksuk, A. Haidoux and J.C.Tedenac, J.Alloys Compd. 462 (2008) 335.

[34] J. W. Hutchinson, Division of Engineering and Applied Sciences, Harvard University, (1996).

[35] P. Nunes, E. Fortunato, P. Tonello, F. BrazFernandes, P. Vilarinho, R.Martins, 64 (2002) 281-285.

[36] Seyed Mohsen Mousavi, Ali Reza Mahjoub, Reza Abazari RSC Adv, 5 (2015), 107378-107388.

[37] Suchea M, Christoulakis S, Katsarakis N, Kitsopoulos T, Kiriakidis G.Thin Solid Films 515 (2007) 6562–6566.

[38] Baik SJ, Jang JH, Lee CH, Cho WY, Lim . Appl Phys Lett. 70 (1997) 3516–3518.

[39] Kim H, Gilmore CM, Pique A, Horwitz JS, Mattoussi H, Murata H, Kafafi ZH, Chrisey DB. J Appl Phys. 86 (1999) 6451–6461.

[40] M. Kul, A. S. Aybek, E. Turan, M. Zor, and S. Irmak, Solar Energy Materials & Solar Cells, 91 (2007) 1927–1933.

[41] D. H. Zhang, T. L. Yang, J. Ma et al. Appl. Surf. Sci. 158 (2000) 43.

[42] G. J. Exarhos. S. K. Sharma,Thin Solid Films, 270 (1995) 27-32.

[43] J. A. Maldonado, A. G. Santiago, M. Dela , L. Olvera, R. C. Perez, G. T. Delgado, Mater. Lett. 59 (2005) 1146–1151.

[44] A. Sanchez-Juarez, A. Tiburcio-Silver, A. Ortizc, E. P. Zironi, J. Rickards, Thin Solid Films. 333 (1998) 196±202.

[45] H. Liang, A. E. Roy, G. Gordon, J. Material Science . 42 (2007) 6388–6399.

[46] S. Ilican, Y. Caglar, M. Caglar, F. Yakuphanoglu, Applied Surface Science. 255 (2008) 2353–2359.

[47] B.N. Pawar, D. H. Ham, R.S. Mane, T. Ganesh, B. W. Cho, S. H. Han, Appl. Surf. Scien. 254 (2008) 6294–6297.

[48] A. El Hichou, A. Bougrine, J. L. Bubendorff, J. Ebothe, M. Addou and M. Troyon, Semicond. Sci. Technol. 17 (2002) 607.

[49] HP. Klug, LE. Alexaander, New York: Wiley; (1974) 662.

[50]P.V.Bhuvaneswari, P.Velusamy, R.R.Babu, S.M.Babu, K.Ramamurthi,M Arivanandhan,Mater. Sci. Semicond. Proc. 16 (2013) 1964–1970.

General Conclusion and perspectives

In this work we have demonstrated the existence of the common features of the growth of undoped and doped ZnO by two kinds of spray pyrolysis, our results were devided into two types the fisrt from the pneumatic spray pyrolysis the second from the ultrasonic spray pyrolysis technique, where we have studied the effect of pressure and its relation with variation of solution flow rate on Structural, optical and electrical properties of undoped ZnO thin films deposited using pneumatic spray pyrolysis. We conclude the properties become worse when the flow rate value is above 200 µl/min. and when the solution flow rate is bigger than 200 µl/min, we have observed that the solution flow rate value is more effective at low deposition pressure. And The X-ray diffraction spectrum indicated that the films were crystalline with hexagonal structure with the only diffraction peak. However, at lower pressure we estimate that highest transparance indicated about 95%. And the (002) diffraction peak was going to high intensity, with low solution flow rate, compare with higher pressure value.

In the other side of this thesis, thin films of undoped and doped zinc oxide were investigated using the ultrasonic spray pyrolysis, where we observed that undoped ZnO thin films have polycrystalline nature and hexagonal wurtzite structure with (100) and (002) preferential orientation at high substrate temperature, and all the thin films showed an average of optical transparency of about 85 in the visible range, then the increase of the optical band gap from the 3.24 eV to 3.28 eV lead a shift in the optical transmittance to highest value ,that when the substrate temperature increasing from 250 ^{o}C to 500^{o}C, also we can observe, that there is an increment on the electrical conductivity of ZnO films was from 3.87×10^{-3} $(\Omega.cm)^{-1}$ to 41.58 $(\Omega.cm)^{-1}$ when the substrate temperature increased from 350 ^{o}C to 500 ^{o}C. As for the other process when ZnO thin films are doped with aliminium and fluorine by ultrasonic spray pyrolysis, its clear that the effect of fluorine is slightly obvious on the ZnO thin films properties, compare to the ZnO doped by aliminium , where whole of AZO thin films were polycrystalline with a peaks (002) correspond to the hexagonal wurtzite stucture, with diffraction peak of about 34^{o} on X-ray diffraction results, also when Aliminiume concentration rate was 5 at%, we observed that all of AZO thin films have a high optical transmittance bigger than 85% with crystal size of about 3.5 µm; that lead us to speech on electrical resistivity,where we observed a decrease on its value as the alimniume doping increase, whereas it has the lowest value 2.32×10^{-3}(Ω.cm) at 5at% of aluminum concentration.

However, as we mentioned in chapter III, the influence of the doping level of the ZnO:F films was investigated also, using ultrasonic spray pyrolysis technique . the results were maybe slightly different ; where as X-ray diffraction revealed that the structural of FZO thin films was hexagonal wurtzite towards (002) peak, and after 2 at% the crystal size was growing to make the surface of FZO thin film more denser, also FZO have exhibited an optical transmittance as high as 90% in the wavelength range of UV-VIS, the electrical conductivity has increased as the concentration rate of fluorine on the ZnO films increased, until to the highest value of $1{,}68\times10^{2}$ $(\Omega.\text{cm})^{-1}$ at 5 at%.

In the early part of the work effort was concentrated on an extensive investigation of the growth and properties of undoped films grown from Zn acetate under a wide range of conditions, deposited using pneumatic spray pyrolysis. The effects of variety in the solution flow rate as well as the deposition pressure were then examined and the solution flow rate proved to be the most effective at lower pressures. Also the highest conductivity value of ZnO thin films prepared using ultrasonic spray pyrolysis were at highest substrate temperatures.

At the end we conclude that there is a very important factor to get the best properties between dopeds and doping rate, affect directly on the structural, optical and electrical characteristics, this brings us to choose an appropriate concentration rate values. However, based to our results AL or F Doped ZnO films have similar electrical and optical properties and they have more advantages than the other due to good stability at high temperatures and lower cost to manufacture.

Abstract:

In our study we were deposited a transparent oxide conducting thin films by two different methods the first one is the pneumatic spray pyrolysis and the second one is the ultrasonic spray pyrolysis, for investigating on five factors and thier effect on zinc oxide thin films characteristics. In the pneumatic spray pyrolysis we have deposited undoped zinc oxide thin films for checking on the effect of spraying flow rate and the deposition air pressure. In the ultrasonic spray pyrolysis we have divided our study into two parts the first was for studying the effect of substrate temperature on the undoped zinc oxide thin films properties the second part was for studying how much the extent of the dopants effect aluminum and fluorine on the zinc oxide thin films. The whole of the zinc oxide thin films were analyzed by many different techniques X-ray diffraction, scanning electron microscopy UV-Vis, Hall effect, four and two probes technique. in the pneumatic spray method we have observed that the films the films processed at 0.5 up to 1.5 bar showed optical band gap of about 3.3965 with electrical conductivity of 0.9×10^{3} $(\Omega.cm)^{-1}$, The X-ray diffraction spectrum indicated that the films were crystalline with hexagonal structure with the only diffraction peak (002).We conclude that there is a very important factor to get the best properties between deposition air pressure and solution flow rate. In the second part we observed that the appropriate substrate temperature is 350° for getting good reaction on top of the substrate, in addition to that the XRD patterns showed that the ZnO films have polycrystalline nature and a hexagonal wurtzite structure with (100) and (002) preferential orientation at high temperature, where the electrical conductivity of ZnO films was increased from 3.87×10^{-3} (Ω.cm)-1 to41.58 $(\Omega.cm)^{-1}$. As well in the study of aluminum doping ZnO, the X-ray diffraction and SEM analysis exhibited that the AZO films were found polycrystalline structure with a hexagonal wurtzite structure along the (002) growth orientation, moreover there is a decreasing in the optical band gap from 3. 38 to 3. 27 eV, the lowest resistivity (2.32×10^{-3} Ω.cm) was observed for AZO films processing with 5 at% ratio. In addition the effect of fluorine doping on ZnO thin films properties is obvious in our study. Where the FZO films showed that the films have peaks correspond to the hexagonal wurtzite structure of ZnO. Where the intense diffraction peak is the (002),the whole of FZO films become denser after 2 at% of fluorine, in the electrical study, we observed that, the electrical conductivity increasing as the fluorine doping increases, where the highest value is $1,68\times102$ $(\Omega.cm)^{-1}$ at 5 at% of fluorine doping.

Résumé

Dans notre étude, nous avons déposé un film transparent d'oxyde transparent par deux méthodes différentes, la première est la pyrolyse par pulvérisation pneumatique et la seconde est la pyrolyse par pulvérisation ultrasonique, pour étudier cinq facteurs et leurs effets sur les caractéristiques des couches minces d'oxyde de zinc. Dans la pyrolyse par pulvérisation pneumatique, nous avons déposé des films minces d'oxyde de zinc non dopés pour vérifier l'effet du débit de pulvérisation et de la pression de l'air de dépôt. Dans la pyrolyse par pulvérisation ultrasonique, nous avons divisé notre étude en deux parties. La première était d'étudier les effets de la température du substrat sur les propriétés des films minces d'oxyde de zinc non dopé et d'étudier l'effet des dopants en aluminium et en le fluor sur des films minces d'oxyde de zinc. L'ensemble des films minces d'oxyde de zinc a été analysé par de nombreuses techniques : la diffraction des rayons X, la microscopie électronique à balayage UV-Vis, l'effet Hall, la technique à quatre et deux pointes. Dans le procédé de pulvérisation pneumatique, nous avons observé que les films déposés à 0,5 jusqu'à 1,5 bar présentés une bande interdite d'environ 3,369 eV avec une conductivité électrique de $0,9 \times 10^{3}$ $(\Omega.cm)^{-1}$. Le spectre de diffraction des rayons X indiquait que les films étaient cristallins avec une structure hexagonale avec le seul pic de diffraction (002). Nous concluons qu'il existe un facteur très important pour obtenir les meilleures propriétés entre la pression de l'air de dépôt et le débit de la solution. Dans la deuxième partie, nous avons observé que la température du substrat était de 350 °C pour obtenir de bonne réaction sur le substrat, en plus que les diagrammes XRD montraient que les films ZnO avaient une nature polycristalline et une structure wurtzite hexagonale d'orientation préférentielle avec (100) et (002) à haute température, où la conductivité électrique des films ZnO est passée de $3,87 \times 10^{-3}$ $(\Omega.cm)^{-1}$ à 41,58 $(\Omega.cm)^{-1}$. Ainsi que dans l'étude du dopage avec de l'aluminium ZnO, la diffraction des rayons X et l'analyse MEB ont montré que les films AZO sont été cristallisés en structure polycristalline avec une structure wurtzite hexagonale selon l'orientation de croissance (002), en outre il y a une diminution de la bande interdite de 3. 38 à 3. 27 eV, le plus faible une résistivité (2,32 x 10^{-3} Ω.cm) a été observée pour les films AZO avec 5 at%. En outre, l'effet du dopage au fluorine sur les propriétés des couches minces de ZnO est évident dans notre étude. Les films FZO ont montré que les films ont des pics qui correspondent à la structure wurtzite hexagonale de ZnO. Là où le pic de diffraction est le (002), l'ensemble des films FZO se densifient après 2% atomique de fluorine. Dans l'étude électrique, on observe que la conductivité électrique augmente lorsque le dopage augmente, 1.68×10^{2} $(\Omega.cm)^{-1}$ à 5at% de dopage au fluorine.

ملخص

في دراستنا قمنا بإيداع الأغشية الرقيقة لأكسيد شفاف ناقل بطريقتين مختلفتين ، أولهما هو الانحلال الحراري بالرش الهوائي ، والثاني هو الانحلال الحراري بالموجات فوق الصوتية ، للتحقيق في خمسة عوامل وتأثيرها على خصائص الأغشية الرقيقة لأكاسيد الزنك. في الانحلال الحراري بالرش الهوائي ، قمنا بترسيب أغشية رقيقة من أكسيد الزنك غير المطعم للتحقق من تأثير معدل تدفق الرش وضغط الهواء الترسيبي، في الانحلال الحراري بالموجات فوق الصوتية قمنا بتقسيم دراستنا إلى جزأين حيث كان الأول لدراسة تأثير درجة حرارة الركيزة على خصائص الطبقة الرقيقة لأكسيد الزنك غير المطعم الجزء و الثاني كان لدراسة مدى تأثير التطعيم بالألمنيوم والفلورين على أغشية أكسيد الزنك الرقيقة. تم تحليل جميع أغشية أكسيد الزنك الرقيقة بالعديد من التقنيات المختلفة : حيود الأشعة السينية والمسح الضوئي بالمنظار الإلكتروني UV-Vis و مفعول هول و تقنيات أربعة مسابير و مسبارين للدراسة الكهربائية. في أسلوب الرش الهوائي ، لاحظنا أن الأفلام التي تمت معالجتها من 0.5 إلى 1.5 بار أظهرت فجوة نطاق ممنوع حوالي 3.396 مع التوصيل الكهربائي 0.9×10^{3} $(\Omega.cm)^{-1}$، وأشار طيف حيود الأشعة السينية إلى أن الأفلام كانت بلورية مع بنية سداسية مع ذروة انعراج فقط نحو(002) حيث نخلص إلى أن هناك عامل مهم جدا للحصول على أفضل الخصائص بين ضغط الهواء الترسيبي ومعدل تدفق المحلول. في الجزء الثاني لاحظنا أن درجة حرارة الركيزة المناسبة هي 350 درجة مئوية للحصول على ملاءمة جيدة فوق الطبقة السفلية ، بالإضافة إلى أن أنماط XRD أظهرت أن أفلام أكسيد الزنك لها طبيعة متعددة البلورات وبنية wurtzite سداسية مع (100) و (002) التوجه التفضيلي عند درجة الحرارة العالية ، حيث زادت الناقلية الكهربائية لأغشية أكسيد الزنك من $(\Omega.cm)^{-1}$ 3.87×10^{-3} إلى $(\Omega.cm)^{-1}$ 41.58 .وكذلك في دراسة أكسيد الزنك المطعم بالألمنيوم ، أظهر حيود الأشعة السينية وتحليل SEM أن أفلام AZO تم العثور عليها على شكل متعدد البلورات مع بنية wurtzite سداسية على طول اتجاه (002) ، بالإضافة إلى وجود انخفاض في فجوة النطاق الضوئي الممنوع من 3.38 إلى 3.27 eV ، لوحظت أدنى مقاومية (2.32×10^{-3} Ω.cm) من أجل AZO الأفلام المطعمة بنسبة 5 ذرة%. بالإضافة إلى ذلك ، فإن تأثير تطعيم الفلورين على خصائص الأغشية الرقيقة ZnO واضح في دراستنا. حيث أظهرت أفلام FZO أن الأفلام لديها قمم تتوافق مع هيكل wurtzite ZnO السداسية عندما تكون ذروة الانعراج هي (002) ، تصبح كل أفلام FZO أكثر كثافة بعد 2 ذرة% من التطعيم بالفلورين ، في الدراسة الكهربائية لاحظنا أن الناقلية الكهربائية تزداد مع زيادة النسبة الذرية للتطعيم بالفلورين ، حيث أن أعلى قيمة كانت $1,68\times10^{2}$ $(\Omega.cm)^{-1}$ في 5 ذرة % من التطعيم بالفلورين.